الجـــــــــــــــــــــــمهـوريـــــة الجـــــــــــــزائـريـة الديمـــــــقـراطيـة

الـشـــــــــعبيـة

People's Democratic Republic of Algeria

وزارة التـــــــــــــــــــــــــعـليـم العـــــــالي و البـــــــــحث العـــــلـمـــي

Ministry of Higher Education and Scientific Research

جـــــــــــــامعة أبي بكـــر بـلـقـايد – تـلمســـــــــــــان –

University of Abou Bekr Belkaid – Tlemcen –
Faculty of Technology

Laboratory of Computational Mechanics

THESIS

Presented for the obtaining the degree of **DOCTORATE 3rd Cycle**

in Mechanical Engineering

Specialty: Mechanical Construction

Presented by: **Hakim BENTRAR**

Subject

Vibration Analysis of Porous FGM Sandwich Plates

Publicly defended, 30/06/2024, in front of the thesis committee:

M. Amirat Mohammed	Professor	Univ. Tlemcen	Chairman
M. Belalia Sid Ahmed	Professor	Univ. Tlemcen	Supervisor
M. Chorfi Sidi Mohammed	Assoc. Prof. 'A'	Univ. Tlemcen	Co-Supervisor
M. Bensaid Ismail	Assoc. Prof. 'A'	Univ. Tlemcen	Examiner 1
M. Serdoun Mohammed Nadjib	Assoc. Prof. 'A'	ESSAT	Examiner 2

Academic year: 2023-2024

بِسْمِ اللَّهِ الرَّحْمَٰنِ الرَّحِيمِ

Dedication

I would like to dedicate this thesis to my parents, whose enduring love and sacrifices fueled my ambitions. To my extended family and dear friends, unwavering support and camaraderie have been vital to my academic journey.

I extend my heartfelt gratitude to every mentor, colleague, and participant who contributed to this study. Your insights and assistance were invaluable. This achievement is not mine alone but a shared triumph made possible by the support of my family, friends, and inspiring individuals who believed in me. Thank you for being a guiding star in my academic odyssey.

Declaration

I hereby declare that this thesis is my original work and has not been submitted for any other degrees, or examinations at any university. All sources of information and assistance used in this thesis is also acknowledged. I understand that any act of plagiarism or academic dishonesty can have severe consequences.

Hakim BENTRAR

2024

Acknowledgements

I begin by expressing my profound gratitude to Allah, whose divine guidance illuminated my path and granted me strength to overcome my challenges.

I extend my sincere appreciation to my dedicated tutor, Pr. Belalia, whose wisdom and mentorship have shaped this research. My heartfelt thanks to my co-tutor, Chorfi, for their invaluable insights. It has been a privilege to work with you all.

I am deeply thankful to my diligent examiners for graciously accepting my responsibility for evaluating my work. My sincere appreciation goes to Aouinat, whose assistance and motivation were invaluable, Berka, Houalef, Moussouni, Hachemi, and Ternan for their support in my research endeavors.

I express my gratitude to all members of the MecaComp lab, my peers, and scientific society for fostering an environment of intellectual growth. Thanks for your trust in my life choices and your support.

To my cherished family and friends, my unwavering support was my pillar of strength. This achievement is as much yours as it is in a mine. Thank you for being the foundation upon which my academic journey rested.

ملخص

تقدم هذه الأطروحة تحليل اهتزاز حر لألواح شطيرة المواد المتدرجة وظيفيا (FGM) مع توزيع المسامية التي أجريت باستخدام النسخة p من طريقة العناصر المحدودة، والتي تعتمد على نظرية تشوه القص من الدرجة الأولى. تتكون لوحة الساندويتش من طبقتين من صفائح الوجه المصنوعة من مواد متدرجة وظيفيًا وطبقة أساسية متجانسة. تم افتراض وتحليل خمسة نماذج لتوزيع المسامية لألواح شطيرة المواد المتدرجة وظيفيا. استكشفت هذه الدراسة بشكل منهجي تأثير نسبة السُمك، والظروف الحدودية، وأسس كسر الحجم، ومعاملات المسامية للطبقات العلوية والسفلية من ألواح شطيرة المواد المتدرجة وظيفيًا على التردد الطبيعي. يمثل هذا العمل أول تحليل شامل لهذه العوامل في ظل ظروف حدودية مختلفة للوحة شطيرة متدرجة وظيفيا، مما يوفر رؤى قيمة حول ديناميكياتها الاهتزازية. تم وضع النتائج في سياق الأدبيات الموجودة وإظهار دقة وكفاءة النموذج، مما يجعله أداة رقمية قوية لدراسة تحليل الاهتزاز الحر لألواح شطيرة المواد المتدرجة وظيفيًا ذات المسامية.

الكلمات مفتاحية : لوحة شطيرة المواد المتدرجة وظيفيا؛ تحليل الاهتزاز الحر. النسخة p من طريقة العناصر المحدودة؛ توزيع المسامية.

Abstract

This thesis presents a free vibration analysis of functionally graded material (FGM) sandwich plates with porosity distribution conducted using the p-version of the finite element method, which is based on the first-order shear deformation theory. The sandwich plate consisted of two FGM face sheet layers and a homogeneous core layer. Five porosity distribution models of FGM sandwich plates were assumed and analyzed. This study systematically explored the impact of the thickness ratio, boundary conditions, volume fraction exponents, and porosity coefficients of the top and bottom layers of FGM sandwich plates on the natural frequency. This work marks the first comprehensive analysis of these factors under various boundary conditions for a functionally graded sandwich plate, providing valuable insights into their vibrational dynamics. The findings are contextualized within the existing literature and demonstrate the accuracy and efficiency of the model, establishing it as a robust numerical tool for studying the free vibration analysis of FGM sandwich plates with porosity.

Keywords: FGM sandwich plate; free vibration analysis; p-version of finite element method; porosity distribution.

Résumé

Cette thèse présente une analyse de vibration libre des plaques sandwich en matériau à gradient fonctionnel (FGM) avec une distribution de porosité en utilisant la méthode des éléments finis de la p-version, basée sur la théorie de la déformation en cisaillement du premier ordre. La plaque sandwich se composait de deux couches de feuilles FGM et d'une couche centrale homogène. Cinq modèles de distribution de porosité des plaques sandwich FGM ont été supposés et analysés. Cette étude a exploré systématiquement l'impact du rapport d'épaisseur, des conditions aux limites, des exposants de fraction volumique et des coefficients de porosité des couches supérieure et inférieure des plaques sandwich FGM sur la fréquence naturelle. Ce travail marque la première analyse complète de ces facteurs sous différentes conditions aux limites pour une plaque sandwich à gradient fonctionnel, offrant des perspectives précieuses sur leur dynamique vibratoire. Les conclusions sont contextualisées dans la littérature existante et démontrent l'exactitude et l'efficacité du modèle, l'établissant comme un outil numérique robuste pour l'étude de l'analyse de vibration libre des plaques sandwich FGM avec porosité.

Mots-clés : plaque sandwich FGM ; analyse de vibration libre ; p-version de la méthode des éléments finis ; distribution de porosité.

Contents

List of Figures

List of Tables

Nomenclature

Abbreviations

FGM	Functionally Graded Material
FEM	Finite Element Method
P-FEM	P-version Finite Element Method
SIFs	Stress Intensity Factors
TDFGPP	Two-Directional Functionally Graded Porous Plates
FSDT	First-order Shear Deformation Theory
CVD	Chemical Vapor Deposition
PVD	Physical Vapor Deposition
EPD	Electrodeposition Methods
PM	Powder Metallurgy
AM	Additive Manufacturing
WAAM	Wire and Arc Additive Manufacturing
FSAM	Friction Stir Additive Manufacturing
FSW	Friction Stir Welding
LB	Langmuir-Blodgett
P-FGM	Power-law Functionally Graded Material
S-FGM	Sigmoid law Functionally Graded Material
E-FGM	Exponential law Functionally Graded Material
CPT	Classical Plate Theory
ESL	Elasticity-based Structural Load
HSDTs	Higher-order Shear Deformation Theories
SCFs	Shear Correction Factors
SCSDT	Second-order Shear Deformation Theories
TSDT	Third order Shear Deformation Theory
SSDT	Sinusoidal Shear Deformation Theory
HSDPT	Hyperbolic Shear Deformation Plate Theory
ESDPT	Exponential Shear Deformation Plate Theory
RPT	Refined Plate Theory
DQM	Differential Quadrature Method

Greek Symbols

ω	Natural Frequency
θ_i	Rotation Vector
ε_{ij}	Strain Tensor
σ_{ij}	Stress Tensor
x, y	Cartesian Coordinates
ξ, η	Local Coordinates
$P^{(l)}$	The Effective Material Properties
$\overline{\Omega}$	Fundamental Frequencies
Ω	Frequency Parameters
$E^{(\mathrm{i})}$	Young's Modulus
$\nu^{(\mathrm{i})}$	Poisson's Ratio
$\rho^{(\mathrm{i})}$	Mass Density
$V^{(\mathrm{i})}$	Volume Fraction
$N_i(\xi,\eta)$	Shape Functions
$g_i(\xi,\eta)$	Uni-dimensional Hierarchical Shape Functions
$P_i(\tau)$	Shifted Legendre Polynomials

Latin Letters

$[K_e]$	Stiffness Matrices
$[M]$	Mass Matrix
$\bar{Q}^i_{jk}$	Elasticity Constants
$\{\bar{\mathrm{q}}_\mathrm{j}\}$	Vector of Generalized in-plane Displacements
$\{\mathrm{q}_\mathrm{j}\}$	Vector of Generalized Transverse Displacement and Rotations
a, b	Plate length and width
h	Plate Thickness
k	Shear Correction Factors
A_{ij}	Extensional Stiffness Coefficients
B_{ij}	Bending-Extensional Coupling Stiffness
D_{ij}	Bending Stiffness Coefficients
S_{ij}	Shear Stiffness Constants
$\mathrm{I}_{\mathrm{i,j}}$	The Inertia Constants
U	Strain Energy

T	kinetic Energy
u_1, u_2, u_3	Displacement Field
(u, v, and w)	Displacements of the Middle Surface
n_1, n_2	Volume Fraction Exponents
ξ_1, ξ_2	Porosity Coefficients
P	Polynomial Order

General Introduction

General Introduction

Scientific advancements in material technology and the evolution of modern industries have spurred the demand for increasingly advanced materials tailored to specific properties. This demand has catalyzed the transformation of materials from their basic states into composites, where the combination of different materials confers superior properties. Composite materials, typically composed of a matrix with embedded reinforcement, offer enhanced properties, such as stiffness, fatigue resistance, and weight reduction. However, conventional composite materials often suffer from issues such as discontinuity of properties and stress concentrations at interfaces, which lead to structural vulnerabilities, particularly in high-temperature environments.

One innovative solution to these challenges is the utilization of Functionally Graded Materials (FGM), where the material properties vary continuously with the thickness. By eliminating sharp interfaces and introducing gradient transitions, FGM offer improved structural integrity and tailored performance, reminiscent of those of natural materials such as bones and teeth. Originally conceptualized in the 1980s for aerospace and fusion reactor applications, FGM have been widely used in various engineering sectors including aerospace, power generation, and machinery. The increasing application of FGM underscores the importance of understanding their complex behavior and performance characteristics.

In this context, this thesis focuses on the application of FGM in sandwich structures. Sandwich structures consisting of lightweight cores sandwiched between strong face sheets offer unique advantages in engineering applications. By integrating FGM into sandwich structures, we aim to enhance their mechanical and functional properties while addressing the current limitations in weight and strength.

One specific challenge addressed in this study is the impact of porosity on the mechanical behavior of FGM sandwich plates. Porosity can lead to reduced strength and stiffness as well as increased susceptibility to fatigue and failure. Investigating the effects of porosity on FGM sandwich plates is a critical aspect of our research as it allows the development of strategies to mitigate these effects and optimize the performance of these structures.

The motivation behind this research stems from the need to advance materials science and engineering, particularly in areas where lightweight and high-strength materials are critical, such as the aerospace and automotive industries. By studying the behavior of FGM sandwich structures, including the effects of porosity, we seek to contribute to the development of innovative solutions to real-world engineering challenges.

FGM sandwich structures exhibit complex behaviors that require sophisticated numerical tools for analysis. The finite element method is a powerful and efficient method that is widely used in the analysis of the complex behavior of these materials. The objectives of this thesis are to investigate the mechanical behavior and manufacturing techniques of FGM sandwich structures, with a specific focus on understanding the effects of porosity on their performance.

In general, the behavior of structural elements made of FGM sandwiches, for instance plates, can be described by three-dimensional (3D) or two-dimensional (2D) theories. Although the 3D approach is more accurate, it is difficult to implement. Therefore, the 2D approach is widely used owing to its simplicity and low computational costs. For decades, classical and first-order shear deformation theories have been used to analyze FGM structural component behaviors.

By addressing these objectives, including the study of porosity effects, we aim to contribute to a broader understanding of FGM and their applications in engineering, paving the way for the development of advanced materials with tailored properties and enhanced performance.

Aims and objectives

The overall aim of this thesis is to advance the understanding of the linear behavior of FGM sandwich plates with porosity using the p-version of the finite element method. This was accomplished by achieving four main objectives:

- Verify p-version of the FEM numerical model based on the first-order shear deformation theory.
- Investigate the linear free-vibration behavior of isotropic and FGM sandwich plates with different parameters.
- We further explored the linear free vibration behavior of the FGM sandwich plate.
- Effect of porosity distribution on free vibration of functionally graded sandwich plate.

Thesis Organization

The present work deals with the free vibrations of an FGM sandwich plate with porosity, which is organized into six chapters as follows:

- Chapter I, presents a brief literature review related to the mechanical behavior of FGM sandwich plates, considering the influence of porosity distribution within the layers and focusing on various aspects of FGM sandwich plates, with particular attention to their vibration characteristics. Special emphasis is placed on investigating the effects of the material gradient distribution, structural composition, and porosity distribution on the vibration response of the FGM sandwich plates.

- Chapter II, provides an overview of the key concepts and methodologies relevant to modeling sandwich structures and FGM. In Section II.1, we delve into the mechanical properties of sandwich structures, encompassing different assembly types, modes of damage, adhesive requirements, and material advantages and drawbacks, while surveying various modeling techniques. section II.2, offers an examination of FGM, including diverse manufacturing approaches, with a particular emphasis on the solid freeform fabrication method owing to its inherent advantages and manufacturing adaptability. Furthermore, it elucidates the multiple application domains.

- Chapter III, we present the main plate theories frequently employed to model FGM sandwich plates, alongside a layered approach aimed at elucidating the interfacial influences observed in conventional composite materials. Additionally, was introduced to describe the particularities of the p-version of the finite element method for modeling the free vibration of plates.

- Chapter IV addresses several key aspects that are essential for our investigation. In Section IV.1, we scrutinized the geometric layout of the FGM sandwich plate model. Subsequently, we delve into the mathematical formulation of the first-order shear deformation theory. In addition, we amalgamate and elaborate on the element description, displacement interpolation, and shape functions pertinent to the P-version

of the finite element method. Moving forward, we elucidate the derivation of equations for strain, kinetic energy, and motion, contributing to a thorough delineation of the plate behavior. Moreover, we discuss the validation study conducted to ascertain the accuracy and dependability of our numerical approach. In Section IV.2, computer implementation and computational considerations are employed to efficiently conduct calculations on the machines. We then embark on a parametric study in section IV.3, aimed at exploring the effects of varying parameters, such as the volumetric fraction of layers, on the free vibration analysis of functionally graded sandwich plates.

- Chapter V, the effect of porosity distribution on free vibration of functionally graded sandwich plate is investigated. In Section V.1, we define five porosity distribution models and study the convergence and comparison of the FGM sandwich plate with porosity with results in the literature to verify the accuracy of the model for intact FGM plates. In Section V.2, we present a comprehensive parametric study to investigate the influence of key factors, including the effect of the thickness ratio, boundary conditions, volume fraction exponents, and porosity coefficients of the top and bottom layers of the FGM sandwich plates on the natural frequency.

- Chapter VI, the conclusions and potential further work are discussed.

Chapter I

Literature Review

Chapter I

Literature Review

In this chapter, a brief literature review is presented, focusing on two key points: the mechanical behavior of functionally graded material sandwich plates and the effects of porosity distribution on the vibration response of the FGM sandwich plates.

I.1 Vibration of FGM plates

In recent years, the study of the mechanical behavior of FGM plates has emerged as a focal point in materials science and engineering. Researchers have turned to sophisticated analytical and computational methods to unravel the complexities of mechanical performance. The analysis of FGM plates has become increasingly important in materials science and engineering because of their spatial variations in material composition and properties, offering diverse applications across industries. This introduction sets the stage for exploring the mechanical intricacies and performance of FGM plates using atomistic methods.

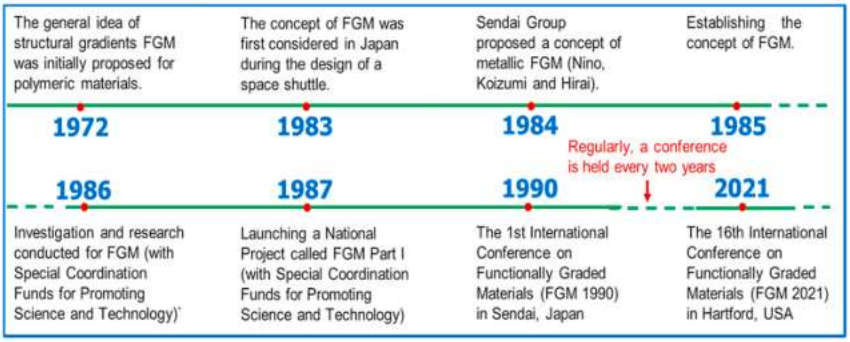

Figure I-1: Historical overview of relevant milestones in the research and development of FGM [1]

Several studies have been conducted on the vibration of FGM plates. Swaminathan et al. [2] provided a comprehensive review encompassing various analytical and numerical methods employed for this purpose, focusing on the stress, vibration, and buckling characteristics of FGM plates. For example, analytical methods such as the classical plate theory and numerical techniques such as finite element analysis have been utilized to predict the behavior of FGM plates under different loading conditions.

Similarly, Swaminathan et al. [3] used thermal analysis to discuss mathematical idealizations, modeling techniques, and solution methods pertinent to FGM plates subjected to thermal loads. They explored various temperature profiles and their effects on the mechanical response of the FGM plates. For instance, linear and nonlinear temperature gradients across the thickness of a plate have been investigated to understand thermal stresses and deformation behaviors.

Alimoradzadeh et al. [4] extended this study by exploring the nonlinear dynamic responses of FGM composite beams on nonlinear viscoelastic foundations under moving mass loads and

temperature variations. They conducted numerical simulations to analyze the influence of the temperature rise, material distribution parameters, and moving mass characteristics on the dynamic behavior of FGM beams. Their study highlighted the importance of considering material nonlinearity and dynamic loading conditions in the design of FGM.

Another facet of research, elucidated by Thai et al. [5], involved a comprehensive review of various theories for modeling and analyzing functionally graded plates and shells, emphasizing single-layer theories and three-dimensional elasticity solutions. They provided examples of theoretical models, such as first-order shear deformation theory, which has been widely used to predict the global responses of functionally graded plates and shells under mechanical and thermal loadings.

Furthermore, Gupta and Talha [6] presented an extensive review of the structural response of FGM and structures, offering insights into thermo-electro-mechanical loadings and fabrication procedures. They discussed case studies of FGM plates and shells subjected to combined thermal and mechanical loading conditions, highlighting the importance of considering material heterogeneity and environmental effects in the design and analysis.

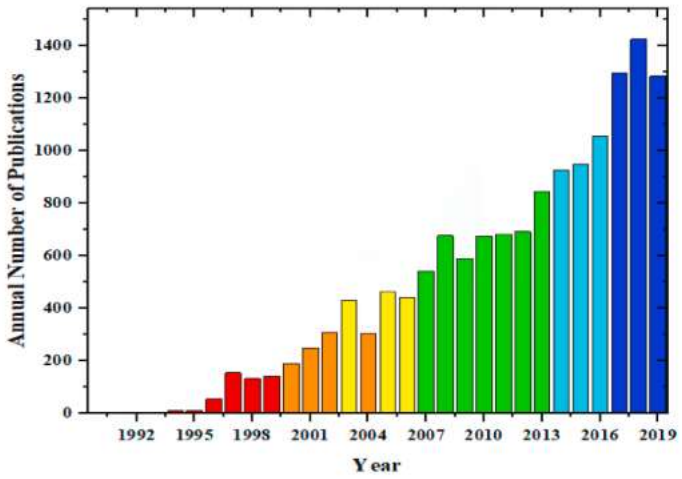

Figure I-2: The annual number of publications using the search titles “functionally graded materials”. (Based on the Web of Science search system in the duration)

Kanu et al. [7] focused on fracture analysis of FGM materials, highlighting computational advances such as multiscale simulations and extended finite element methods. They provided examples of crack propagation studies in FGM structures using advanced numerical techniques, demonstrating the utility of these methods in predicting the fracture behavior and structural integrity.

Additionally, Toudehdehghan et al. [8] provided an overview of FGM applications, manufacturing processes, and mathematical idealizations, underscoring the need for simplified homogenization schemes for efficient analysis. They discussed examples of homogenization techniques used to model FGM microstructures and predict macroscopic material properties, highlighting the importance of accurate material characterization and modeling assumptions.

The reviewed literature underscores the multifaceted exploration of FGM plates, encompassing various analytical, numerical, and experimental approaches. These investigations have significantly contributed to the understanding of the mechanical, thermal, and dynamic responses of FGM structures, paving the way for advancements in material science and engineering applications.

I.2 Vibration of FGM sandwich plates

In recent years, the study of vibrations in FGM plates has become a focal point of research. Research on the vibration behavior of FGM sandwich plates has been extensively explored by scholars aiming to enhance our understanding of these complex structures in various applications. Garg et al. [9] conducted a thorough literature review on sandwich FGM structures and explored analysis methods and theories across plates, beams, and shells, considering factors such as porosity and hygrothermal loading, to set a benchmark for future research.

Dat et al. [10] investigated the free vibration of functionally graded sandwich plates with stiffeners using the finite element method. They employed a power-law distribution for the material properties in the thickness direction and conducted a parametric study to analyze the influence of the material distribution and stiffener parameters on the plate vibration characteristics. Wang [11] aims to develop a robust algorithm for analyzing the free vibration of moderately thick circular cylindrical shells under various conditions, crucial for applications in structural, rock, and aerospace engineering. By proposing an adaptive finite element method, they sought to enhance the accuracy and reliability of solutions compared to conventional finite element methods for such analyses. Wang et al. [12] address the dynamic behavior of moderately thick circular cylindrical shells commonly used in engineering applications, emphasizing the impact of micro-crack damage on vibration characteristics. They highlighted the importance of accurately capturing free vibration frequency and mode changes due to stiffness weakening in damaged regions and proposed improvements to conventional finite element methods for better precision in local oscillation solutions.

Belalia examined the free vibrations of FGM sandwich plates using von Karman’s assumptions and a geometrically nonlinear formulation [13]. The p-version of the FEM was

used for the geometrically nonlinear free vibration of the bi-FGM sandwich plates [14]. The bi-FGM sandwich elliptic plates' linear and geometrically nonlinear free vibrations was explored by Belalia [15] using a curved hierarchical finite element. Wang [16] tackles precision challenges in eigensolutions and buckling load predictions for curved beams with crack damage, introducing a finite element method and advocating for adaptive mesh refinement to enhance solution accuracy. Wang et al. [17] proposed an hp-version adaptive finite element method for precise eigensolutions in moderately thick circular cylindrical shell vibrations, integrating error homogenization and higher-order interpolation to efficiently achieve high-precision results. Burlayenko et al. [18] developed a three-dimensional modeling approach to understand the free vibrations and static responses of FGM sandwich plates. Their work utilized the finite element method within the ABAQUSTM code, incorporating a 3-D brick graded finite element for an accurate representation. Parametric studies were conducted by varying the volume fraction profile and ceramic volume fraction, providing insights into material behavior. Irfan et al. [19] reviewed finite element formulations developed after 2000 for analyzing sandwich plates, covering theories such as first-order shear deformation, higher-order shear deformation, and mixed solid-shell elements. Their comprehensive review addressed emerging areas, including piezoelectric structures, and reflected the evolution of analytical methods for understanding the behavior of complex sandwich structures. Yaylacı et al. [20] tackled the continuous and discontinuous contact problems of functionally graded layers on rigid foundations. The study involved analytical and finite-element solutions, demonstrating the compatibility between the two approaches. Their work emphasized the importance of material properties and loading conditions in understanding the contact behavior of FGM layers. Zhang et al. [21] delved into stress intensity factors (SIFs) in linear elastic fracture mechanics, extracting SIFs for various crack configurations using the p-version finite element method (P-FEM). Their study verified the effectiveness and accuracy of P-FEM in comparison with other numerical methods, highlighting its significance in assessing structural and material damage.

Recent studies by Ghazwani and Van Vinh introduced novel theories for the bending and free vibration analysis of bifunctionally graded sandwich plates. Ghazwani's [22] study focused on establishing an nth-order shear deformation theory and simplifying the analysis by incorporating only four unknown displacement functions. Van Vinh [23] proposed a hybrid quasi-3D theory, combining polynomial and trigonometric functions to capture the distribution of transverse shear strains and thickness stretching effects. Both studies contributed to advancing the understanding of complex sandwich plate structures.

Kumar et al. [24] conducted a comprehensive review of the literature on buckling and free vibration analysis of shear deformable isotropic and laminated composite sandwich plates and shells. Their article covered various theories, finite-element models, and experimental methods. Meksi et al. [25] introduced a new shear deformation plate theory for illustrating the bending, buckling, and free vibration responses of functionally graded material sandwich plates. Their theory involves a displacement field with integrals, accounting for a quasi-parabolic distribution of the transverse shear stress. The proposed model was validated through analytical solutions and the influence of critical parameters on the behavior of functionally graded sandwich plates.

In summary, the culmination of these research endeavors to understand the dynamics and behavior of functionally graded material sandwich plates and lay a solid foundation for future investigations in the field of structural mechanics. Areas ripe for exploration include the development of advanced analytical and computational methods to more accurately model the complex behaviors exhibited by FGM sandwich plates under various loading conditions. Furthermore, there is a growing need to explore novel materials and manufacturing techniques that can further enhance the performance and functionality of FGM sandwich plates, particularly in demanding applications, such as aerospace, automotive, and civil engineering. Additionally, future research could delve deeper into the optimization of the porosity distribution patterns and material compositions to tailor the mechanical properties of FGM sandwich plates for specific applications, thereby maximizing their efficiency and effectiveness.

I.3 Vibration of FGM sandwich plates with porosity

In the fabrication process of FGM sandwich plates, the constituent materials have different solidification temperatures, which causes the creation of porosities or microscopic voids. Many studies have been conducted that have considered the impact of porosity on the free vibration of FGM sandwich plates. Hadji et al. [26] investigates the effect of porosity distribution pattern on the free vibration analysis of porous FG plates, considering various boundary conditions and material variations. Heshmati and Jalali [27] explored the free vibration behavior of sandwich circular and annular plates with a core made of materials with functionally graded porosity and analyzed different porosity distributions in the radial direction.

Figure I-3: A top view of a radial cross-section of a cylinder showing graded porosity distribution in the radial direction [27]

Daikh and Zenkour [28] propose a new porosities distribution for bending analysis of FGM sandwich plates, while Daikh and Zenkour [29] study the free vibration and mechanical buckling of porous functionally graded sandwich plates, utilizing a new and simple higher-order shear deformation theory.

Zhang et al. [30] presented a comprehensive analysis of the free vibration and damping properties of porous FG sandwich plates by considering a modified Fourier-Ritz method and investigating the effects of evenly and unevenly distributed porosities within the face layers. Tran et al. [31] utilizes an edge-based smoothed finite element method to investigate the static bending and free vibration of functionally graded porous plates, examining the influence of geometric parameters and material properties on plate behavior.

Quan et al. [32] focused on the nonlinear vibration of porous FG sandwich plates under blast loading by employing an analytical approach to study the effects of volume fraction index, porosity coefficient, and type of porosity distribution.

Van Vinh and Huy [33] establish a finite element model to study the static bending, free vibration, and buckling of functionally graded sandwich plates with porosity, considering the effects of various parameters on plate response. Kumar Sah and Ghosh [34] analyze the free vibration and buckling of multi-directional porous FGM sandwich plates, investigating the influence of porosity models and geometric parameters. Hirannaiah et al. [35] investigate the effects of thermo-mechanical load coupling and porosity distributions on the vibration and

buckling characteristics of FGSPs with cutouts, employing a Finite Element (FE) formulation to study plate behavior under different loading conditions.

Belkhodja et al. [36] analyzed the thermal buckling and thermomechanical bending responses of sandwich plates with FGM face layers, considering the effects of thermal loads and porosity distributions on plate behavior. Karakoti [37] develop a finite element formulation for the nonlinear transient response of porous FGM sandwich plates and shell panels, examining the effects of volume fraction index, porosity model, and blast load parameters. Merdaci et al. [38] examined the free vibration response of functionally graded plates with different porosity distributions, and evaluated the influence of material properties and porosity volume fractions on plate behavior. Shivaramaiah et al. [39] investigate the nonlinear behavior of two-directional functionally graded porous plates (TDFGPP) using various porosity distributions and material properties, exploring the effects of volume fraction gradation profiles on plate response.

These studies collectively contribute to advancing our understanding of the mechanical behavior and vibrational characteristics of functionally graded porous materials, offering insights for engineering applications.

I.4 Gaps in existing literature

FGM sandwich structures are subjected to non-symmetric charges in many engineering fields and industries. However, in the manufacturing process, the constituent materials of the two thin face sheets have different solidification temperatures, leading to the generation of two different microvoids or porosities inside the layers on the top and bottom face sheets of the FGM sandwich plates. However, a notable research gap emerges from the absence of comprehensive studies dedicated to investigating the free vibration of FGM sandwich plates with various porosity coefficients and volume fraction exponents in the top and bottom layers. To the best of our knowledge, there are no publications in the available literature that address this specific aspect. This conspicuous void underscores the need for further research in this area.

Addressing this gap is imperative, and prompts the scientific community to conduct rigorous inquiries. Delving into this unexplored territory will help scientists avoid problems associated with different porosity coefficients for the top and bottom layers, thereby advancing our understanding and contributing to the enhancement of FGM sandwich plate design and performance. Through comprehensive analysis, this research contributes to the advancement of FGM technology and lays the groundwork for future studies in this field.

I.5 Summary

This chapter provides a comprehensive and in-depth review of the vibration behavior of FGM sandwich plates, specifically focusing on the impact of varying porosity distributions. It traces the historical evolution of research in this domain, incorporating recent advancements and identifying critical avenues for further exploration, notably emphasizing the role of porosity. With clearly delineated objectives aimed at bridging existing research gaps, this chapter provides a comprehensive framework for targeted and purposeful investigations, laying a strong foundation for subsequent studies. In the ensuing chapter, we will delve into diverse theories, development methods, and methodologies employed in modeling sandwich structures and FGM, expanding upon the insights gleaned from this examination.

Chapter II

Preliminaries

Chapter II

Preliminaries

This chapter focuses on the synergistic potential of sandwich structures and FGM, which are two advanced composite materials known for their unique properties and applications. Sandwich structures, composed of lightweight cores sandwiched between high-strength face sheets, offer exceptional stiffness-to-weight ratios and customizable performance attributes. In contrast, FGM exhibit gradient compositions and properties, allowing for precise control over their mechanical, thermal, and electrical characteristics. By exploring the characteristics and applications of both sandwich structures and FGM, this chapter aims to elucidate their combined potential in innovative engineering solutions across diverse industries and applications.

II.1 Sandwich structures

Sandwich panels have been successfully utilized for many years in the aviation and aerospace industries as well as in marine, mechanical, and civil engineering applications. This is attributed to their high rigidity and strength-to-weight ratio [40]. The use of sandwich construction in aerospace structures can be traced back to World War II, when the British bomber de havilland mosquito employed such construction [41].

Initially, the sandwich structure was a simple assembly featuring basic coverings made of fabric, thin metal, and soft wood used as the core. The classical sandwich construction comprises a relatively thick core and low-density material that separates the relatively thin yet rigid upper and lower faceplates. The materials employed in sandwich constructions have been diverse, but recently there has been increased interest owing to the introduction of novel materials for use in facings and cores [42].

The advancement of modern technologies demands the utilization of materials possessing specific high mechanical properties tailored to their applications, while maintaining low densities. This aim primarily targets a reduction in the structural mass. Composite materials fulfill these criteria, offering low density, high strength, significant rigidity, and excellent durability. Sandwich materials are among the most commonly used composite materials and occupy a significant niche in the construction of composite components.

II.1.1 Definition

A sandwich material consists of a core, which is typically lightweight with poor mechanical characteristics, sandwiched between two skins made of a material possessing strong mechanical properties. Thin, rigid, and resilient skin adheres to a core composed of soft, lightweight materials. This configuration provides sandwich materials with an excellent bending strength and remarkable lightness. The overall performance of sandwich structures depends on their constituent material properties (face sheets, adhesive, and core), geometric dimensions, and loading type. The effective design and application of sandwich construction necessitate thorough characterization and understanding of not only the constituent sandwich materials but also the overall structure under quasi-static and dynamic loads [43].

II.1.2 Sandwich ingredients

The sandwich concept is a well-established construction technique that combines lightweight properties with rigidity and strength. Essentially, a sandwich structure comprises a

low-density material onto which two thin layers of stronger and more rigid materials are adhered.

The skin (or layers) must withstand bending moments and can vary in nature, for example, metal, laminate, wood (plywood), or even thermoplastic sheets. The core, which is the central element of a sandwich structure, typically exhibits poor mechanical characteristics. Its role involves resisting shear stresses resulting from skin sliding under a load and maintaining separation. Figure II-1 illustrates the various constituent elements of a composite material used in sandwich construction.

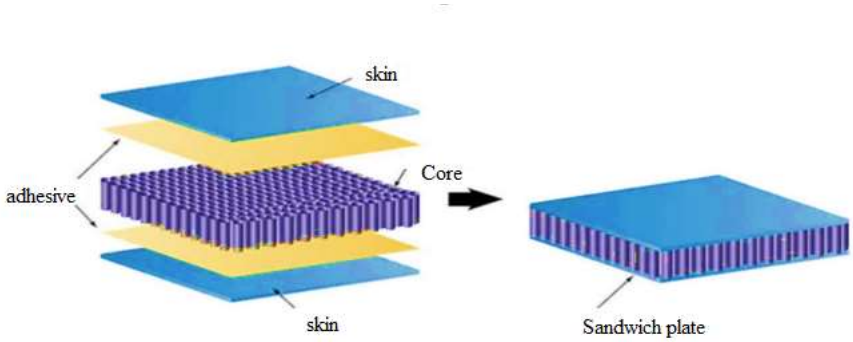

Figure II-1: Diagram of a sandwich plate

II.1.2.1 The skins

Generally, thin skins can be made of any material that can be obtained in a layered form, including wood, metal, or composite materials. The choice of the material nature and sequence depends on the use of composite materials. Skins aim to withstand bending forces, which are reflected in the normal stresses (tension or compression). Quoting Allen [44], 'Nearly all structural materials available in thin sheet form can be used to form the faces of a sandwich panel,' offering a wide variety in material selection. This flexibility allows for efficient design that enables the use of each material component to its utmost potential. The key properties crucial for the skin include the following:

- Impact resistance
- Surface finish
- Wear resistance
- High stiffness providing elevated flexural rigidity
- High tensile and compressive strength
- Environmental resistance (chemical, UV, heat, etc.)

Commonly used skin materials can be categorized into two main groups: metallic and non-metallic. The first group comprises steel, stainless steel, and aluminum alloys, which offer a wide variety of alloys with different strength properties, while exhibiting limited stiffness variation. The larger of the two groups is the latter, encompassing materials such as plywood, cement, veneers, reinforced plastics, and fiber composites.

The most significant nonmetallic materials are fiber composites, which have had a substantial impact on sandwich construction since their introduction. This is because most composites offer strength properties similar or even superior to those of metals, although their stiffness is often lower. Hence, to achieve the required stiffness, composites are frequently sandwiched between lightweight cores [45].

II.1.2.2 The core

The core, which is typically lightweight, generally has very low bending strength. The fundamental function of a sandwich structure is to transmit mechanical actions from one skin to another through transverse shear. The cores used in load-bearing sandwich constructions can be categorized into four groups: corrugated cardboard, honeycomb, balsa wood, and foams.

First, the core must have a low density to add minimal weight to the total sandwich. The key properties of interest for the core include the following.

- Density
- Shear modulus
- Shear strength
- Stiffness perpendicular to faces
- Thermal insulation
- Sound insulation

There are two types of cores:

- Solid cores [46] encompassing the:
  - Balsa or cellular wood (Figure II-2a)
  - Various cellular foams (Figure II-2b)
  - Resins filled with hollow glass microspheres are referred to as syntactic foam. This solid or cellular core was considered isotropic.

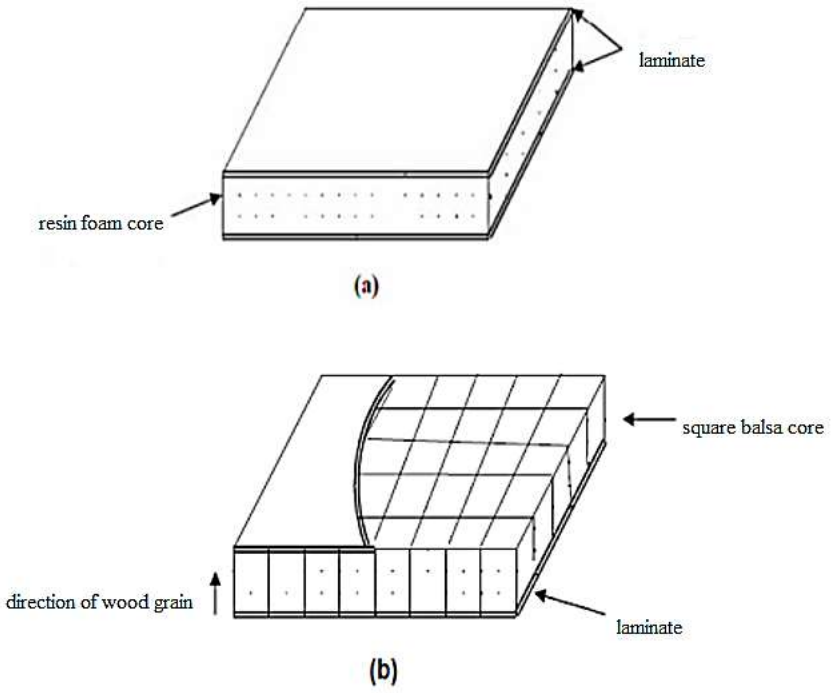

Figure II-2: Solid core sandwich materials

- Hollow cores [46], primarily honeycomb in type (Figure II-3), comprising the following:
  - Lightweight metallic alloys
  - Kraft papers
  - Polyamide papers, such as Nomex paper.

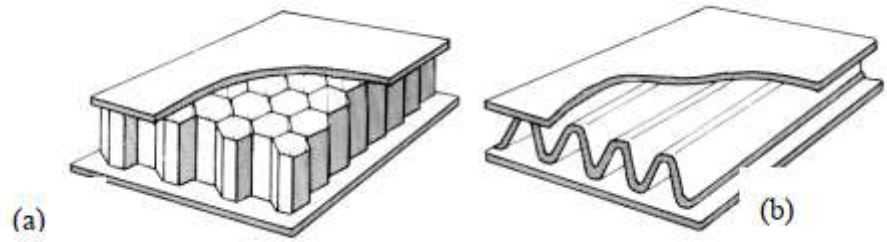

Figure II-3: Hollow core sandwich materials: (a) honeycomb; (b) corrugated core

The core can be made from the following materials:

- Foams: Lightweight, inexpensive, easily machinable, yet with very poor mechanical properties.

- Balsa: Known for its various uses and qualities, including lightness, high thermal and acoustic insulation, and resistance to thermal variation.
- Honeycomb: Typically made from thin-plate materials (aluminum alloy, polyamide paper).

II.1.2.3 The interface

Sandwich structures can be assembled through bonding, welding, or brazing. Numerical simulations typically assume a flawless bond between components, irrespective of the layer assembly method. This component is of crucial importance because it bonds the core and skin together. It must enable solid assembly of the structure by forming a continuous, nonporous, and uniform thickness bond.

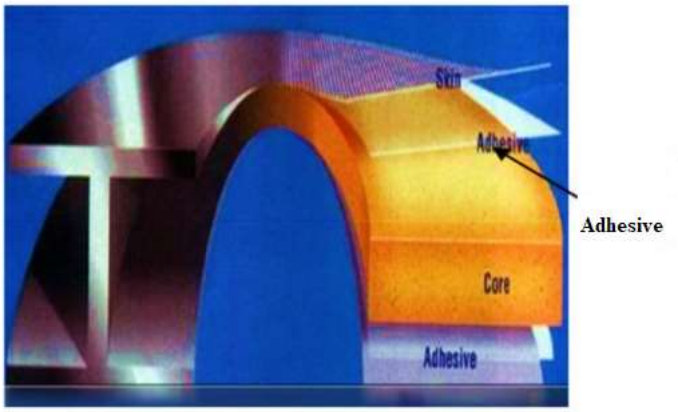

Figure II-4: Adhesion mechanisms

II.1.3 Type of sandwich structures

Currently, a wide variety of sandwich cores are employed in structural engineering, as depicted in Figure II-5.

II.1.4 Applications for sandwich materials

The use of sandwich structures continues to increase rapidly for various applications, including satellites, aircraft, ships, automobiles, railcars, wind turbines, and bridge construction. The sandwich method finds extensive application in naval and maritime construction, with new markets on the horizon.

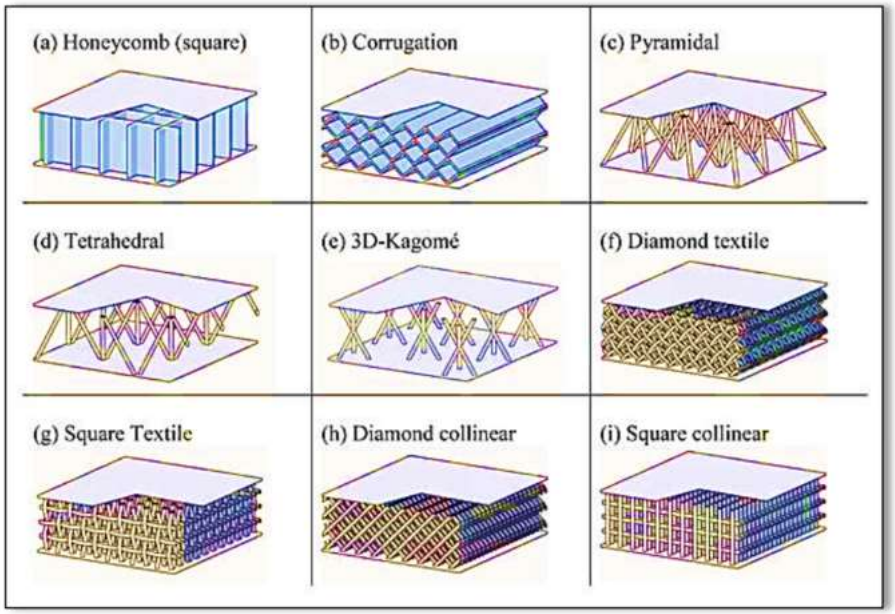

Figure II-5: Variety of cellular networks configured as cores of sandwich panel structures

Contemporary land designs mostly limit the use of concrete, steel, and a few aluminum alloys. Sandwich materials assembled through bonding also find applications in automotive and railway construction. In this study, glass/polyester laminate skins and expanded polystyrene foam cores were used.

Sandwich materials are in demand for metro and tramway systems, which require frequent starts. Access doors made of sandwich panels with composite glass/polyester or aluminum skins adhered by internal adhesives are prevalent, utilizing cores of aluminum honeycombs or Nomex.

Aerospace construction involves the use of sandwich panels and co-cured composite laminates (carbon/epoxy, kevlar/epoxy) for landing gear doors and various fairings (between fuselage wings, engine pylons, flap tracks).

Engine cowls are commonly constructed using carbon/epoxy skins that adhere to aluminum honeycomb cores. Numerous helicopter parts are either monolithic or sandwiched, featuring composite skins bonded to honeycomb cores [47].

In astronautics and defense sectors, where heat and thermal variations are critical, solar reflectors use carbon/epoxy skins and Nomex honeycomb cores. In the future, the sandwich concept may serve as a substitute material for various modules constituting these structures.

II.1.5 Manufacturing processes

In many cases, the manufacturing of sandwich structures involves standard composite processing technologies, such as contact molding, vacuum bag molding, resin injection molding, press molding, filament winding, and centrifugation. These methods enable integration of a core within the thickness of the manufactured structure. This section highlights the most commonly used process for developing a sandwich structure.

II.1.5.1 Wet process technologies (direct impregnation)

Traditionally, sandwiches are obtained through implementation processes known as 'wet lay-up," in which dry reinforcements are impregnated with thermosetting resin during shaping. This can be achieved through contact molding, simultaneous spraying, resin injection, or filament winding. Structures produced via contact or simultaneous spraying exhibit average mechanical properties, particularly if the skins are made from chopped fibers. The resin content, porosity rate, and overall laminate quality depend on the molder skill. Those generated by filament winding or resin injection (vacuum or pressure) showcase higher mechanical properties due to the potential use of continuous fiber reinforcements (unidirectional, fabrics) and achieving higher fiber content.

II.1.5.2 Dry process technologies (indirect impregnation)

Dry lay-up methods or indirect impregnation processes involve the creation of sandwich structures with skins obtained from a pre-impregnated material. Implementation occurs under vacuum in an oven, heated press, or vacuum autoclave. The use of pre-impregnated materials ensures uniform and high-quality reinforcement impregnation, granting the sandwich component good mechanical properties owing to the high fiber content. Excess resin in the pre-impregnated material, which is extracted through appropriate pressure and temperature applications, can be used for core-to-skin bonding.

- Bonding Assembly: Bonding remains a prevalent method for assembling sandwiches, involving the joining of preformed cores and skins using adhesives. The shaping and assembly phases were distinct. Surface preparation is crucial to ensure high-quality bonding.
  - Cleaning to eliminate grease or dust and enhance the surface roughness.
  - Priming via chemical treatment of metallic skin adhesives tailored to the constituent materials of the sandwich must be uniformly applied. The stack (core + adhesive +

skin) is heated and placed under pressure, which can be applied using a press, vacuum autoclave, or vacuum bag molding.

II.1.6 Designing sandwich structures

Although primarily intended to withstand bending forces, sandwich structures are also engineered to meet other requirements, such as thermal and acoustic insulation. The choice of the sandwich type depends predominantly on its intended application. The key goals for a 'sandwich' designer include selecting appropriate materials constituting the structure and determining the respective thicknesses of the skin and core to withstand bending moments, shear, and axial stresses induced by applied forces. Generally, the design is based on sandwich theory (homogeneous beam theory) and the selection of materials possessing the requisite properties.

II.1.7 Geometric characteristic of sandwiches

Owing to the fabrication of sandwiches, the mechanical properties are tailored by varying the nature of the skin (whether identical or not), core, and thickness of each phase. Generally, the skins have the same thickness, t_f, and the ratio t_f / h_c (where h_c is the core thickness) falls between 0.01 and 0.1, sandwiches are classified into three categories based on the value of the d/t_f ratio [42], where d represents the distance between the neutral axes of the sandwich skins:

- For a d/t_f ratio below 5.77, the sandwich is termed as thick-skinned.
- For a d/t_f ratio between 5.77 and 100, the sandwich is termed thin-skinned.
- For a d/t_f ratio above 100, the sandwich is termed very thin-skinned.

These limits were defined in relation to the contribution of each constituent to the bending and shear stiffness of the sandwich.

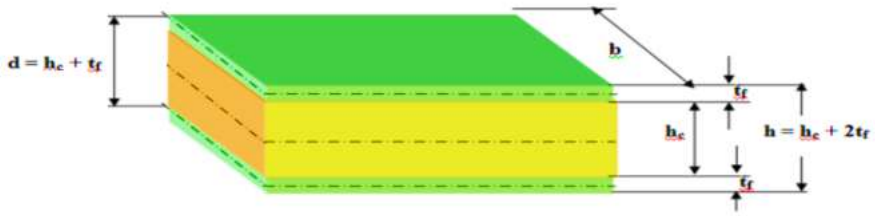

Figure II-6: Diagram of a sandwich

II.1.8 Sandwich materials plates

A sandwich material consists of a low-density material (core) bonded to high-stiffness and high-strength layers (skins). The primary function of the core is to transmit mechanical action from one skin to another through transverse shear. The skins can be made of laminates or metallic materials with thicknesses h_1 (lower skin) and h_2 (upper skin). The core thickness was denoted as h_c, and the total sandwich thickness was H ($H = h_1 + h_c + h_2$). At each point in the sandwich structure, the coordinate system is selected such that the (x, y) plane represents the mid-plane [48].

The assumptions underlying the theory of sandwich materials are as follows [48].

- Core thickness was greater than that of the skin ($h_c > > h_1, h_2$).
- The core displacements u_c and v_c in the x- and y-directions are linear functions of the z-coordinate.
- The displacements u and v in the x- and y-directions were uniform within the skin thickness.
- The transverse displacement w is independent of the variable z, and strain ε_{zz} is neglected.
- The core only transmits transverse shear stresses σ_{xz}, σ_{yz}; stresses σ_{xx}, σ_{yy}, σ_{xy}, and σ_{zz} are neglected.
- The transverse shear stresses τ_{xz} and τ_{yz} were neglected within the skin.
- Finally, the theory addresses elasticity problems in small deformations.

II.1.9 Assembling techniques for sandwich materials

II.1.9.1 The bonding of skin on the soul

For sandwich structures to fulfill their roles effectively, it is crucial to ensure perfect bonding between the core and skin to distribute the loads evenly between them. Assembly was achieved, as depicted in Figure II-7, through bonding using resins compatible with the materials involved.

II.1.9.2 Folding technique

After the implementation, sandwich panels can be formed by folding, as illustrated in Figure II-8. The process begins by stripping a strip of one of the coverings along the folding axis and to a width determined by the plate thickness and the desired folding angle. The material was then folded and the angle was held in the chosen position.

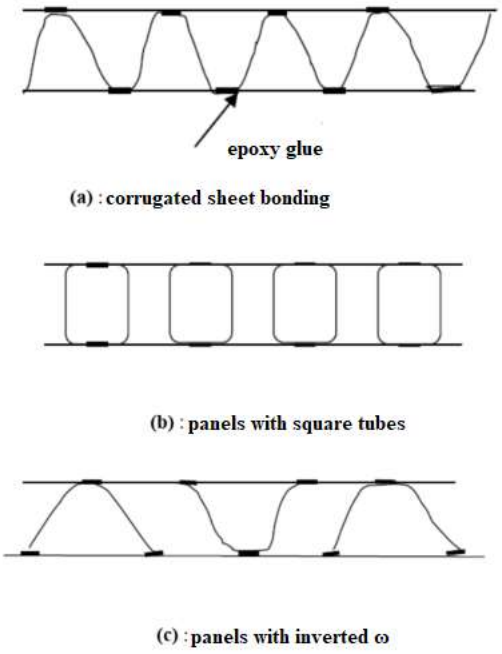

Figure II-7: panels made by gluing from various profiles

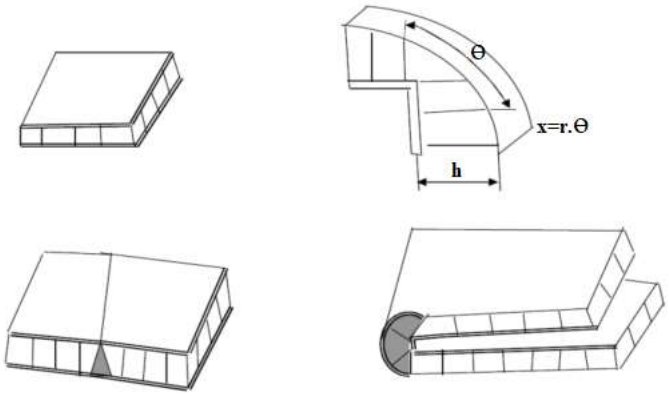

Figure II-8: Folding sandwich panels

II.1.10 Advantages of sandwich structures

The primary advantage of sandwich structures over traditional monolithic composites is their exceptionally high specific stiffnesses. Core density typically ranges from approximately 100 kg/m^{-3}. By altering the nature and thickness of the skin and/or core, the structure can be tailored to suit the specific requirements. Enhancing the stiffness, which is indicative of the material's bending behavior, is achieved by increasing either the core thickness, leading to an increase in its moment of inertia, or the elastic modulus of the skin. Because the core possesses a low density, the mass of the composite does not significantly increase.

Composite sandwich materials offer significant advantages over conventional materials. They provide various functional benefits such as lightweight, mechanical and chemical resistance, reduced maintenance, and design flexibility. They can prolong the equipment lifespan owing to their mechanical and chemical properties, contributing to enhanced safety through better impact and fire resistance. In addition, they offer superior thermal or acoustic insulation, and in some cases, good electrical insulation. These materials expand design possibilities by enabling lightweight structures and complex forms capable of fulfilling multiple functions. Across diverse application markets (automotive, construction, electrical, industrial equipment, etc.), these remarkable performances have driven innovative technological solutions.

II.2 Functionally graded materials

FGM represent one of the latest developments in revolutionizing material design in the 21st century. They have extensive application in various fields. Enhancing the structural part performance often leads to seeking different, often conflicting, but locally optimized properties within the same material. The development of composite materials has enabled the combination of the specific properties of different materials within a single piece. Locally optimizing these properties, for instance, combining a high-hardness material on the surface with a tough material, poses challenges, such as addressing interface issues. For example, adhering a ceramic layer to a metallic structure forms a thermal barrier coating for high-temperature applications. Sudden transitions in the material properties across discrete material interfaces can lead to interlaminar stress or high stress concentrations, resulting in plastic deformation or cracking.

FGM have been employed to mitigate these adverse effects. In recent years, FGM have been developed owing to their excellent mechanical properties, high performance, and heat resistance. Initially designed as barrier materials in reactors and high-temperature applications, FGM have expanded into the military, automotive, biomedical, and semiconductor industries, and various high-temperature environments.

II.2.1 FGM concept

A material with gradient properties is a type of composite material composed of two or more materials with varying volume fractions and a microstructure designed to have a spatial continuity of variables. An FGM was created by continuously changing the volume fractions throughout its thickness to achieve a specific profile.

FGM are typically made from a blend of metals and ceramics (Figure II-9) using a powder metallurgy process. The metal-rich side is usually placed in regions where mechanical properties such as hardness need to be high. Conversely, the ceramic-rich side, which has lower conductivity and higher temperature resistance, is positioned in regions with significant temperature gradients.

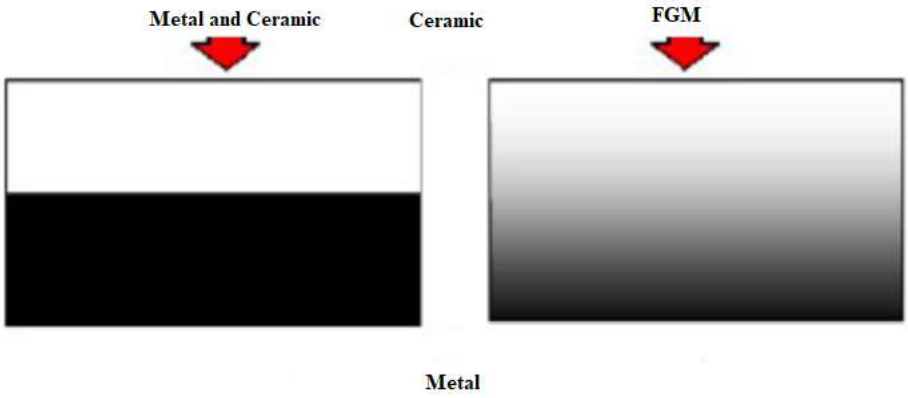

Figure II-9: type of ceramic and metal FGM material

The concept of FGM was developed by a group of scientists in Japan at the in 1984. The idea was to create materials that could be used as thermal barriers in space structures and fusion reactors [49], [50], [51]. An example of such a material is shown in Figure II-10 [52], in which spherical or nearly spherical particles are embedded in an isotropic matrix.

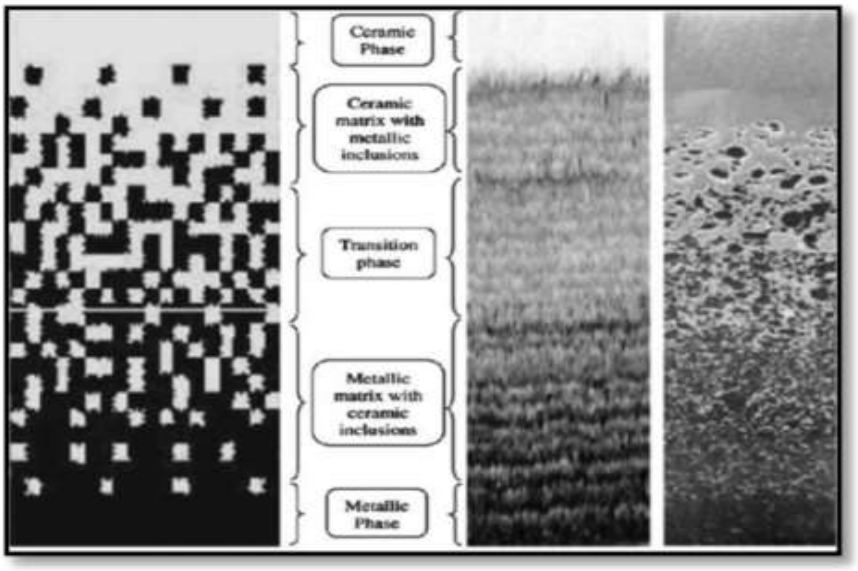

Figure II-10: FGM with the volume fractions of the constituent phases graduated in a single direction [52]

By gradually varying the volume fraction of the constituent materials, their material properties showed minimal and continuous changes from one point to another, addressing interface issues and alleviating thermal stress concentrations. This is because the ceramic components of FGM can withstand high temperatures, resulting in better thermal resistance, whereas the metallic constituents provide stronger mechanical strength and reduce the likelihood of catastrophic failure. Therefore, a typical FGM is a nonhomogeneous compound composed of different material phases (usually ceramic-metal), enabling a continuous transition of desired properties through a composition gradient.

Most FGM consist of ceramics and metals with specific mechanical properties:

- High-temperature side for ceramics
  - Good thermal resistance
  - Resistance to oxidation
  - Low thermal conductivity
- Low-temperature side for metals
  - Good mechanical strength
  - High thermal conductivity
  - Very good toughness
- Intermediate layers for material continuity
  - Addressing interface issues
  - Alleviating thermal stress

The continuous change in composition, and thus in the microstructure of an FGM material, is illustrated in Figure II-11, resulting in a gradient that determines the properties of the FGM.

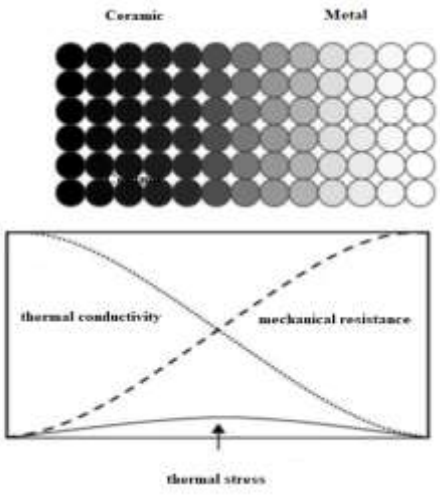

Figure II-11: Concept of materials with graded properties [54]

II.2.2 FGM development methods

Our literature review revealed the various fabrication methods employed to create FGM. These techniques are briefly described below:

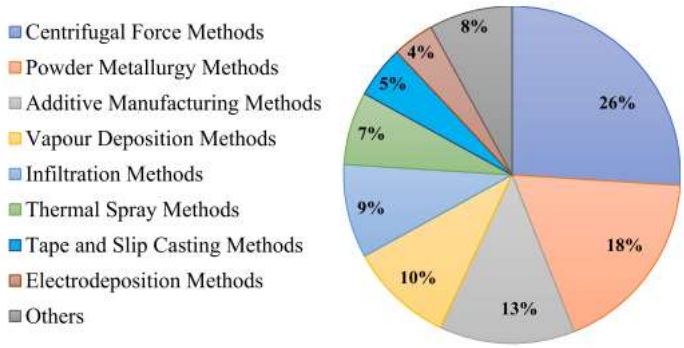

Figure II-12: Contribution of manufacturing methods in the production of FGM (Based on the Web of Science search system in the duration of 1990–12/2019)

II.2.2.1 Deposition based methods

a. Chemical Vapor Deposition (C.V.D) and Physical Vapor Deposition (P.V.D)

Chemical and physical vapor deposition techniques involve the deposition of atoms from the source material onto the substrate surface. C.V.D. and P.V.D. techniques can be employed to prepare FGM on complex-shaped substrates [53].

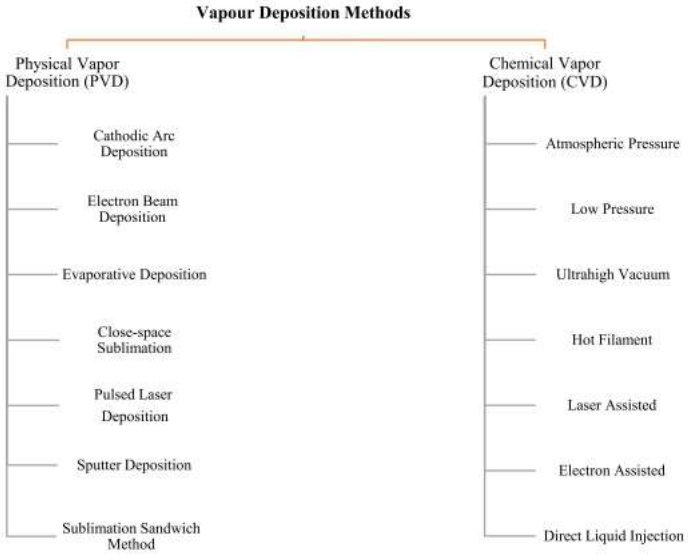

Figure II-13: Classifications of Vapor Deposition Methods used to produce FGM [54]

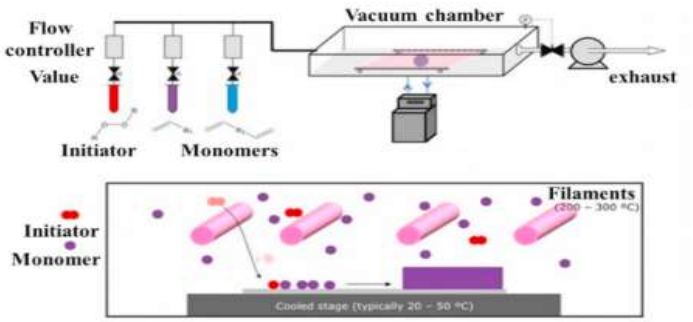

Figure II-14: Chemical Vapor Deposition (CVD) process [55]

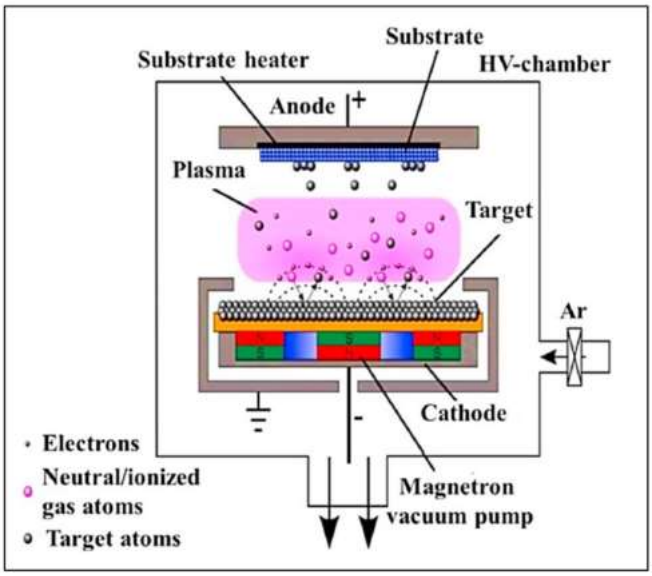

Figure II-15: Physical Vapor Deposition (PVD) process [54]

b. Electrodeposition methods (EPD)

Electrophoretic deposition is a process in which a stable colloidal suspension is placed in a cell that contains two electrodes. It involves the movement of charged particles within the solution towards either the cathode or anode based on the charge of the particles, owing to an applied electric field [56].

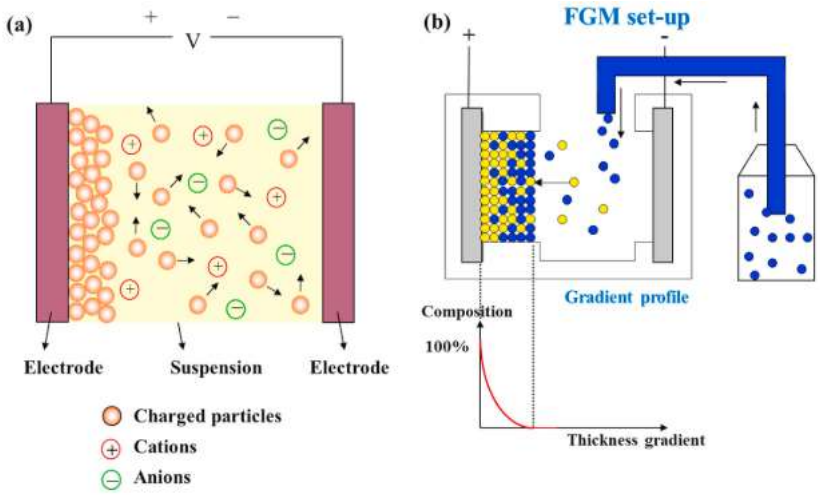

Figure II-16: (a) Schematic diagram of EPD process, and (b) Concept of EPD process for produced FGM [57]

c. Thermal spray method

The thermal spray technique is fundamental for producing FGM and generating thin surface coatings via spraying. These coatings provide vital protection against corrosion, wear, and thermal and electrical factors, which are crucial for components enduring diverse service conditions. Various processes under thermal spray coating were employed to fabricate FGMs with graded properties, as illustrated in Figure II-17 [58].

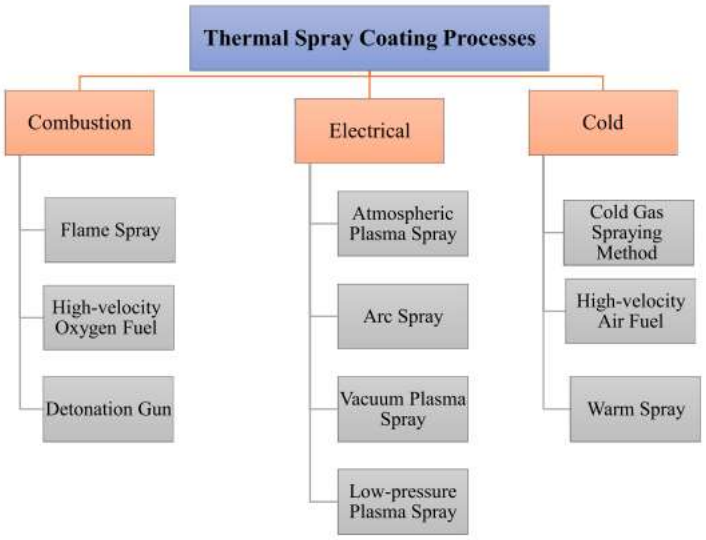

Figure II-17: Types of thermal spray coating processes [58]

II.2.2.2 Solid state methods

a. Powder metallurgy (PM)

In this technique, the powders were successively poured into a steel mold. Slight compression was applied upon pouring each powder. Subsequently, all layers are compacted. Typically, this process is followed by isostatic pressure and lubrication. Densification is the final stage [59].

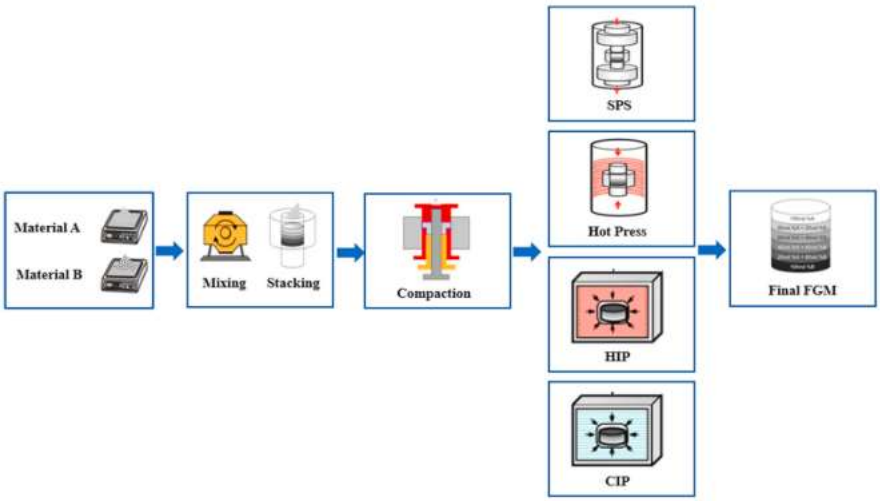

Figure II-18: Fabrication process of the FGM by powder Metallurgy [59]

b. Additive manufacturing methods

Recently, additive manufacturing (AM) methods have emerged as influential tools for advancing FGM development, shifting from conventional metal production models to sophisticated layer-by-layer fabrication, as depicted in Figure II-19 [60]. This transition replaced the traditional approach of using intricate machinery with a simpler mold-based process.

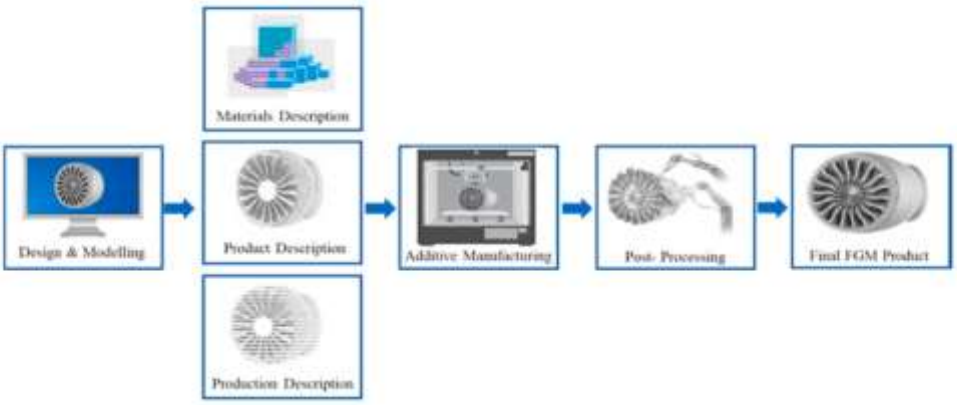

Figure II-19: Concept of functionally graded additive manufacturing method [60]

c. Hybrid methods with additive manufacturing

Owing to the high costs and time associated with additive manufacturing (AM) for producing FGMs, researchers have sought alternative methods while retaining the key properties achieved by AM [61], such as the Wire and Arc Additive Manufacturing (WAAM) method and the Friction Stir Additive Manufacturing (FSAM) method. FSAM, a new technique for FGM production, leverages the benefits of Friction Stir Welding (FSW) and offers improved manageability and advantages over traditional approaches [62].

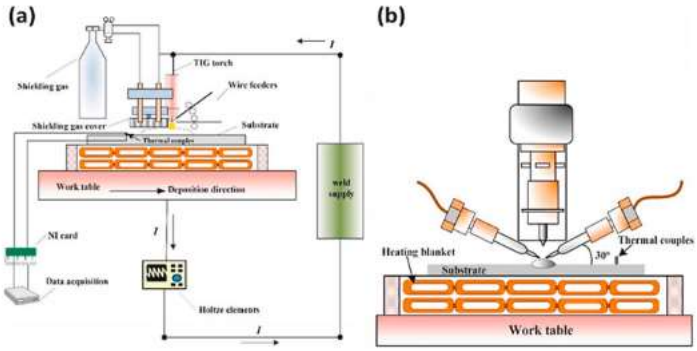

Figure II-20: (a) Concept of WAAM process for produced FGM, (b) double-wire feeding units [54]

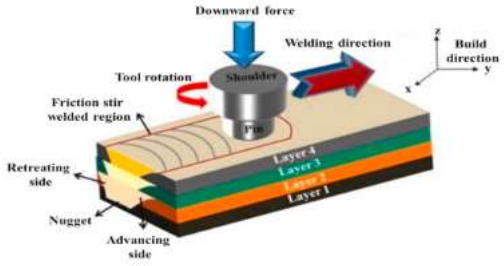

Figure II-21: Concept of FSAM process for manufactured FGM [54]

II.2.2.3 Liquid state methods

a. Centrifugal force methods

Numerous methods, including centrifugal force techniques, slip casting, tape casting, and infiltration, fall under the liquid-state principle for producing FGM with gradient properties. While these methods offer cost advantages and can generate materials with continuous properties [63], challenges include difficulties in controlling the gradation and wettability between materials, as well as issues related to molten metal [1].

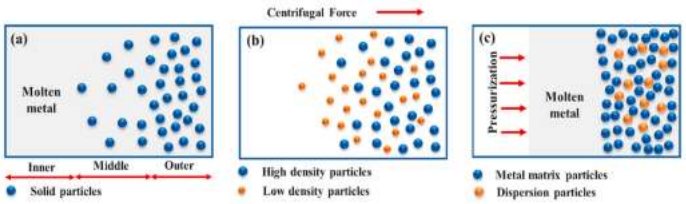

Figure II-22: Centrifugal force methods for producing FGM (a) centrifugal casting method, (b) centrifugal slurry method, and (c) centrifugal pressurization method [54]

b. Slip casting method

Slip casting involves pouring a suspension into a porous mold that drains liquid owing to capillary forces, leaving a compacted powder layer on the surface of the mold. A green body was obtained upon drying. Slip casting comprises two essential stages:

- Formation of the layer or 'setting.'
- Consolidation of the layer or 'solidification'.

Filtration, which occurs during casting, is a process in which a portion of the water in the slip is eliminated. This water migrates through the already formed layer as follows:

- Suction capability of plaster [64] (conventional casting).
- Pressure is applied to slip (pressure casting).

In the case of manufacturing multilayers, after the formation of the first layer, deposition of the second layer occurs such that the slip does not penetrate the formed layer. This process was repeated sequentially for subsequent layers.

c. Tape casting method

Tape casting involves pouring a slurry of fine powders in an aqueous or nonaqueous suspension onto a flat support in thin and uniform layers. The resulting products were sheets with controlled thicknesses (25-1000 µm). After the paste solidified, the sheets were demolded and cut. The solvent used must have a very low boiling point and viscosity. It should be soluble with the binder, plasticizer, and other additives but should not be soluble or reactive with the ceramic powder. The binder provides high mechanical strength to the green product, allowing handling. Typically, a plasticizer is added to a binder to reduce its viscosity. The binder, plasticizer, and deflocculant were completely removed during the drying process. The tape-casting process is widely used to produce laminated composite materials using two methods: either by directly creating multilayered tapes through a system of multiple blades, as in the case

of tri-layers developed by [65], or by stacking separately prepared layers, which are then bonded through a thermocompression step [66].

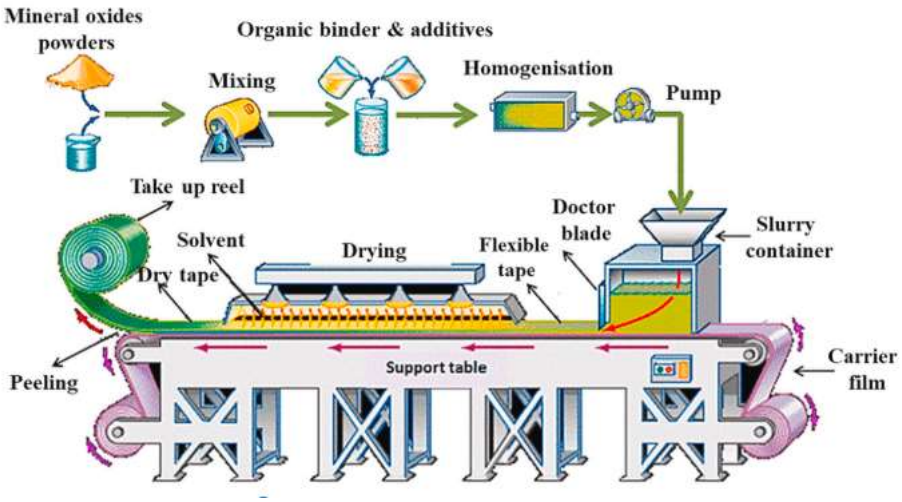

Figure II-23: Schematic illustration of tape casting process [67]

d. Infiltration method

Infiltration is a liquid-state process for producing FGM, wherein a molten matrix fills the space between the dispersed stages containing preformed ceramic particles [68]. This method can be conducted with or without pressure, utilizing capillary action or gaseous/mechanical pressure, as shown in Figure II-24. This process involves chemical interactions at the interface, resulting in the formation of the FGM structure, offering advantages such as rapid preparation.

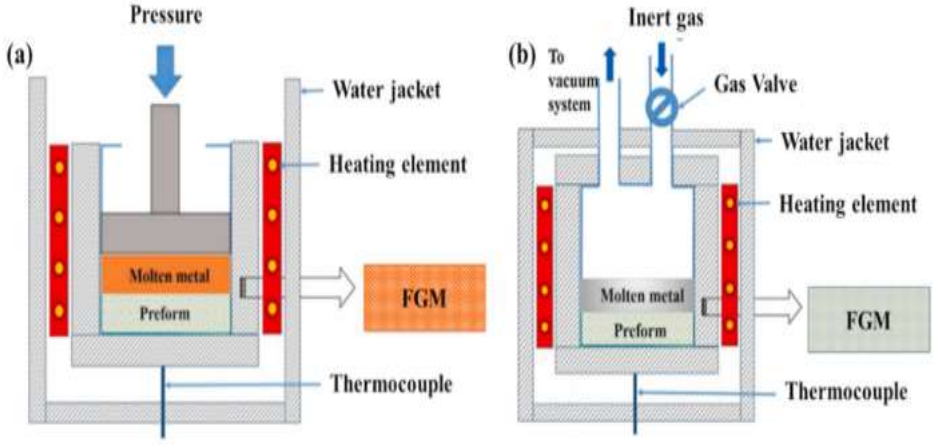

Figure II-24: Schematic illustration of infiltration process (a) squeeze casting method, (b) pressure method [54]

e. Langmuir-Blodgett method

In recent years, the Langmuir-Blodgett (LB) film method has garnered increasing interest among researchers and engineering communities for producing graded structures. This process facilitates the deposition of uniform film materials with high precision down to a single-molecular-layer thickness [54]. LB films, utilized as active layers or passive insulators in electronic applications, offer the advantages of precisely controlled internal layer structures at the molecular level and precise regulation of film thickness.

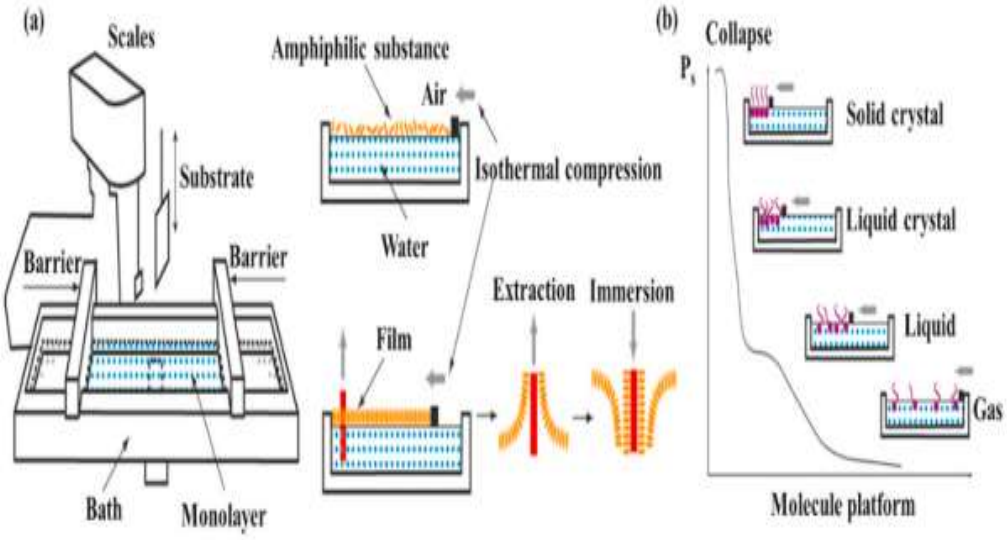

Figure II-25: Schematic illustration of the Langmuir-Blodgett method [54]

II.2.3 Physical and mechanical properties of FGM

The FGM material chosen for this work is (Aluminium-Ceramic). The Physical and mechanical properties of Aluminium and Ceramic are presented in Table II-1.

II.2.4 Applications of FGM

In the present era, with the adaptable production of composite materials to meet specific application needs and functional requirements, the use of FGM spans across an extensive range. Figure II-26 outlines diverse application domains for FGM, which holds significant potential for applications facing severe operational conditions or requiring precise sensitivity [55]. These applications span aerospace, automotive, biomedical, defense, energy, marine, and civil engineering, as detailed in the subsequent subsections.

Table II-1: Physical and mechanical properties of Aluminium and Ceramic

properties	Aluminium	Ceramic
Physical	• Aluminum's melting temperature: Around 660°C, facilitating foundry operations. • Highly ductile, allowing easy shaping. • Density: 2700 kg/m³.	• Fusion advantage in foundry operations. • Density: 3800 kg/m^3. • Utilization across various sectors: housing, design, ceramic and metallurgical industries, aerospace, medical, and coatings.
mechanical	• Tensile strength. • Penetration resistance (hardness). • Malleability (forming into sheets). • Ductility (forming into wires).	• High Young's Modulus (covalent and ionic bonding). • High hardness (abrasives, cutting tools, friction surfaces requiring wear resistance, high mechanical strength, heat resistance, high rigidity). • Excellent compressive strength, not suitable for tension (Compression strength = 200 MPa).

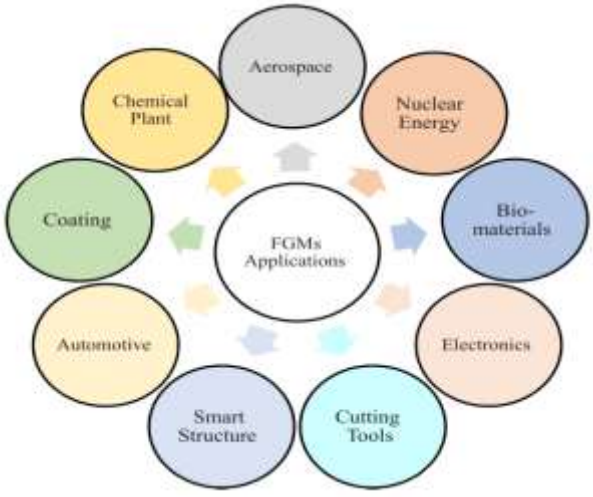

Figure II-26: Areas of practical applications for FGM [54]

II.2.4.1 Aerospace applications

Initially utilized in spacecraft to mitigate thermal stresses between external and internal surfaces, FGM have found applications in diverse aerospace applications. Presently, a multitude of aircraft and spacecraft components leverage FGM, including rocket nozzles, heat exchange panels, solar panels, turbine wheels, spaceplane noses, protective layers for combustion chambers, structural elements, rocket engine parts, reflectors, camera housings, caps, and the leading edges of missiles and space shuttles, as shown in Figure II-27 [54]. Moreover, FGM serve as thermal barriers, lining the walls of planes (such as spaceplane frames) and offering resistance against heat generated from air friction on the aircraft's exterior.

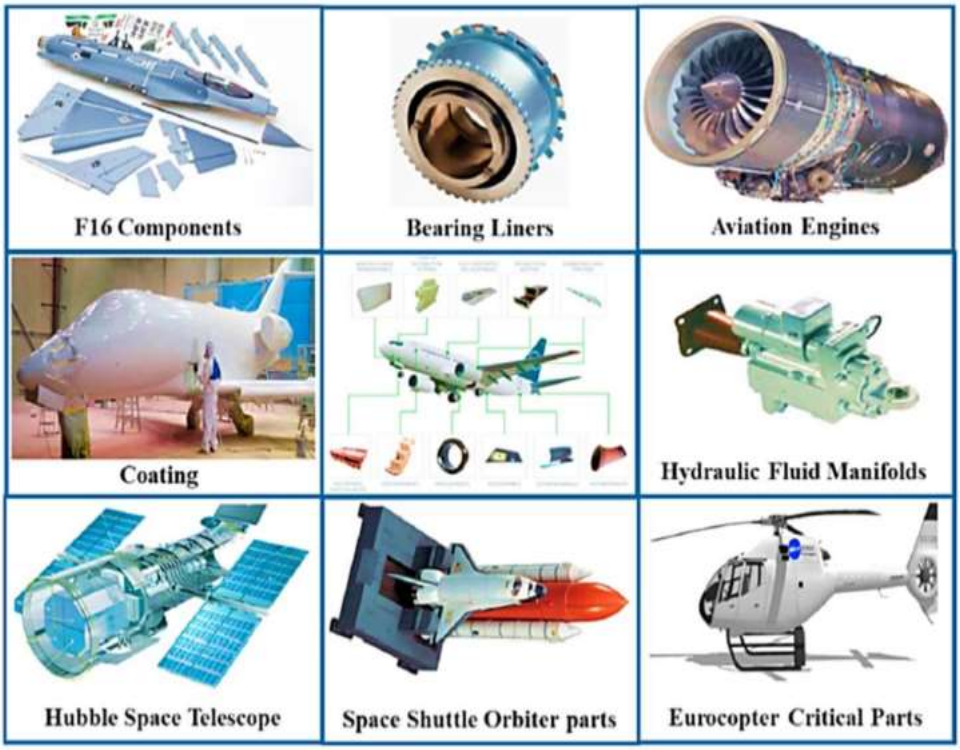

Figure II-27: FGM parts in Aerospace applications [54]

II.2.4.2 Automotive applications

Because of their high cost [69], FGM have limited applications in the automotive sector, primarily in critical components such as diesel engine pistons, cylinder liners, combustion chambers, racing car brakes, driveshafts, and flywheels, as depicted in Figure II-29. Additionally, FGM can be used in coatings for automotive bodies [54].

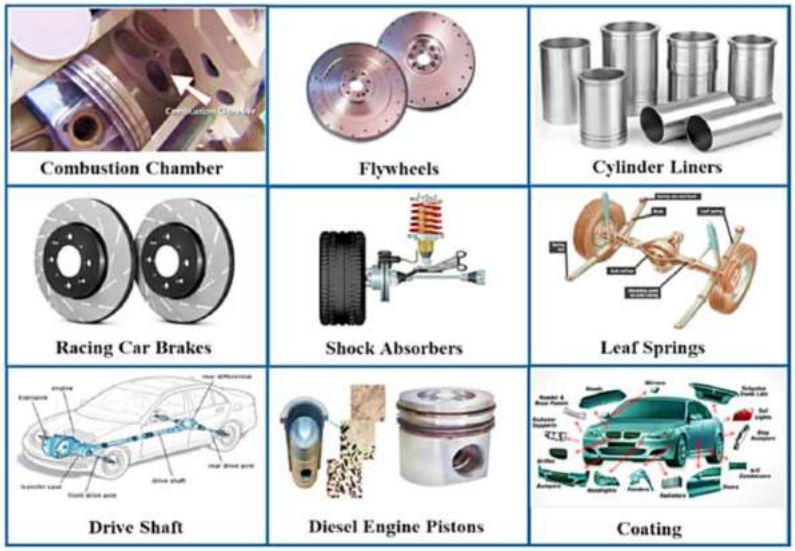

Figure II-28: FGM parts in automotive applications [54]

II.2.4.3 Biomedical applications

Human tissues such as bones and teeth exhibit natural FGM properties. In instances where damage occurs and necessitates replacement, a compatible material that fulfills the original function of the tissue is needed. Functionally graded materials are ideal for this purpose. FGM have diverse applications in the dental [70] and orthopedic fields, specifically in tooth and bone replacement [71]. Figure II-29 illustrates a schematic view of an FGM dental implant featuring a graded material composition [72].

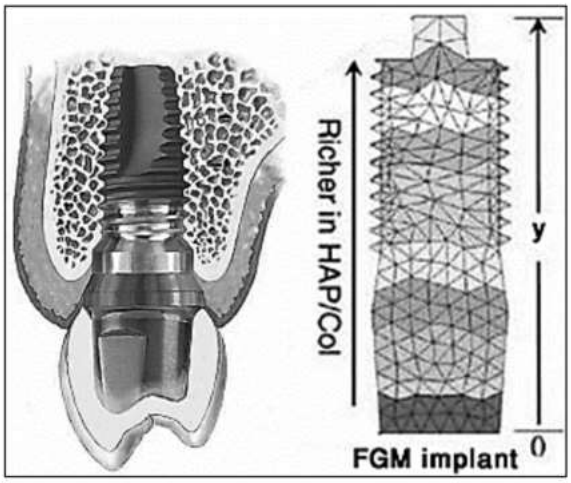

Figure II-29: Schematic view of the FGM dental implant with graded material composition [72]

II.2.4.4 Defense applications

The capability of FGM to impede crack propagation is crucial, especially in defense applications. They serve as effective penetration-resistant materials used in armor plates and bulletproof vests [73]. Additionally, FGM have significant applications in the construction of bulletproof vehicle bodies.

II.2.4.5 Energy applications

FGM play a crucial role in the energy sector by providing efficient thermal barriers and protective coatings for blades in gas turbine engines. They are also instrumental in applications such as thermoelectric generators, energy-conversion devices, solar cells, and sensors [74].

II.2.4.6 Electrical/electronic applications

FGM are used in the electrical and electronics industries in many ways, including field stress relaxation in the electrode and field-spacer interface, diodes, semiconductors, insulators, and sensors. Thermal-shielding elements in microelectronics are also made from functionally graded carbon nanotube materials [69].

II.2.4.7 Marine applications

FGM play a role in the marine and submarine industries and are applied in propeller shafts, diving cylinders, sonar domes, composite piping systems, and cylindrical pressure hulls [69].

II.2.4.8 Civil engineering applications

The functional grading of concrete elements aligns their internal compositions with their distinct structural and thermal performance requirements. This alignment involves continuously altering material traits, such as porosity, strength, or rigidity, across up to three dimensions, aiming to minimize mass and achieve multifunctional properties. A lower porosity enhances structural traits, whereas a higher porosity improves heat insulation. Figure II-30 depicts curves illustrating the characteristics of hardened concrete with varying porosities [75].

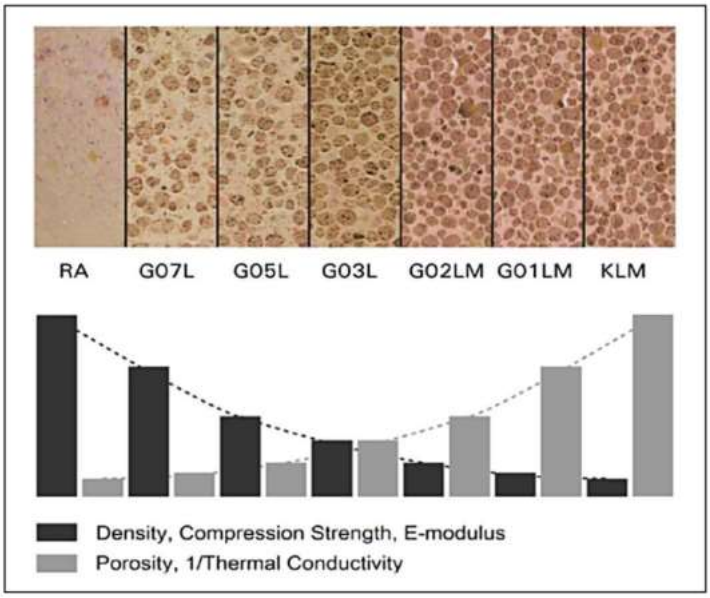

Figure II-30: Curves of hardened concrete characteristics depending of the porosity [75]

II.2.4.9 Other miscellaneous applications

FGM find applications in cutting tool insert coatings, heat exchangers, tribology, fire retardant doors, and defense pads to prevent crack propagation. The scope of their application is poised to grow further if future advancements lead to reduced production costs for these materials.

II.2.5 Material properties of the FGM structures

Materials with property gradients can be created by continuously altering the constituents of materials with non-uniform microstructures, resulting in spatially graduated macro properties. An FGM can be defined by the variation in the volume fractions. Most researchers utilize power, exponential, or sigmoid functions to describe volume fractions [76].

Researchers commonly employ the power, exponential, and sigmoid laws to describe the volume fractions when designing the variation of the desired property in an FGM across any direction.

II.2.5.1 Power-law (P-FGM)

The power law for material gradation, has been extensively employed by researchers and is prevalent in the stress analysis of FGM [77]. For the analysis of an FGM plate with uniform

thickness 'h,' as depicted in Figure II-31, the effective material property P(z) in a specific direction (along z) can be determined according to this law.

$$P(z) = P_2 + (P_1 + P_2)\, V(z) \tag{II.1}$$

where n represents each effective material property. P_1 and P_2 correspond to the material properties at the topmost (z = + h/2) and bottommost (z = − h/2) surfaces of the plate, respectively. The material properties depend on the volume fraction V of the FGM, following the power law as follows:

$$V(z) = \left(\frac{1}{2} + \frac{z}{h}\right)^n \tag{II.2}$$

where ($0 \leq n \leq \infty$) is the volume fraction exponent (or power-law index).

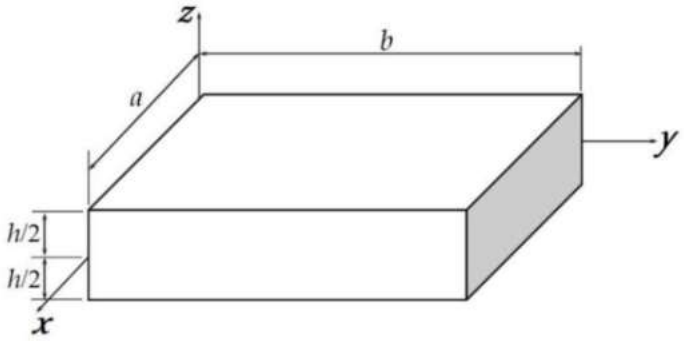

Figure II-31: Coordinate system for a gradient property FGM sandwich plate

II.2.5.2 Sigmoid law(S-FGM)

When a single FGM power law function is added to the multilayered composite, stress concentrations appear at one of the interfaces in which the material is continuous but changes rapidly. Therefore, Chung and Chi [78] developed another law called the sigmoid law, which is a combination of two power-law functions, to ensure the smooth distribution of stresses among all interfaces. This law is also used to reduce the stress intensity factors in cracked structures [79]. The two power law functions are defined as follows:

$$V_1(z) = \frac{1}{2}\left(\frac{h/2 - z}{h/2}\right)^n \quad \text{For } 0 \leq z \leq h/2 \tag{II.3}$$

$$V_2(z) = \frac{1}{2}\left(\frac{h/2 + z}{h/2}\right)^n \quad \text{For } -h/2 \leq z \leq 0 \tag{II.4}$$

By using the rule of mixture, the effective properties of the S-FGM can be calculated by

$$P(z) = P_2 + (P_1 - P_2)\left(1 - \frac{1}{2}\left(\frac{h/2-z}{h/2}\right)^n\right) \quad \text{For } 0 \le z \le h/2 \tag{II.5}$$

$$P(z) = P_2 + (P_1 - P_2)\left(\frac{1}{2}\left(\frac{h/2+z}{h/2}\right)^n\right) \quad \text{For } -h/2 \le z \le 0 \tag{II.6}$$

II.2.5.3 Exponential law (E-FGM)

The exponential law is commonly applied to address issues related to the fracture mechanisms of FGM. This law, introduced by Kim and Paulino [80] and further elaborated by Zhang et al. [81], defines the distribution of properties across the thickness of the FGM plates as follows:

$$P(z) = P_2 e^{\frac{1}{h}\left(ln\frac{P_1}{P_2}\right)\left(z+\frac{h}{2}\right)} \tag{II.7}$$

The effective mass density (ρ) was determined using the rule of mixtures, irrespective of the micromechanical model employed [82]. The impact of Poisson's ratio on deformation is considered significantly lower than that of Young's modulus, as reported by Delale and Erdogan [83]. Consequently, Poisson's ratio of the plates was assumed to remain constant.

II.3 Summary

In this chapter, we provide an overview of the key concepts and methodologies relevant to modeling sandwich structures and FGM. Initially, we delved into the mechanical properties of sandwich structures, encompassing different assembly types, modes of damage, adhesive requirements, and material advantages and drawbacks, while surveying various modeling techniques. Subsequently, the chapter offers an examination of FGM, including diverse manufacturing approaches, with a particular emphasis on the solid freeform fabrication method owing to its inherent advantages and manufacturing adaptability. Furthermore, it elucidates multiple application domains and explores avenues for enhancing and broadening these domains by means of cost-reduction strategies tied to optimizing the most promising manufacturing technique. Given the broad applicability of sandwich structures and FGM, a thorough investigation of their behavior is imperative. Accordingly, the succeeding chapter elaborates on the array of theories utilized for analyzing FGM sandwich structures.

Chapter III

Modeling of FGM sandwich plates

Chapter III

Modeling of FGM sandwich plates

The utilization of FGM in engineering applications, such as plates, beams, and shells, has surged owing to their tailored material properties, which are often achieved by blending two distinct materials such as ceramics and metals. FGM effectively mitigate thermal stresses, withstand high temperatures, and resist corrosion. In the realm of FGM sandwich plates, two common configurations exist: sandwich plates with FGM cores and isotropic skins and those with isotropic cores and FGM skins. To harness their benefits, a comprehensive understanding of their vibration, bending, dynamic, and buckling behaviors is imperative. Typically, the behavior of FGM plates is elucidated using either three-dimensional (3D) or two-dimensional (2D) theories. Although the former boasts superior accuracy, its implementation is challenging, leading to the popularity of the latter owing to its simplicity and computational efficiency.
The prevalent 2D plate theories are as follows:

- The Classical Plate Theory (CPT) is ideal for thin plates but disregards transverse shear effects.
- First-order shear deformation theory (FSDT) caters to moderately thick plates by incorporating transverse shear effects.
- Higher-Order Shear Deformation Theories (HSDTs), tailored for thicker plates.

These models rely on assumptions regarding the strains or stresses through the thickness of the plate, thereby facilitating the reduction of 3D complexities to 2D formulations. Given their extensive application in modeling FGM plates, this chapter briefly outlines these theories and examines the particularities of the p-version of the finite element method in order to use them to model freely vibrating plates using a quadrilateral p-element.

III.1 Different plate theories for FGM sandwich modeling

A plate is characterized as a solid object enclosed by two parallel flat surfaces, known as faces, with substantial lateral dimensions (width and length for rectangular plates or diameter for circular plates) compared to the thickness of the plate.

Plates are categorized into thin and thick groups, where a plate is considered thin when the ratio of thickness to side length is less than 1/20 [84].

III.1.1 Classical plate theory (CPT)

The Classical Plate Theory (CPT) is based on the Love-Kirchhoff assumptions, asserting that a normal to the plate's mid-plane remains perpendicular after deformation, effectively neglecting the transverse shear deformation effects. This theory, deemed the simplest among Elasticity-based Structural Load (ESL) theories, is suitable only for thin plates, where the deflection caused by transverse shear deformations is negligible compared with that induced by the curvature of the plate. For a homogeneous isotropic plate, the shear contribution to deflection is directly linked to the slenderness ratio (L/h) [85], [86]. In the vast majority of thin-plate scenarios, Classical Plate Theory (CPT) provides accurate results that closely align with those derived from the 3D theory of elasticity. Given the aforementioned assumptions, the displacement field of CPT can be represented as follows [83], [87].

$$u\,(x,y,z) = u_0(x,y) - z\frac{\partial w_0}{\partial x} \tag{III.1a}$$

$$v\,(x,y,z) = v_0(x,y) - z\frac{\partial w_0}{\partial y} \tag{III.1b}$$

$$w\,(x,y,z) = w_0(x,y) \tag{III.1c}$$

Where (u_0, v_0, w_0) represents the displacement field components on the mid-plane of the plate ($z = 0$).

In Classical Plate Theory, the following assumptions are considered, as established by [88]:

- No deformation occurred in the midplane of the plate.
- The normal stress σ_z is negligible compared to other components.
- Normal to the mid-plane before deformation remained normal to the mid-plane after deformation.
- The effect of the rotational inertia is negligible.

Let's consider an FGM plate with length "a" and width "b," having a thickness "h." Here, u (x, y, z), v (x, y, z), and w (x, y, z) represent the displacements of the plate, while u_0, v_0, and w_0 are the components of the displacement field on the mid-plane of the plate (see Figure III-1).

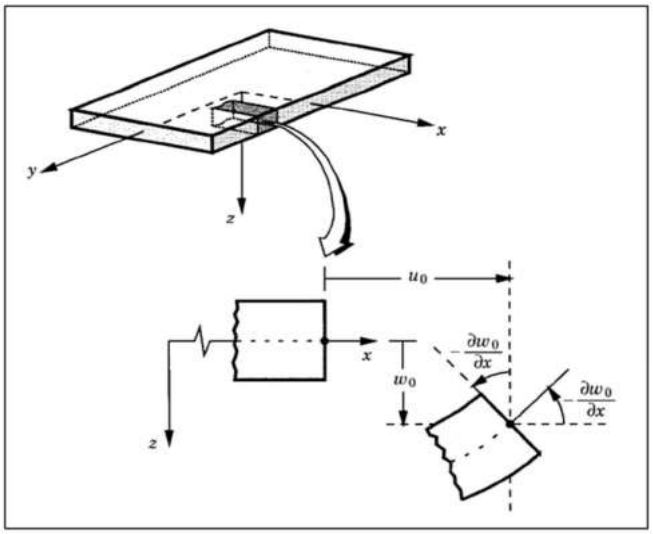

Figure III-1: Undeformed and deformed geometry of a plate under Kirchhoff's hypotheses [86]

Given the neglect of transverse shear effects in the Classical Plate Theory, the obtained results are inaccurate for thick plates, particularly those composed of advanced composites. To address this limitation, the First-Order Shear Deformation Theory has been developed.

III.1.2 First-order shear deformation theory (FSDT)

The First-order shear deformation theory, also known as the Mindlin-Reissner theory [89], [90], or the Mindlin plate theory, expanded upon the classical plate theory by incorporating the effects of transverse shear strains. In accordance with this theory, transverse straight lines maintain their straightness after deformation but may not necessarily be normal to mid-plane post-deformation (see Figure III-2 [83]). Consequently, the transverse shear strain remained uniform throughout the thickness. In addition, this theory assumes a zero value for transverse normal stress σ_z.

The displacement field of FSDT is expressed as follows [83], [87]:

$$u\,(x,y,z) = u_0(x,y) + z\emptyset_x\,(x,y) \quad \text{(III.2a)}$$

$$v\,(x,y,z) = v_0(x,y) + z\emptyset_y(x,y) \quad \text{(III.2b)}$$

$$w\,(x,y,z) = w_0(x,y) \quad \text{(III.2c)}$$

In this formulation, u_0 , v_0, and w_0 represent the displacements of a point on the plane $z = 0$,while $\emptyset_x$ and $\emptyset_y$ denote the rotations about the y and x axes, respectively.

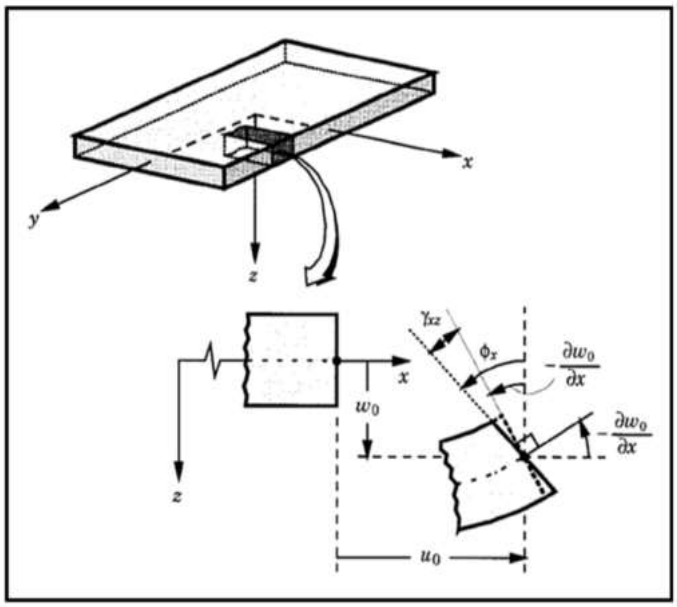

Figure III-2: Undeformed and deformed geometries of a plate under the assumptions of the FSDT [86]

Owing to the constancy of the transverse shear strains throughout the plate thickness, the transverse shear stress also remains constant. However, in practice, the shear stress typically varies parabolically with the plate thickness. Therefore, the FSDT requires a shear correction factor to account for this parabolic variation and ensure adherence to the shear stress-free boundary conditions on the plate surfaces, where the shear stress must be zero at the top and bottom surfaces of the plate.

III.1.3 Higher-order shear deformation theories (HSDTs)

To address the drawbacks of CPT and FSDT, such as achieving a realistic variation of transverse shear strains and stresses across the plate thickness and avoiding the necessity of Shear Correction Factors (SCFs), numerous higher-order shear deformation theories have been devised [91], [92], [93], [94], [95], [96], [97]. These models operate on the premise of nonlinear stress distribution throughout the thickness and can depict section warping in the deformed state, as depicted in Figure III-3 [86].

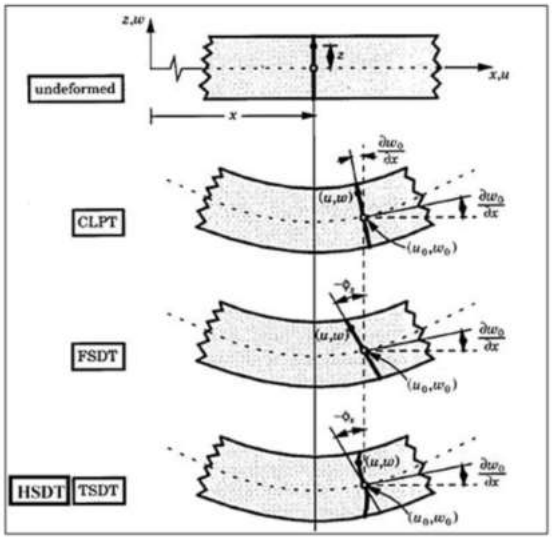

Figure III-3: Undeformed and deformed geometry of a plate according to the CPT, FSDT and HSDT [86]

The most advanced HSDT rely on Taylor series expansions of displacement fields to approximate the 3D theory [98]. The displacement is thus assumed to follow the form:

$$u_i(x,y,z) = u_i(x,y) + z\emptyset_i^{(1)}(x,y) + z^2\emptyset_i^{(2)}(x,y) + \ldots\ldots + z^j\emptyset_i^{(j)}(x,y) \quad \text{(III.3)}$$

Where i = 1,2,3, and j defines the order used in the theory.

The Reissner-Mindlin first-order theory corresponds to the Taylor series expansion up to the order j=1 and $\emptyset_3^{(1)} = 0$. When a first-order model fails to adequately address a specific problem, it becomes necessary to transition to a higher-order model (2nd order, 3rd order, or beyond) in the series expansion of displacements.

III.1.3.1 Second-order shear deformation theories (SCSDT)

Second-order shear deformation theories (SCSDT) [99] generally produce slightly improved results compared to FSDT but encounter similar limitations, necessitating correction factors. In these theories, the displacement field is typically described as follows:

$$u(x,y,z) = u_0(x,y) + z\emptyset_x(x,y) + z^2\Psi_x(x,y) \quad \text{(III.4a)}$$

$$v(x,y,z) = v_0(x,y) + z\emptyset_y(x,y) + z^2\Psi_y(x,y) \quad \text{(III.4b)}$$

$$w(x,y,z) = w_0(x,y) + z\emptyset_z(x,y) + z^2\Psi_z(x,y) \quad \text{(III.4c)}$$

where the parameters Ψ_x, $\Psi_y$and Ψ_z are the second order functions.

III.1.3.2 Third order shear deformation theory (TSDT)

Numerous Third-order Shear Deformation Theories (TSDT), also known as Parabolic Shear Deformation Theory, have been proposed by various researchers [94], [95], [96]. The displacement field according to Reddy's TSDT is as follows:

$$u(x,y,z) = u_0(x,y) + z\emptyset_x(x,y) + z^2\Psi_x(x,y) + z^3\zeta_x(x,y) \quad \text{(III.5a)}$$

$$v(x,y,z) = v_0(x,y) + z\emptyset_y(x,y) + z^2\Psi_y(x,y) + z^3\zeta_y(x,y) \quad \text{(III.5b)}$$

$$w(x,y,z) = w_0(x,y) \quad \text{(III.5c)}$$

where the parameters Ψ_x, Ψ_y , ζ_x , ζ_y are the high order functions.

As the order of expansion increases, the number of additional parameters also increases, often making the interpretation challenging. To mitigate this complexity, simplifications were devised to reduce the displacement parameters. These simplifications involve truncating the latter terms of the Taylor series through the introduction of a "shear function." Subsequently, the proposed displacement field form is expressed as follows:

$$u(x,y,z) = u_0(x,y) - z\frac{\partial w_0}{\partial x} + f(z)\theta_x(x,y) \quad \text{(III.6a)}$$

$$v(x,y,z) = v_0(x,y) - z\frac{\partial w_0}{\partial y} + f(z)\theta_y(x,y) \quad \text{(III.6b)}$$

$$w(x,y,z) = w_0(x,y) \quad \text{(III.6c)}$$

In the provided expression, $f(z)$ represents the shear function, dictating the distribution of transverse shear strains and stresses throughout the plate's thickness, denoted by h. Furthermore, w_{xx} and w_{yy} are given by $\frac{\partial w}{\partial x}$ and $\frac{\partial w}{\partial y}$, respectively, where $\emptyset_x$ and $\emptyset_y$ represent rotations about the y and x axes, respectively.

In accordance with equation (III-6), the displacement field of the CPT is derived by setting $f(z) = 0$, while that of the FSDT is derived by setting $f(z) = z$. Furthermore, the displacement field of Reddy's TSDT [86], [96] is obtained by utilizing the following function:

$$f(z) = z - \frac{4z^3}{3h^2} \quad \text{(III.7)}$$

This theory facilitates a parabolic distribution of the transverse shear stress and ensures compliance with the shear stress-free surface conditions at the top and bottom surfaces of the plate. Consequently, it offers a favorable approximation of transverse shear stresses in comparison to solutions derived from three-dimensional elasticity.

III.1.3.3 Sinusoidal Shear Deformation Theory (SSDT)

Another variant of HSDT, known as Sinusoidal Shear Deformation Theory (SSDT), was introduced by Touratier [100]. This theory uses a sinusoidal trigonometric function and represents a significant example within the family of trigonometric HSDT. This was implemented in the following setting:

$$f(z) = \frac{h}{\pi} sin\ \left(\frac{\pi z}{h}\right) \tag{III.8}$$

III.1.3.4 Hyperbolic Shear Deformation Plate Theory (HSDPT)

An HSDPT was introduced by Soldatos [101] and derived using the following expression:

$$f(z) = h\ sin\ h\ \left(\frac{z}{h}\right) - z\ cos\ h\ (\frac{1}{2}) \tag{III.9}$$

III.1.3.5 Exponential Shear Deformation Plate Theory (ESDPT)

The ESDPT developed by Karama et al. [102] was formulated using the following expression:

$$f(z) = ze^{-2(z/h)^2} \tag{III.10}$$

III.1.3.6 Refined Plate Theory (RPT)

Although HSDT eliminates the need for SCF, their equations of motion are more intricate than those of the FSDT. Thus, Shimpi [103] devised a simplified plate theory called the RPT, which decomposes the transverse displacement into bending and shear components. Notably, Shimpi's theory involves fewer unknowns (four) and governing equations than the FSDT, and it does not require SCF, providing a parabolic shear distribution across the plate thickness. Moreover, the RPT shares many similarities with the CPT concerning the equations of motion, boundary conditions, and stress resultant expressions. The displacement field of the RPT is expressed as follows:

$$u(x,y,z) = u_0(x,y) - z\frac{\partial w_b(x,y)}{\partial x} + f(z)\frac{\partial w_s(x,y)}{\partial x} \tag{III.11a}$$

$$v(x,y,z) = v_0(x,y) - z\frac{\partial w_b(x,y)}{\partial y} + f(z)\frac{\partial w_s(x,y)}{\partial y} \tag{III.11b}$$

$$w(x,y,z) = w_b(x,y) + w_s(x,y) \tag{III.11c}$$

Where w_b and w_s are the bending and shear components of transverse displacement, respectively.

III.1.3.7 quasi-3D theory

It is important to acknowledge that the aforementioned plate theories neglect the thickness stretching effect (i.e., ε_z =0) by assuming a constant transverse displacement throughout the thickness. This effect becomes notable in moderately thick and thick plates and warrants further consideration. Quasi-3D theories, which are HSDT, incorporate a higher-order variation of both in-plane and transverse displacements through the thickness, thereby accounting for both shear deformation and thickness stretching effects [104]. The displacement field of quasi-3D theory is represented as follows:

$$u(x,y,z) = u_0(x,y) - z\frac{\partial w_0}{\partial x} + f(z)\varphi_x(x,y) \quad \text{(III.12a)}$$

$$v(x,y,z) = v_0(x,y) - z\frac{\partial w_0}{\partial y} + f(z)\varphi_y(x,y) \quad \text{(III.12b)}$$

$$w(x,y,z) = w_0(x,y) + g(z)\varphi_z(x,y) \quad \text{(III.12c)}$$

Where u_0, v_0, w_0, φ_x, φ_y and φ_z are six unknown displacements of the midplane of the plate**,** and g(*z*) and f (*z*) are shear functions with

$$g(z) = \frac{df(z)}{dz} \quad \text{(III.13)}$$

All the previously mentioned theories have been widely utilized by numerous researchers to precisely forecast the behavior of FGM sandwich plates.

III.2 Layered approach

These approaches are specifically aimed at describing the interfacial effects of conventional composite materials. Various models based on layered approaches have been proposed [96], [105], [106]. The multilayer approach is subdivided into substructures (corresponding to each layer or group of layers). An FSDT or HSDT model was applied to each substructure, imposing a displacement field that satisfied the continuity at the interfaces between different layers. Models of this type are relatively costly (the order of the behavior equations depends on the number of layers), but they allow for more accurate results, particularly concerning out-of-plane stress calculations. In general, models derived from the layered approach can be classified into two groups: discrete layer models, in which each layer is considered as a plate, imposing continuity conditions in displacements or stresses at the interfaces, and zigzag models, in which the kinematics inherently satisfy contact conditions and are independent of the number of layers (Figures. III-4 and III-5).

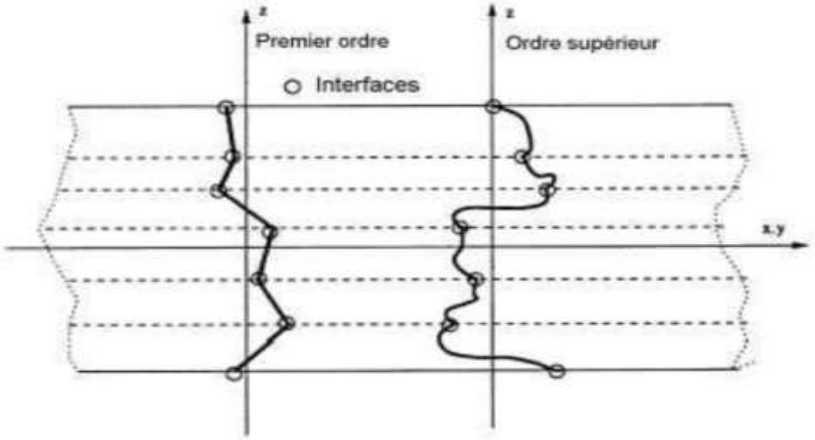

Figure III-4: Displacement fields of discrete layer models, kinematic approach [107]

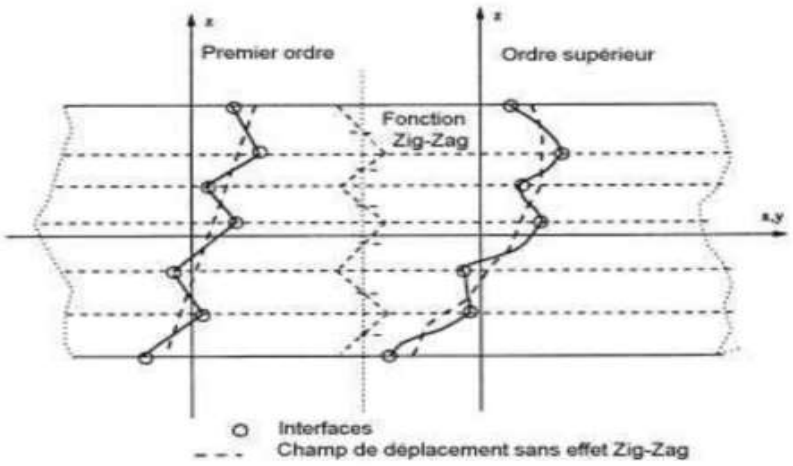

Figure III-5: Displacement fields of zig-zag models, kinematic approach [107]

III.2.1 Zigzag models

To reduce the number of unknown parameters, Di Sciuva was the first to propose a first-order zigzag model [108]. In this model, membrane displacements result from the superposition of the overall displacement field of the FSDT and a zigzag function (using the Heaviside function). The zigzag function contributes to membrane displacements that are continuous in z; however, its first derivative is discontinuous at the interface (see Figure III-6).

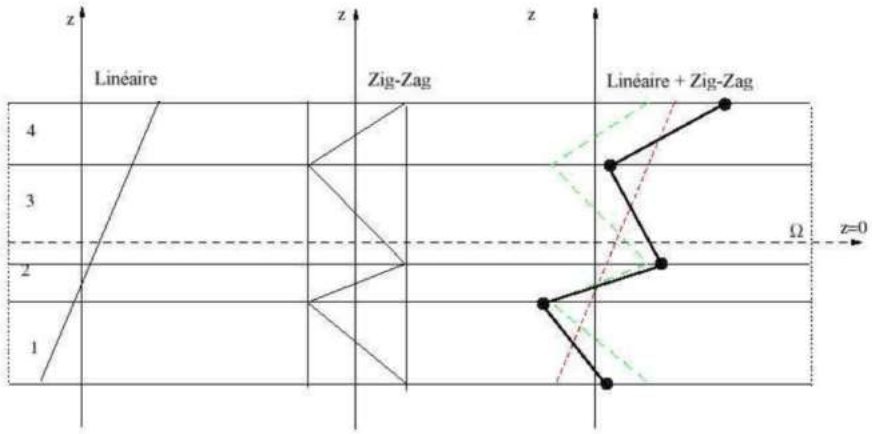

Figure III-6: Displacement fields of first order zig-zag models [107]

Thus, the transverse deformations were discontinuous, ensuring continuity of the transverse shear stresses at the interfaces. Building on this concept [109], several authors have made significant improvements to the zigzag model. The primary enhancement was the introduction of a nonlinear displacement distribution. The zigzag field (piecewise linear) was superimposed on a higher-order displacement field (often cubic) (see Figure III-7).

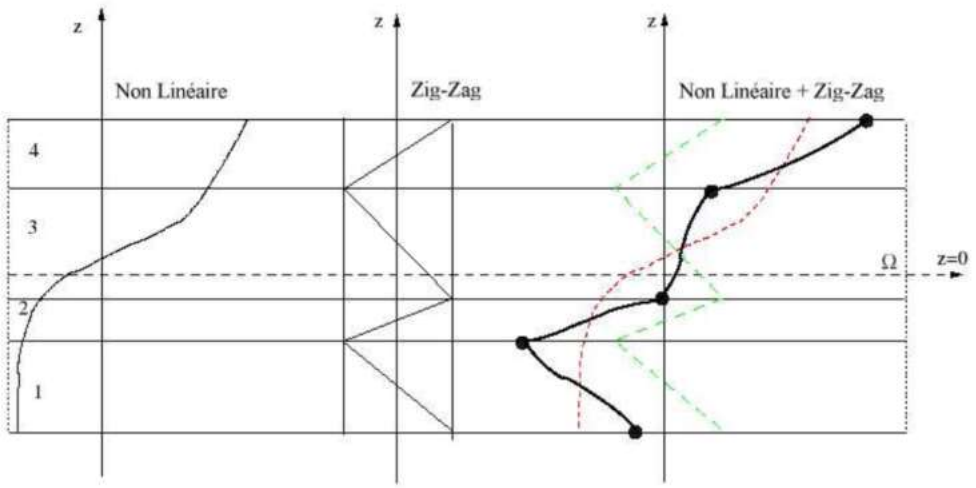

Figure III-7: Displacement fields of higher order zig-zag models [107]

The compatibility conditions were satisfied on the upper and lower surfaces of the plates to reduce the number of parameters. In the works of Ossadzow [110] and Karama [111], the zigzag function was added to the "sin" displacement function [100] to refine shear effects. The zigzag model ensures a good compromise between the solution accuracy and computational cost.

However, as the slenderness decreases, the calculation of transverse shear stresses becomes less precise [109].

III.3 P-version of the finite element method

The p-version of the finite element method originated from the work of Babuška [112], [113] and Szabó [114]. While maintaining the initial mesh, it involves introducing new degrees of freedom by increasing the degree of interpolation of shape functions in certain areas. The history of the p-version of the finite element method has been marked by significant milestones, including the proposal of hierarchical shape function concepts and use of high-degree Lagrange functions. Additionally, hierarchical functions were introduced into finite elements to detect the emergence of an efficient p-version [115], the study of p-version convergence [112].

The p-version requires simpler meshing, a solid theoretical foundation, and a reputation for providing robust and accurate solutions that converge exponentially to various problems.

III.3.1 Mesh adaptation

Modification of the discretization parameters is necessary to enhance the accuracy of a finite element solution for a linear elasticity problem. Thus, the mesh can be refined, and the interpolation degree used on the elements can be increased or both simultaneously. Various procedures exist for refining finite-element solutions. Broadly speaking, these are divided into two categories. H-refinement, in which the same class of elements continues to be used but with changes in size, enlarging, and reducing size in certain areas to allow for maximum economy in seeking the desired solution. P-refinement, where we continue to use the same element size and simply increase, usually hierarchically, the polynomial order used in their definition.

To solve a physical problem using the finite element method, the engineer must make a series of assumptions and approximations to transform a real object into a numerical model. The discretization thus obtained, defined by a mesh and the approximation degrees of the elements, allows us to obtain an approximate solution. Based on the above, we determine the displacement field of the element and the corresponding vibration equation.

Each element has a continuous displacement field expressed by approximation functions and displacements at selected points in the space of the element. These points are often the corner nodes. According to the simplest linear form of the approximation function, the displacement field{u}of the element can be expressed as follows [113]:

$$\{u\} = \sum_{i=1}^{n} Ni\ di = [N_i]\{d_i\} \qquad \text{(III.14)}$$

where [Ni] comprise the shape functions of the first-order element, {di} is the vector of unknown nodal displacements, and i indicates the node number and number of corner nodes, respectively.

III.3.2 Implementation of the p-version

III.3.2.1 Legendre polynomials

The orthogonal Legendre polynomial Pi(ξ) for a domain defined between [-1, +1] is defined as

$$P_0(\xi) = 1 \tag{III.15}$$

$$P_n(\xi) = \frac{1}{2^n \mathrm{n!}} \frac{d^n}{dx^n}[(x^2 - 1)], \text{ for n = 1, 2, 3, ...} \tag{III.16}$$

These are solutions of the following differential equation for n = 0, 1, 2, ...:

$$(1 - x^2)y'' - 2xy' + n(n+1)y = 0 \tag{III.17}$$

III.3.2.2 Shifted legendre polynomials

The shape functions used were constructed from shifted Legendre polynomials [116]. Shifted Legendre polynomials form a set of functions analogous to Legendre polynomials but are defined on the interval [a, b]:

$$P_n^*(\xi) = P^n\left(\frac{2\xi - \mathrm{a} - \mathrm{b}}{\mathrm{b} - \mathrm{a}}\right) \tag{III.18}$$

They are orthogonal to interval [a, b].

Unlike the Legendre polynomials defined in [-1, 1], the shifted Legendre polynomials are defined in [0, 1]. Therefore, Equation (III-18) becomes

$$P_n^*(\xi) = P_n(2\xi - 1) \tag{III.19}$$

III.3.2.3 P-version and hierarchical interpolation functions

Since the inception of the finite element method, high interpolation degrees have been tested with varying degrees of success. A finite element approximation,

$$u_h = \sum_{i=1}^{n} N_i a_i \tag{III.20}$$

is said to be hierarchical if the transition from n to n+1 does not alter the shape functions. Among the advantages of the p-version, the hierarchical formulation is as follows:

- Allows for the utilization of an 'industrial' mesh with consistent element sizes throughout computations,

- Provides solutions less sensitive to numerical inaccuracies,
- Maintains a favorable convergence rate most of the time,
- Offers an economic error indicator necessary for the implementation of an automated computational procedure.

a. One-dimensional elements

Linear elasticity and other problems can be formulated and solved by using simple element shapes. Once the element and corresponding shape functions have been determined, the following operations follow a well-defined standard path. To interpolate the problem for each element, a basis must be established for each element. Several choices are possible, but generally, the base functions used for finite elements interpolate, meaning that the nodal values are the values of the unknowns at the nodes, and interpolation is performed based on these values. The simplest method involves using displaced Legendre polynomials. In this method, the characteristics of the displaced Legendre polynomials are employed to obtain hierarchical shape functions for a one-dimensional element.

$$N_1(\xi) = 1 - \xi \tag{III.21a}$$

$$N_2(\xi) = \xi \tag{III.21b}$$

$$N_{i+1}(\xi) = \sqrt{2i-1}\int_0^{\xi} P_{i-1}^{*}(t)dt \qquad i \geq 2 \tag{III.21c}$$

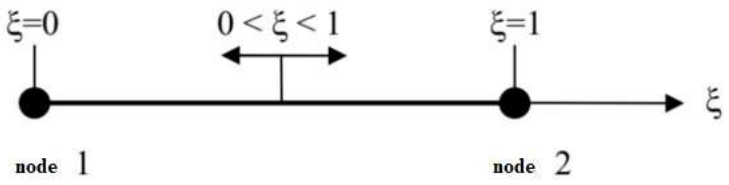

Figure III-8: One-dimensional elements

where N_1 and N_2 are the nodal or external shape functions of nodes (1 and 2) of the one-dimensional p-element, respectively. Ni (i = 3, 4, ...) are internal shape functions. The internal shape functions are termed 'hierarchical' because the set of shape functions of degree p includes those of lower degrees p-1, p-2, ..., 1. The nodal shape functions connect with other elements to ensure the continuity of displacements, whereas the hierarchical shape functions enrich the

displacement field within the element. Figure III-9 illustrates the hierarchical structure of a stiffness matrix corresponding to a polynomial degree p=3.

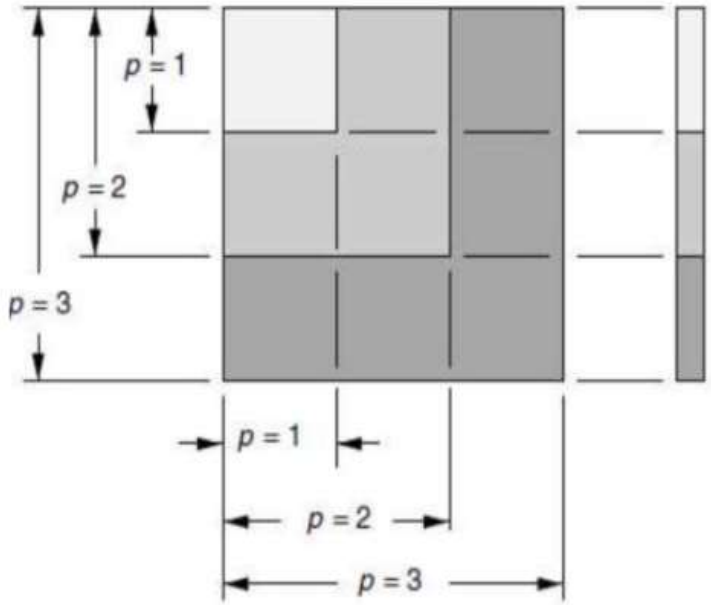

Figure III-9: Hierarchical structure of a stiffness matrix corresponding to the polynomial degree p=3

b. Two-dimensional p-elements

- **Polynomial spaces**

For a square domain $\Pi = \{0 \leq \xi, \eta \leq 1\}$, three commonly used two-dimensional polynomial spaces exist [117].

- **Serendipity family space $S^P(\Pi)$**

This corresponds to the set of monomials $\xi^i \eta^j$ with $i, j = 0,1,\ldots\ldots,p$ where $i + j = 0,1,\ldots\ldots,p$ including the monomial $\xi\,\eta$ if $p = 1$ and the monomials $\xi^p\,\eta$ and $\eta^p\,\xi$ if $p \geq 2$.

By using Pascal's triangle for a hierarchical quadrilateral element, this polynomial space can be represented as follows:

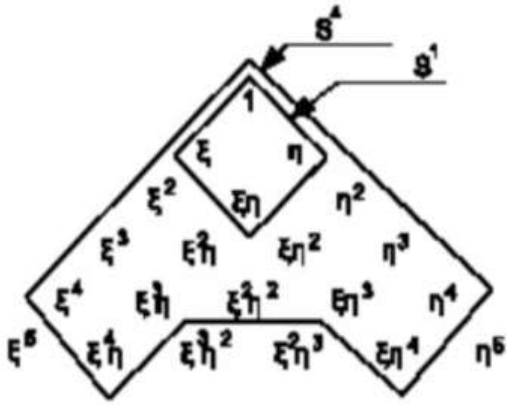

Figure III-10: Serendipity Family [118]

- **Lagrange family space $S^{p,q}$ (II)**

This corresponds to the set of monomials $\xi^i \eta^j$ with $i = 0,1,\ldots\ldots,$ p and $i,j = 0,1,\ldots\ldots,$ q. Polynomial space is represented as follows:

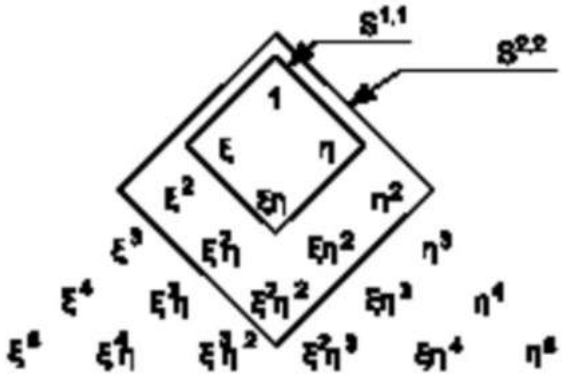

Figure III-11: Lagrange Family [118]

- **Mixed family space $\tilde{S}^{p,q}$**

It consists of the set of monomials common to both the aforementioned polynomial spaces; formally, $\tilde{S}^{p,q} = S^p \cap S^{p,q}$. Côté and Charron [117] compared the Lagrange and Serendipity families in the case of plate vibrations using the p-version of FEM. They concluded a better convergence of the Lagrange family compared to the Serendipity family, and they developed another polynomial family derived from the Serendipity family, called the enriched Serendipity family.

c. Quadrilateral element-p

The intersection of four one-dimensional elements in different directions forms a square element containing four corner nodes, four sides, and one face (Figure III-12). The combination of shape functions from two one-dimensional elements with two different directions (ξ and η) yields shape functions for the quadrilateral element, which are divided into three groups corresponding to the geometry of the element, as follows:

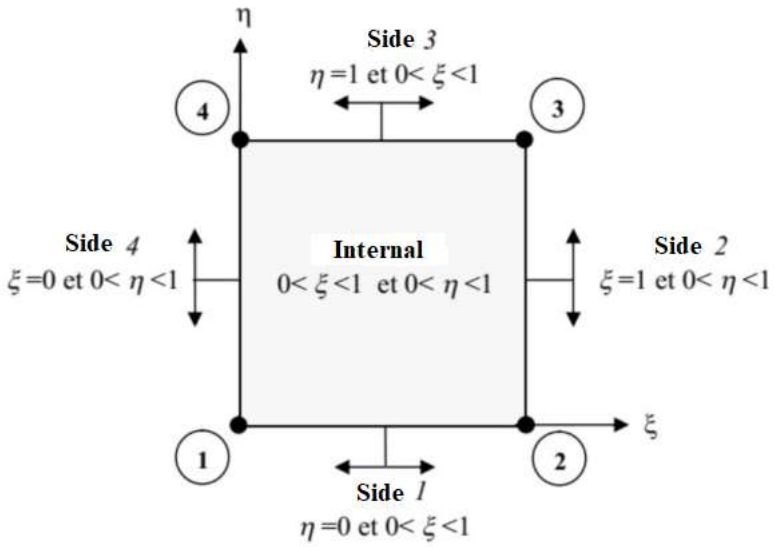

Figure III-12: Quadrilateral element

- **Corner node shape functions**

Each corner node of the quadrilateral element contains a bilinear function.

$$\text{Node 1: } N^{n1}(\xi,\eta) = N_1(\xi)N_1(\eta) \quad \text{(III.22a)}$$

$$\text{Node 2: } N^{n2}(\xi,\eta) = N_2(\xi)N_1(\eta) \quad \text{(III.22b)}$$

$$\text{Node 3: } N^{n3}(\xi,\eta) = N_2(\xi)N_2(\eta) \quad \text{(III.22c)}$$

$$\text{Node 4: } N^{n4}(\xi,\eta) = N_1(\xi)N_2(\eta) \quad \text{(III.22d)}$$

as shown in Figure III-13.

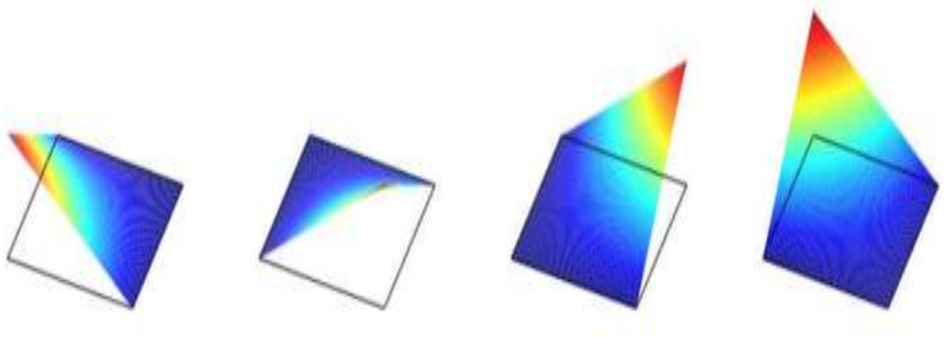

Figure III-13: Shape functions on the quadrilateral element [118]

- **Shape Functions on the Sides**

There are (p-1) shape functions for each side of the element, as shown in Figure III-14.

$$\text{Side 1: } N^{s1}(\xi,\eta) = N_{i+2}(\xi)N_1(\eta) \quad \text{(III.23a)}$$

$$\text{Side 2: } N^{s2}(\xi,\eta) = N_2(\xi)N_{i+2}(\eta) \quad \text{(III.23b)}$$

$$\text{Side 3: } N^{s3}(\xi,\eta) = N_{i+2}(\xi)N_2(\eta) \quad \text{(III.23c)}$$

$$\text{Side 4: } N^{s4}(\xi,\eta) = N_1(\xi)N_{i+2}(\eta) \quad \text{(III.23d)}$$

where i=1, …., p

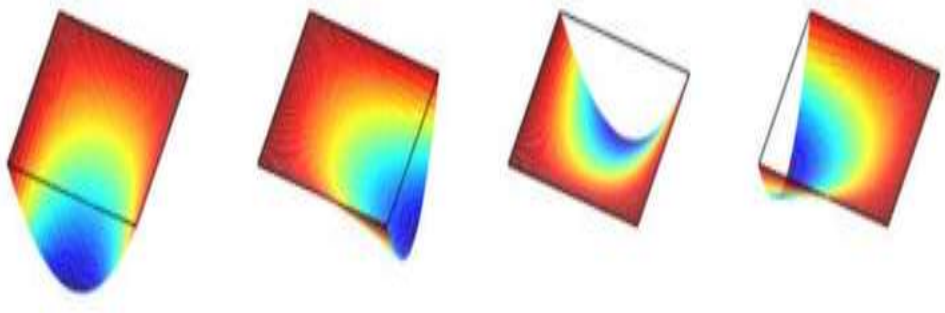

Figure III-14: Quadratic shape functions on the sides of the quadrilateral element [118]

- **Internal Shape Functions**

There are (p-1) and (p-1) internal shape functions corresponding to the element face, as shown in Figure III-15.

$$\text{Face: } N^{int}(\xi,\eta) = N_{i+2}(\xi)N_{i+2}(\eta) \tag{III.24}$$

where $i,j = 0,1,\ldots\ldots,\mathrm{p}\ ;\ i+j = 0,1,\ldots\ldots,\mathrm{p}$

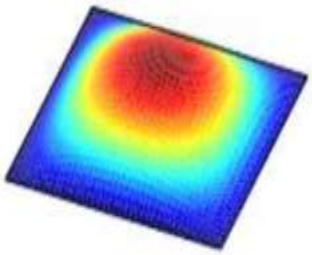

Figure III-15: Quadratic internal shape function on the quadrilateral element [118]

III.4 Summary

In this chapter, we introduce the primary plate theories commonly used for modeling FGM sandwich plates. The earliest and simplest theory, known as CPT, lacks consideration of transverse shear deformation effects, thus effectively describing only the behavior of thin plates. The FSDT assumes a uniform transverse displacement field across the plate thickness, leading to constant transverse shear stress throughout. However, the actual transverse shear stresses exhibit a parabolic distribution through the thickness, necessitating a shear correction factor for accurate characterization, which is contingent upon factors such as the end conditions, material properties, and thickness profile. In HSDTs, the in-plane displacement field is expanded with respect to the thickness coordinate to capture the intricate variations. A layered approach is introduced to describe the interfacial effects of conventional composite materials. Finally, a was introduced to describe the particularities of the p-version of the finite element method to use them to model free vibration plates.

Chapter IV

Vibration Analysis of FGM Sandwich Plates Using p-version of The Finite Element Method

Chapter IV

Vibration Analysis of FGM Sandwich Plates Using p-version of The Finite Element Method

In this chapter, we address several key aspects that are essential to our investigation. Initially, we examined the geometric configuration of the model FGM sandwich plate to provide a foundational understanding of its structural layout. Following this, we delve into the mathematical formulation of first-order shear deformation theory, elucidating its principles and significance within our analytical framework. Additionally, we integrate and detail the element description, displacement interpolation, and shape functions relevant to the p-version of the finite element method, which serve as fundamental components of the numerical analysis. Moving forward, we present the derivation of equations for strain, kinetic energy, and motion, contributing to a comprehensive characterization of plate behavior. Furthermore, we discuss the validation study conducted to ensure the accuracy and reliability of our analytical approach. This chapter includes a detailed implementation of the code used to analyze the vibration of the system. Finally, we embark on a parametric study aimed at exploring the effects of varying parameters, such as the volumetric fraction of layers, on the free vibration analysis of functionally graded sandwich plates.

IV.1 Geometric configuration

Figure IV-1 presents an illustration of a rectangular FGM sandwich plate with uniform thickness depicted within a rectangular coordinate system (X, Y, Z). In this configuration, the top and bottom face sheets of the sandwich plates are situated at z = ±h/2, whereas the vertical positions of the bottom, the two interfaces, and the top are denoted as h_0 = -h /2, h_1, h_2, and h_3 = h /2, respectively.

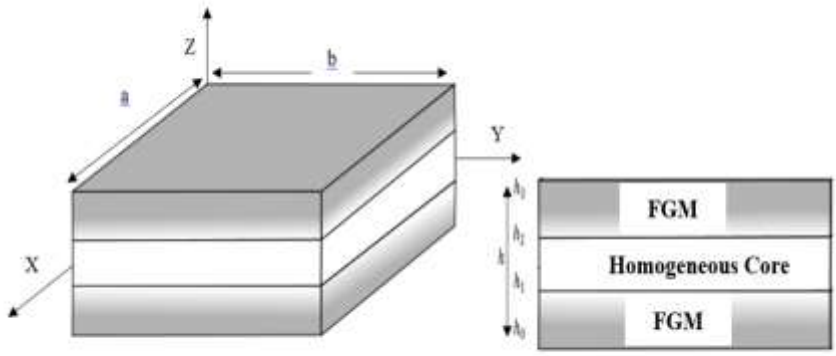

Figure IV-1: Geometry of sandwich plate with FGM skins and homogeneous core

The stress-strain relationships for each layer in x, y directions under plane stress conditions are related by

$$\begin{Bmatrix} \sigma_{xx} \\ \sigma_{yy} \\ \tau_{xy} \\ \tau_{xz} \\ \tau_{yz} \end{Bmatrix}^{i} = \begin{bmatrix} \bar{Q}_{11}^{i} & \bar{Q}_{12}^{i} & 0 & 0 & 0 \\ & \bar{Q}_{22}^{i} & 0 & 0 & 0 \\ & & \bar{Q}_{66}^{i} & 0 & 0 \\ & sym & & \bar{Q}_{44}^{i} & 0 \\ & & & & \bar{Q}_{55}^{i} \end{bmatrix}^{i} \begin{Bmatrix} \varepsilon_{xx} \\ \varepsilon_{yy} \\ \gamma_{xy} \\ \gamma_{xz} \\ \gamma_{yz} \end{Bmatrix}^{i} \quad \text{(IV.1)}$$

where, $(\sigma_{xx}, \sigma_{yy}, \tau_{xy}, \tau_{xz}, \tau_{yz})$ and $(\varepsilon_{xx}, \varepsilon_{yy}, \gamma_{xy}, \gamma_{xz}, \gamma_{yz})$ represent the stress and strain components, respectively.

The elasticity constants $\bar{Q}_{jk}^{i}$ are expressed as a function of the effective material properties, such as Young's modulus $E^{(i)}(z)$ and Poisson's ratio $\nu^{(i)}(z)$, and are defined as follows:

$$\bar{Q}_{11}^{i} = \bar{Q}_{22}^{i} = \frac{E^{(i)}(z)}{1-\left(\nu^{(i)}(z)\right)^{2}} \quad \text{(IV.2a)}$$

$$\bar{Q}_{12}^{i} = \nu^{(i)}(z)\, \bar{Q}_{11}^{i} \quad \text{(IV.2b)}$$

$$\bar{Q}_{44}^{i} = \bar{Q}_{55}^{i} = \bar{Q}_{66}^{i} = \frac{E^{(i)}(z)}{2\left(1+\nu^{(i)}(z)\right)} \quad \text{(IV.2c)}$$

The effective material characteristics of the FGM layers, such as mass density $\rho^{(i)}(z)$, are considered to be graded in the thickness direction according to a power-law distribution and can be written as [15].

$$\begin{bmatrix} E^i(z) \\ \nu^i(z) \\ \rho^i(z) \end{bmatrix} = \begin{bmatrix} V^{(i)}(z) & 0 & 0 \\ 0 & V^{(i)}(z) & 0 \\ 0 & 0 & V^{(i)}(z) \end{bmatrix} \begin{bmatrix} E_c - E_m \\ \nu_c - \nu_m \\ \rho_c - \rho_m \end{bmatrix} + \begin{bmatrix} E_m \\ \nu_m \\ \rho_m \end{bmatrix} \quad \text{(IV.3)}$$

where, the indices (c) and (m) denote ceramic and metal materials, respectively.

$V^{(i)}(z)$ denotes the volume fractions of the FGM sandwich for the (i) layer (i = 1, 2, 3) and assumes they are as follows:

$$V^{(1)}(z) = \left(\frac{z-h_0}{h_1-h_0}\right)^{n_1}, \ z \in [h_0, h_1] \quad \text{(IV.4a)}$$

$$V^{(2)}(z) = 1, \qquad z \in [h_1, h_2] \quad \text{(IV.4b)}$$

$$V^{(3)}(z) = \left(\frac{z-h_3}{h_2-h_3}\right)^{n_2}, \ z \in [h_2, h_3] \quad \text{(IV.4c)}$$

where n_1 and n_2 denotes the volume fraction exponents of the bottom and top layers, respectively, $(0 \leq n_1, n_2 \leq +\infty)$.

IV.2 Mathematical formulation

IV.2.1 Displacement field

According to the FSDT, the displacement field u_1, u_2 and u_3 at point (x, y, z) are defined as [86].

$$u_1(x, y, z, t) = u(x, y, t) + z\theta_y(x, y, t) \quad \text{(IV.5a)}$$

$$u_2(x, y, z, t) = v(x, y, t) - z\theta_x(x, y, t) \quad \text{(IV.5b)}$$

$$u_3(x, y, z, t) = w(x, y, t) \quad \text{(IV.5c)}$$

This theory uses three displacements of the middle surface and five variables to characterize the deformation (u, v, and w) and two rotations ($\theta_x$and θ_y) of transverse normal to the midplane about the x and y axes, respectively. However, the Mindlin plate theory approach fails to fulfill the transverse shear boundary conditions at the top and bottom surfaces because of its assumption of a constant shear angle throughout the thickness, maintaining the plane sections as a plane after deformation. Consequently, shear correction factors (k) are necessary for the equilibrium considerations. Mindlin suggests that these factors are linearly dependent on Poisson's ratio (ν), providing two estimations based on comparisons with the more precise

solution of three-dimensional elasticity. The initial estimation yields $0.75 \leq k \leq 0.91$ for $0 \leq \nu \leq 0.5$, while the second estimation, derived from shear wave velocity, results in $k \approx 0.86$ when $\nu = 0.3$, aligning well with the commonly assumed value of $k = 5/6$ [119].

The Green strain tensor can be expressed in terms of displacement gradients by [120].

$$\varepsilon_{xx} = \frac{\partial u_1}{\partial x} \tag{IV.6a}$$

$$\varepsilon_{yy} = \frac{\partial u_2}{\partial y} \tag{IV.6b}$$

$$\varepsilon_{zz} = \frac{\partial u_3}{\partial z} \tag{IV.6c}$$

$$\gamma_{xy} = \frac{\partial u_1}{\partial y} + \frac{\partial u_2}{\partial x} \tag{IV.6d}$$

$$\gamma_{xz} = \frac{\partial u_1}{\partial z} + \frac{\partial u_3}{\partial x} \tag{IV.6e}$$

$$\gamma_{yz} = \frac{\partial u_3}{\partial y} + \frac{\partial u_2}{\partial z} \tag{IV.6f}$$

Using the Mindlin plate theory and inserting Eq. (IV.5) into Eq. (IV.6), the strain-displacement [120] relationships are expressed as.

$$\varepsilon_{xx} = \frac{\partial u}{\partial x} \tag{IV.7a}$$

$$\varepsilon_{yy} = \frac{\partial v}{\partial y} \tag{IV.7b}$$

$$\gamma_{xy} = \frac{\partial u}{\partial y} + \frac{\partial v}{\partial x} \tag{IV.7c}$$

$$\gamma_{xz} = \theta_y + \frac{\partial w}{\partial x} \tag{IV.7d}$$

$$\gamma_{yz} = -\theta_x + \frac{\partial w}{\partial y} \tag{IV.7e}$$

$$\chi_x = \frac{\partial \theta_y}{\partial x} \tag{IV.7f}$$

$$\chi_y = -\frac{\partial \theta_x}{\partial y} \tag{IV.7g}$$

$$\chi_{xy} = \frac{\partial \theta_y}{\partial y} - \frac{\partial \theta_x}{\partial x} \tag{IV.7h}$$

IV.3 P-version of the finite element method

IV.3.1 Element description

A rectangular, four-node finite element based on first-order shear deformation theory, with five degrees of freedom per node, was used to perform free vibration of the FGM sandwich

plates. Figure IV-2 shows the geometry and the corresponding nodal variables of the finite element.

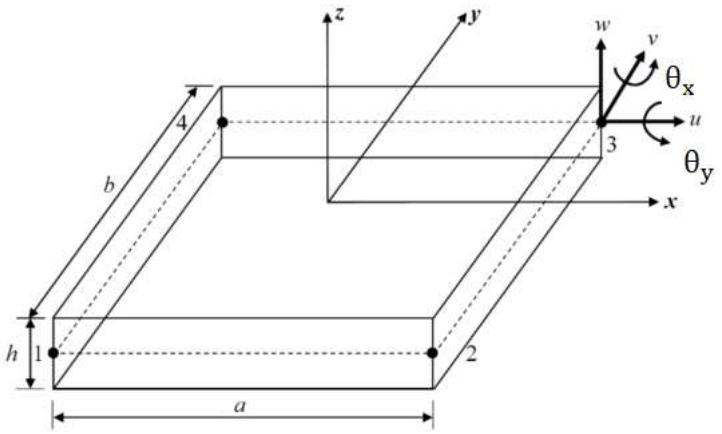

Figure IV-2: Geometry and corresponding nodal variables of the element finite

IV.3.2 Displacement interpolation and shape functions

The in-plane displacements (u, v) and out-of-plane displacements (w, θ_x and θ_y) are denoted as

$$\begin{Bmatrix} u \\ v \end{Bmatrix} = \sum_{j=1}^{r} \bar{N}_j \bar{q}_j \tag{IV.8}$$

where

$$\bar{N}_j = \begin{bmatrix} N_j(\xi,\eta) & 0 \\ 0 & N_j(\xi,\eta) \end{bmatrix}, \text{ and } \qquad \bar{q}_j = \begin{Bmatrix} \bar{q}_{2j-1} \\ \bar{q}_{2j} \end{Bmatrix} \tag{IV.9}$$

and

$$\begin{Bmatrix} w \\ \theta_y \\ \theta_x \end{Bmatrix} = \sum_{j=1}^{r} N_j q_j \tag{IV.10}$$

where

$$N_j = \begin{bmatrix} N(\xi,\eta) & 0 & 0 \\ 0 & N(\xi,\eta) & 0 \\ 0 & 0 & N(\xi,\eta) \end{bmatrix}, \text{ and } \qquad q_j = \begin{Bmatrix} q_{3j-2} \\ q_{3j-1} \\ q_{3j} \end{Bmatrix} \tag{IV.11}$$

where $\bar{q}_j$ is the vector of generalized in-plane displacements, q_j represents the vector of generalized transverse displacement and rotations, respectively, and $N(\xi,\eta)$ are the shape functions of rectangular finite p-element.

In the p-element, shape functions are classified into three categories. Firstly, the shape functions of the nodes at the vertices of the element, secondly the shape functions of the four

sides of the element and finally the functions of the internal shapes. The shape functions used in the present p-element are given as:

- Four shape functions of vertex

$$N_1(\xi,\eta) = g_1(\xi)g_1(\eta) \quad \text{(IV.12a)}$$
$$N_2(\xi,\eta) = g_2(\xi)g_1(\eta) \quad \text{(IV.12b)}$$
$$N_3(\xi,\eta) = g_2(\xi)g_2(\eta) \quad \text{(IV.12c)}$$
$$N_4(\xi,\eta) = g_1(\xi)g_2(\eta) \quad \text{(IV.12d)}$$

- $(p-1)$ hierarchical shape functions on each side

$$N^{Side\ 1}(\xi,\eta) = g_{i+2}(\xi)g_1(\eta) \quad \text{(IV.13a)}$$
$$N^{Side\ 2}(\xi,\eta) = g_2(\xi)g_{i+2}(\eta) \quad \text{(IV.13b)}$$
$$N^{Side\ 3}(\xi,\eta) = g_{i+2}(\xi)g_2(\eta) \quad \text{(IV.13c)}$$
$$N^{Side\ 4}(\xi,\eta) = g_1(\xi)g_{i+2}(\eta) \quad \text{(IV.13d)}$$

- $(p-1)^2$ internal hierarchical shape functions

$$N^{Internal}(\xi,\eta) = g_{i+2}(\xi)g_{i+2}(\eta) \quad \text{(IV.14)}$$

where $g_i(\xi)\ and\ g_i(\eta)$ are the uni-dimensional hierarchical shape functions and are given as:

$$g_1(\xi) = 1-\xi,\ g_2(\xi) = \xi,\ g_{i+1}(\xi) = \sqrt{2i-1}\int_0^{\xi} P_{i-1}(\tau)\,d\tau \quad i \geq 2 \quad \text{(IV.15a)}$$
$$g_1(\eta) = 1-\eta,\ g_2(\eta) = \eta,\ g_{i+1}(\eta) = \sqrt{2i-1}\int_0^{\eta} P_{i-1}(\tau)\,d\tau \quad i \geq 2 \quad \text{(IV.15b)}$$

and $P_i(\tau)$ is shifted Legendre polynomials and are given as:

$$P_0(\tau) = 1,\ P_1(\tau) = 2\tau - 1 \quad \text{(IV.16a)}$$
$$P_{j+1}(\tau) = \frac{1}{j+1}\left[(-2j-1+(4j+2)j)P_j(\tau) - jP_{j-1}(\tau)\right],\quad j = 1,2,\ldots \quad \text{(IV.16b)}$$

IV.4 Strain, Kinetic Energy, and Motion Equations

The strain energy U and kinetic energy T of the functionally graded moderately thick plate can be written as follows:

$$U = \frac{1}{2}\iint [A_{11}\varepsilon_{xx}^2 + A_{22}\varepsilon_{xx}^2 + 2A_{12}\varepsilon_{xx}\varepsilon_{yy} + A_{66}\gamma_{xy}^2 + 2\left(B_{11}\varepsilon_{xx}\chi_x + B_{12}\varepsilon_{xx}\chi_y + B_{12}\varepsilon_{yy}\chi_x + B_{22}\varepsilon_{yy}\chi_y + B_{66}\chi_{xy}^2\right) + \left(D_{11}\chi_x^2 + D_{22}\chi_y^2 + 2D_{12}\chi_x\chi_y + D_{66}\chi_{xy}^2\right) + \left(S_{44}\gamma_{xz}^2 + S_{55}\gamma_{yz}^2\right)]dxdy \quad \text{(IV.17)}$$

$$T = \frac{1}{2}\iint \left[I_1 \left(\left(\frac{\partial u}{\partial t}\right)^2 + \left(\frac{\partial v}{\partial t}\right)^2 + \left(\frac{\partial w}{\partial t}\right)^2 \right) + I_3 \left(\left(\frac{\partial \theta_x}{\partial t}\right)^2 + \left(\frac{\partial \theta_y}{\partial t}\right)^2 \right) \right] dxdy \quad \text{(IV.18)}$$

where A_{ij}, B_{ij}, D_{ij}, and S_{ij} are extensional, bending-extensional, bending and shear stiffness constants and $I_{1,3}$ are the inertia constants of the FGM plate and are given by

$$\left(A_{ij}, B_{ij}, D_{ij}\right) = \sum_{i=1}^{3} \int_{h_{i-1}}^{h_i} \bar{Q}_{jk}^{(i)} (1, z, z^2) dz \quad (j,k = 1,2,6) \quad \text{(IV.19a)}$$

$$\left(S_{ij}\right) = \sum_{i=1}^{3} k \int_{h_{i-1}}^{h_i} \bar{Q}_{jk}^{(i)} dz \quad (j,k = 4,5) \quad \text{(IV.19b)}$$

$$(I_1, I_3) = \sum_{i=1}^{3} \int_{h_{i-1}}^{h_i} \rho^{(i)}(z)(1, z^2) dz \quad \text{(IV.19c)}$$

where k is a shear correction factor of FSDT ($k = 5/6$) [119], $\bar{Q}_{jk}^{(i)}$ are the coefficients of the elasticity matrix.

Lagrangian of the system is given by

$$L = T - U \quad \text{(IV.20)}$$

$$\frac{d}{dt}\left(\frac{\partial L}{\partial \dot{q}_i}\right) - \left(\frac{\partial L}{\partial q_i}\right) = 0 \quad \text{(IV.21)}$$

We obtain the following motion equation

$$[K_e]\{Q\} + [M]\{\ddot{Q}\} = 0 \quad \text{(IV.22)}$$

The substitution of $\{\ddot{Q}\} = -\omega^2\{Q\}$ in the above equation leads to

$$([K_e] - \omega^2[M])\{Q\} = 0 \quad \text{(IV.23)}$$

Using Eqs. (IV.17)– (IV.18) in conjunction with Lagrange's equations, the final equation of motion yields.

$$[K - K_2^T K_1^{-1} K_2 - \omega^2 M]\{Q\} = 0 \quad \text{(IV.24)}$$

Where $\{Q\} = \left\{Q_w \; Q_{\theta_y} \; Q_{\theta_z}\right\}$ in the vector of generalized amplitudes and $[K_e] = [K - K_2^T K_1^{-1} K_2]$.

Where $[K_1]$ is the submatrix of internal degrees of freedom, $[K_2]$ is the submatrix of the coupling terms, and $[K]$ is the submatrix of the main degrees of freedom.

The element mass matrix M, and element stiffness matrices K, K_1 and K_2 are given as

$$M = \int_0^1 \int_0^1 \begin{bmatrix} I_1 N_i N_j & 0 & 0 \\ 0 & I_3 N_i N_j & 0 \\ 0 & 0 & I_3 N_i N_j \end{bmatrix} abd\xi d\eta \quad \text{(IV.25)}$$

K

$$= \int_0^1 \int_0^1 \begin{bmatrix} S_{44}\frac{\partial N_i}{\partial \xi}\frac{\partial N_j}{\partial \xi} + S_{55}\frac{\partial N_i}{\partial \eta}\frac{\partial N_j}{\partial \eta}, & -S_{44}\frac{\partial N_i}{\partial \eta}N_j, & S_{55}\frac{\partial N_i}{\partial \xi}N_j \\ -S_{44}N_i\frac{\partial N_j}{\partial \eta}, & D_{66}\frac{\partial N_i}{\partial \xi}\frac{\partial N_j}{\partial \xi} + D_{22}\frac{\partial N_i}{\partial \eta}\frac{\partial N_j}{\partial \eta} + S_{44}N_iN_j, & -D_{12}\frac{\partial N_i}{\partial \eta}\frac{\partial N_j}{\partial \xi} - D_{66}\frac{\partial N_i}{\partial \xi}\frac{\partial N_j}{\partial \eta} \\ S_{55}N_i\frac{\partial N_j}{\partial \xi}, & -D_{12}\frac{\partial N_i}{\partial \xi}\frac{\partial N_j}{\partial \eta} - D_{66}\frac{\partial N_i}{\partial \eta}\frac{\partial N_j}{\partial \xi}, & D_{66}\frac{\partial N_i}{\partial \eta}\frac{\partial N_j}{\partial \eta} + D_{11}\frac{\partial N_i}{\partial \xi}\frac{\partial N_j}{\partial \xi} + S_{55}N_iN_j \end{bmatrix} abd\xi d\eta$$

(IV.26)

$$K_1 = \int_0^1 \int_0^1 \begin{bmatrix} A_{11}\frac{\partial N_i}{\partial \xi}\frac{\partial N_j}{\partial \xi} + A_{66}\frac{\partial N_i}{\partial \eta}\frac{\partial N_j}{\partial \eta}, & A_{12}\frac{\partial N_i}{\partial \xi}\frac{\partial N_j}{\partial \eta} + A_{66}\frac{\partial N_i}{\partial \xi}\frac{\partial N_j}{\partial \eta} \\ A_{21}\frac{\partial N_i}{\partial \eta}\frac{\partial N_j}{\partial \xi} + A_{66}\frac{\partial N_i}{\partial \eta}\frac{\partial N_j}{\partial \xi}, & A_{22}\frac{\partial N_i}{\partial \eta}\frac{\partial N_j}{\partial \eta} + A_{66}\frac{\partial N_i}{\partial \xi}\frac{\partial N_j}{\partial \xi} \end{bmatrix} abd\xi d\eta \quad \text{(IV.27)}$$

$$K_2 = \int_0^1 \int_0^1 \begin{bmatrix} 0, & B_{12}\frac{\partial N_i}{\partial \xi}\frac{\partial N_j}{\partial \eta} - B_{66}\frac{\partial N_i}{\partial \eta}\frac{\partial N_j}{\partial \xi}, & B_{11}\frac{\partial N_i}{\partial \xi}\frac{\partial N_j}{\partial \eta} + B_{66}\frac{\partial N_i}{\partial \eta}\frac{\partial N_j}{\partial \xi} \\ 0, & B_{22}\frac{\partial N_i}{\partial \eta}\frac{\partial N_j}{\partial \eta} - B_{66}\frac{\partial N_i}{\partial \xi}\frac{\partial N_j}{\partial \xi}, & B_{12}\frac{\partial N_i}{\partial \eta}\frac{\partial N_j}{\partial \xi} + B_{66}\frac{\partial N_i}{\partial \xi}\frac{\partial N_j}{\partial \eta} \end{bmatrix} abd\xi d\eta \quad \text{(IV.28)}$$

IV.5 Code implementation

The final section of this chapter focuses on code implementation to determine the natural frequencies of the FGM sandwich plate. Based on the first-order plate theory and formulation using the quadrilateral p-element, the Fortran 90 code. First, we introduce the programming environment, software, and hardware used, followed by a program flowchart to explain the development steps. A general description of parameter dictionaries, data files, and output files is provided in this section. The final section includes a detailed explanation of each subroutine's task of executing the calculation code.

IV.5.1 Programming environment

Building upon the detailed mathematical formulas from the preceding chapter, a FORTRAN 90 program was developed based on the p-version of the finite element method to determine the natural frequencies of a plate under various physical and geometric parameters and boundary conditions.

The software utilized in this study includes Origin 9.0, for graph plotting and mode analysis, and MATLAB for the symbolic computation of shape functions and their derivatives. The program was executed on a PC equipped with a Core i5 processor (2.30 GHz) and 8 GB of RAM.

The calculation program comprises three main components.

- Input files
- Calculation program
- Output file.

IV.5.2 Main program

The various stages involved in developing a calculation program are illustrated in the flowchart (Figure IV-3).

IV.5.3 Program description

IV.5.3.1 Data file

All the necessary data for implementing the calculation program are contained within the data file. The data can be divided into four categories.

a. Geometric Parameters

The parameters required to define the geometry of the plate were as follows:

- H: Plate thickness.
- X(i), Y(i): Coordinates of the nodes at the vertices of the elements, where they are utilized in blending functions (refer to Chapter III).

b. Physical Parameters

The physical parameters utilized in the program include the following.

- PRm: Poisson's ratio.
- SC: Shear correction factor.
- Em: Young's modulus of the metal.
- Ec: Young's modulus of the ceramic.
- ROm: Surface mass density of the metal.
- ROc: Surface mass density of the ceramic.
- EN1: Volume fraction (bottom layer).
- EN2: volume fraction (top layer).
- XCI1: Porosity coefficient (bottom layer).
- XCI2: Porosity coefficient (top layer)

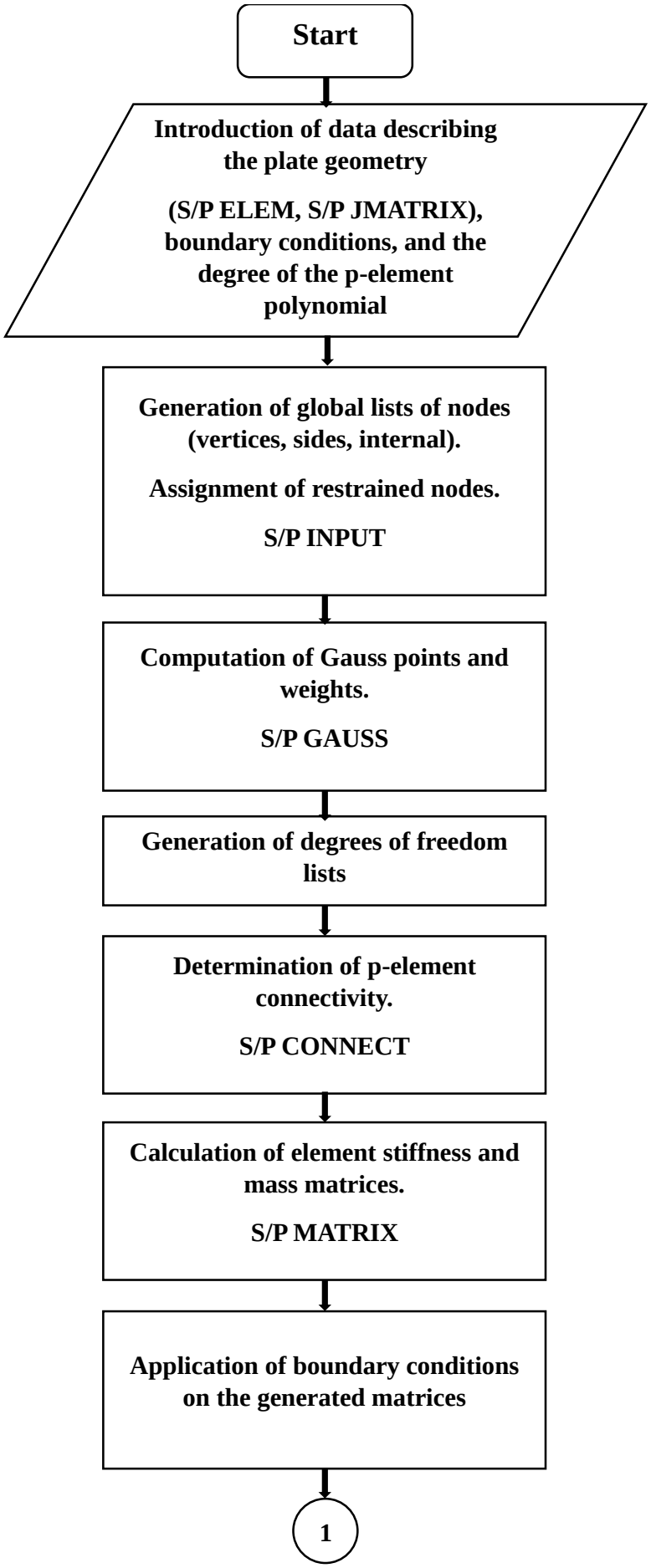
Start
Introduction of data describing the plate geometry
(S/P ELEM, S/P JMATRIX), boundary conditions, and the degree of the p-element polynomial
Generation of global lists of nodes (vertices, sides, internal).
Assignment of restrained nodes.
S/P INPUT
Computation of Gauss points and weights.
S/P GAUSS
Generation of degrees of freedom lists
Determination of p-element connectivity.
S/P CONNECT
Calculation of element stiffness and mass matrices.
S/P MATRIX
Application of boundary conditions on the generated matrices
1

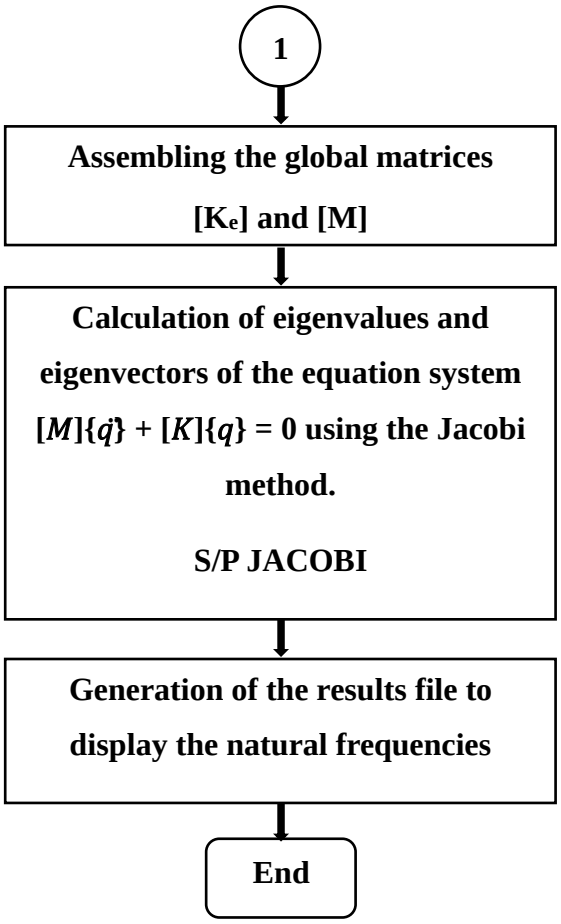

Figure IV-3: Flowchart of the developed program

c. Element Parameters

All necessary parameters that identify the p-element are stored in the data file.

- NTE: Total number of elements.
- NTN: Total number of nodes.
- NTC: Total number of sides.
- NNR: Number of restrained nodes.
- NCR: Number of restrained sides.
- NMH: Degree of p-element polynomial.
- NMODE: Specific mode number.

d. Boundary Conditions

To facilitate the solution of the generalized eigenvalue problem, it is crucial to consider the significance of boundary conditions. To solve the system of equations, it is sufficient to

incorporate the imposed (zero) values of the boundary-node displacements into these equations. The quadrilateral p-element depicted in Figure IV-4 contains four nodes at the vertices and four sides, with each node having three degrees of freedom:

- w: displacement along the z-axis.
- θ_x: rotation of the cross section around the x-axis.
- θ_y: rotation of cross-section around the y-axis

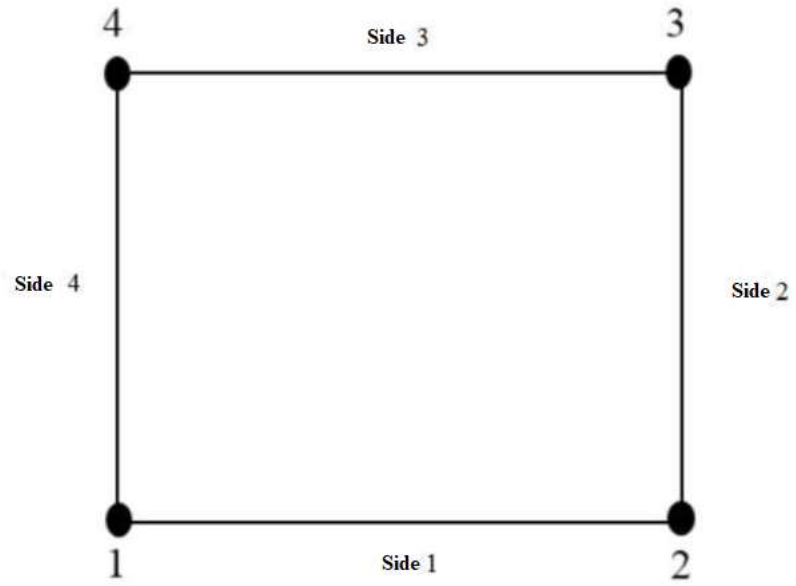

Figure IV-4: Numbering of nodes and sides of the p-element

In the subroutine (S/P INPUT), a numbering order for nodes and sides of the quadrilateral p-element exists to ensure the accurate assignment of boundary conditions.

The boundary conditions for the plate element in the data file are introduced following the layout indicated in Tables IV-1 and IV-2.

In the tables below, the value (0 or 1) defines the state of freedom of the nodes and sides of the p element. A value of '1' indicates that the degree of freedom is restricted, whereas '0' signifies that the degree of freedom is free. In the context of applying boundary conditions in the calculation program, the rows and columns of the stiffness and mass matrices corresponding to the restricted degrees of freedom were removed.

Table IV-1: Introduction of node boundary conditions

nodes	u	v	ω	θ_x	θ_y
1	1 Or 0	1 Or 0	1 Or 0	1 Or 0	1 Or 0
2	1 Or 0	1 Or 0	1 Or 0	1 Or 0	1 Or 0
3	1 Or 0	1 Or 0	1 Or 0	1 Or 0	1 Or 0
4	1 Or 0	1 Or 0	1 Or 0	1 Or 0	1 Or 0

Table IV-2: Introduction of side boundary conditions

side	u	v	ω	θ_x	θ_y
1	1 Or 0	1 Or 0	1 Or 0	1 Or 0	1 Or 0
2	1 Or 0	1 Or 0	1 Or 0	1 Or 0	1 Or 0
3	1 Or 0	1 Or 0	1 Or 0	1 Or 0	1 Or 0
4	1 Or 0	1 Or 0	1 Or 0	1 Or 0	1 Or 0

IV.5.3.2 Programming

The calculation program developed in this study allows for the analysis of the linear free vibration of plates with arbitrary geometric shapes using a quadrilateral p-element. This enables the determination of frequencies and eigenvectors. The flowchart in Figure IV-3 illustrates the main subroutines and development steps of this program. The following subroutines are deemed essential for executing the calculation program:

a. Geometric description of the plate by the p-element

The subroutine ELEM performs the task of geometric description of the plate using Cartesian coordinates (x, y) of the nodes at the vertices, and parametric functions of the sides describing the plate boundaries and their derivatives with respect to local coordinates (ξ, η).

b. Jacobian Matrix

The subroutine JMATRIX calculates the determinant and components of the Jacobian matrix to be used in the calculation of element stiffness and mass matrices.

c. Execution of boundary conditions

The INPUT subroutine is responsible for executing the two main tasks.

- The first task involved generating a global list of nodes (real and fictitious). The first list is dedicated to real vertex nodes. The second is reserved for fictitious nodes on the sides, whereas the third contains all nodes within the p-element. In addition, the node lists are designed based on the degree of interpolation polynomial p.
- The second task performed by the S/P INPUT is the assignment of the degrees of freedom for the restrained nodes.

d. Numerical integration

Using the Gauss-Legendre quadrature, the integrals presented in the element stiffness and mass matrices were numerically calculated because of the inability to compute these integrals analytically. The GAUSS subroutine calculates the abscissas of the Gauss points and the corresponding weights required for the numerical integration.

e. Lists of degrees of freedom

After ensuring node and side connectivity, assignments of degrees of freedom lists are performed by the CONNECT subroutine to achieve a hierarchy of degrees of freedom. These lists of degrees of freedom were identified earlier by S/P INPUT.

f. Formation of element matrices

Element stiffness and mass matrices were calculated using the S/P MATRIX subroutine.

g. Calculation of eigenvalues and eigenvectors by the jacobi method

Once the element matrices were formed, they were assembled into global matrices by neglecting the rows and columns corresponding to the restrained nodes and sides that were previously read from the data file. Thus, the equation of motion for global free vibration can be expressed as

$$([K_e] - \omega^2[M])\{Q\} = 0 \qquad \text{(IV.29)}$$

In the JACOBI subroutine, a system of equations is solved using the Jacobi algorithm to obtain the corresponding eigenvalues and eigenvectors.

h. Shape functions and their derivatives

The hierarchical shape functions for the quadrilateral p-element are given in terms of shifted Legendre orthogonal polynomials. In our calculation program, the shape functions and their derivatives with respect to the local coordinates (ξ, η) were computed using the GFUNCT subroutine.

IV.5.3.3 Output file

All the parameters calculated by the developed program are stored in an output file, including

- NMH: Degree of p-element polynomial.
- NEQ: Number of equations in the system.
- NMODE: Specific mode number.
- OMLOC: Local frequency parameter.
- TE: Execution time (seconds).

IV.6 Validation study

The validity of the results was confirmed through comparisons with existing literature. In the first case, we compared the fundamental frequency parameters of isotropic rectangular and square plates as functions of the thickness ratio (h/b), as presented in Table IV-3 and Table IV-4, respectively.

Table IV-3: Fundamental frequencies $\overline{\Omega} = (\omega a^2/2\pi)\sqrt{\rho h/D}$ of an isotropic simply supported rectangular plate $(b = 2a)$

h/b	Present	TSDT [122]	SSDT [123]	DQM [121]
0.005	1.96305	1.96305	1.96305	1.96299
0.01	1.96171	1.96171	1.96171	1.96179
0.02	1.95639	1.95639	1.95640	1.95667
0.1	1.80970	1.80974	1.80993	1.81513
0.2	1.51803	1.51230	1.51294	1.53118

The present results using the p-version of the FEM are in excellent agreement obtained by isotropic plates with those analytical [121] and semi-analytical solutions [122], [123].

Six types of simply supported FGM sandwich plates with homogenous ceramic cores were considered, as listed in Table IV-5. The designation (1-0-1) indicates an absence of the core, signifying that the plate solely consists of two equally thick face layers made of FGM sandwich; (1-1-1) in this type, the plate comprises three layers of equal thickness; (1-2-1) here, the core thickness equals twice the thickness of each face layer; (2-1-2), the core thickness equates to half the thickness of each face layer; (2-1-1) is a non-symmetric sandwich plate where the core thickness aligns with one face thickness and is half the thickness of the other; and (2-2-1) is a

non-symmetric sandwich plate where the core thickness equals the thickness of one face and twice the thickness of the other.

Table IV-4: Fundamental frequencies $\bar{\Omega} = (\omega a^2/2\pi)\sqrt{\rho h/D}$ of an isotropic simply supported square plate

h/b	Present	TSDT [122]	SSDT [123]	DQM [121]
0.1	3.03428	3.03433	3.03445	3.03828
	7.23879	7.23897	7.23973	7.26053
	11.10811	11.10688	11.10867	11.15740
	13.53498	13.52929	13.53217	13.60580
0.2	2.77703	2.77669	2.77717	2.78935
	6.07210	6.04919	6.05177	6.12471
	8.77740	8.67383	8.67960	8.87880
	10.36847	10.17716	10.18547	10.50360

Table IV-5: FGM sandwich model

Thickness	1-0-1	1-1-1	1-2-1	2-1-2	2-2-1	2-1-1
h_0	-h/2	-h/2	-h/2	-h/2	-h/2	-h/2
h_1	0	-h/6	-h/4	-h/10	-h/10	0
h_2	0	h/6	h/4	h/10	3h/10	h/4
h_3	h/2	h/2	h/2	h/2	h/2	h/2

The properties of metal (Aluminum- Al) and ceramic (Alumina-Al_2O_3) mixture are shown as

- Alumina-Al_2O_3:$E_c = 380Gpa, \nu_c = 0.3, \rho_c = 3800Kg\ m^{-3}$.
- Aluminum- Al:$E_m = 70Gpa, \nu_m = 0.3, \rho_m = 2707Kg\ m^{-3}$.

For convenience, the following dimensionless variables are applied to graphically illustrate some numerical results.

The frequency parameters:

$$\Omega = (\omega a^2/h)\sqrt{\rho_0/E_0} \tag{IV.30}$$

where Young's modulus and material density, denoted as $E_0 = 1$ GPa and $\rho_0 = 1\, kg/m^3$, respectively.

Table IV-6 provides a comprehensive comparison of the fundamental frequency parameters of square FGM sandwich plates with those predicted by alternative theories, exhibiting convergence among these values, as noted in the studies by Zenkour [123] and Van Vinh and Huy [33]. By incrementally increasing the polynomial order from two to eight, the desired level of accuracy in the numerical results for simply supported configurations is attained. The tabulated data clearly illustrate a pronounced trend of rapid convergence with an escalating polynomial order. In particular, a significant convergence pattern becomes increasingly conspicuous as the polynomial order surpasses and reaches *p* =6, underscoring the efficacy and stability of the convergence process, and affirming its robustness in achieving precise solutions with higher polynomial orders.

IV.7 Parametric study

The contour plots of the linear frequency parameters of the symmetric FGM sandwich plates are shown in Figure IV-5. This contour was plotted for the calculated values of the linear frequency parameters as functions of the volume fraction exponents of layers 1 (n_1) and 3 (n_2). The two volume fraction exponents varied from 0 to 10. As can be seen in the figure, the increase in the volume fraction exponents in the direction of (n_1) or (n_2) produces a reduction in the frequency parameters. Symmetric FGM plates produce plots for plates with geometrical and physical symmetries.

Table IV-6: The convergence and comparison of fundamental frequencies parameters of FGM sandwich plate with other theories (h/a=0.1)

n	Methods	*p*	1-0-1	2-1-2	2-1-1	1-1-1	2-2-1	1-2-1
0.0	Present	2	1.93283	1.93283	1.93283	1.93283	1.93283	1.93283
		4	1.82470	1.82470	1.82470	1.82470	1.82470	1.82470
		6	1.82442	1.82442	1.82442	1.82442	1.82442	1.82442
		8	1.82442	1.82442	1.82442	1.82442	1.82442	1.82442
	TSDT [123]		1.82445	1.82445	1.82445	1.82445	1.82445	1.82445
	SSDT [123]		1.82452	1.82452	1.82452	1.82452	1.82452	1.82452
	HypSDT [33]		1.82563	1.82563	1.82563	1.82563	1.82563	1.82563
0.5	Present	2	1.52837	1.57066	1.60105	1.60809	1.64303	1.66709
		4	1.44191	1.48182	1.51004	1.51719	1.54982	1.57298
		6	1.44168	1.48159	1.50981	1.51695	1.54958	1.57274
		8	1.44168	1.48159	1.50981	1.51695	1.54958	1.57274
	TSDT [123]		1.44424	1.48408	1.51253	1.51922	1.55199	1.57451
	SSDT [123]		1.44436	1.48418	1.51258	1.51927	1.55202	1.57450
	HypSDT [33]		1.44513	1.48500	1.50735	1.52017	1.54813	1.57553
1.0	Present	2	1.31531	1.37575	1.42765	1.43234	1.49032	1.52388
		4	1.24051	1.29749	1.34520	1.35093	1.40468	1.43745
		6	1.24032	1.29729	1.34500	1.35072	1.40446	1.43722
		8	1.24032	1.29729	1.34500	1.35072	1.40446	1.43722
	TSDT [123]		1.24320	1.30011	1.34888	1.35333	1.40789	1.43934
	SSDT [123]		1.24335	1.30023	1.34894	1.35339	1.40792	1.43931
	HypSDT [33]		1.24393	1.30089	1.33421	1.35415	1.39652	1.44024
5.0	Present	2	0.99965	1.03836	1.13666	1.10538	1.21424	1.24286
		4	0.94271	0.97886	1.06771	1.04200	1.14135	1.17177
		6	0.94256	0.97870	1.06755	1.04183	1.14118	1.17159
		8	0.94256	0.97870	1.06755	1.04183	1.14118	1.17159
	TSDT [123]		0.94598	0.98184	1.07432	1.04466	1.14731	1.17397
	SSDT [123]		0.94630	0.97207	1.07445	1.04481	1.14741	1.17399
	HypSDT [33]		0.94650	0.98240	1.03120	1.04527	1.10963	1.17468

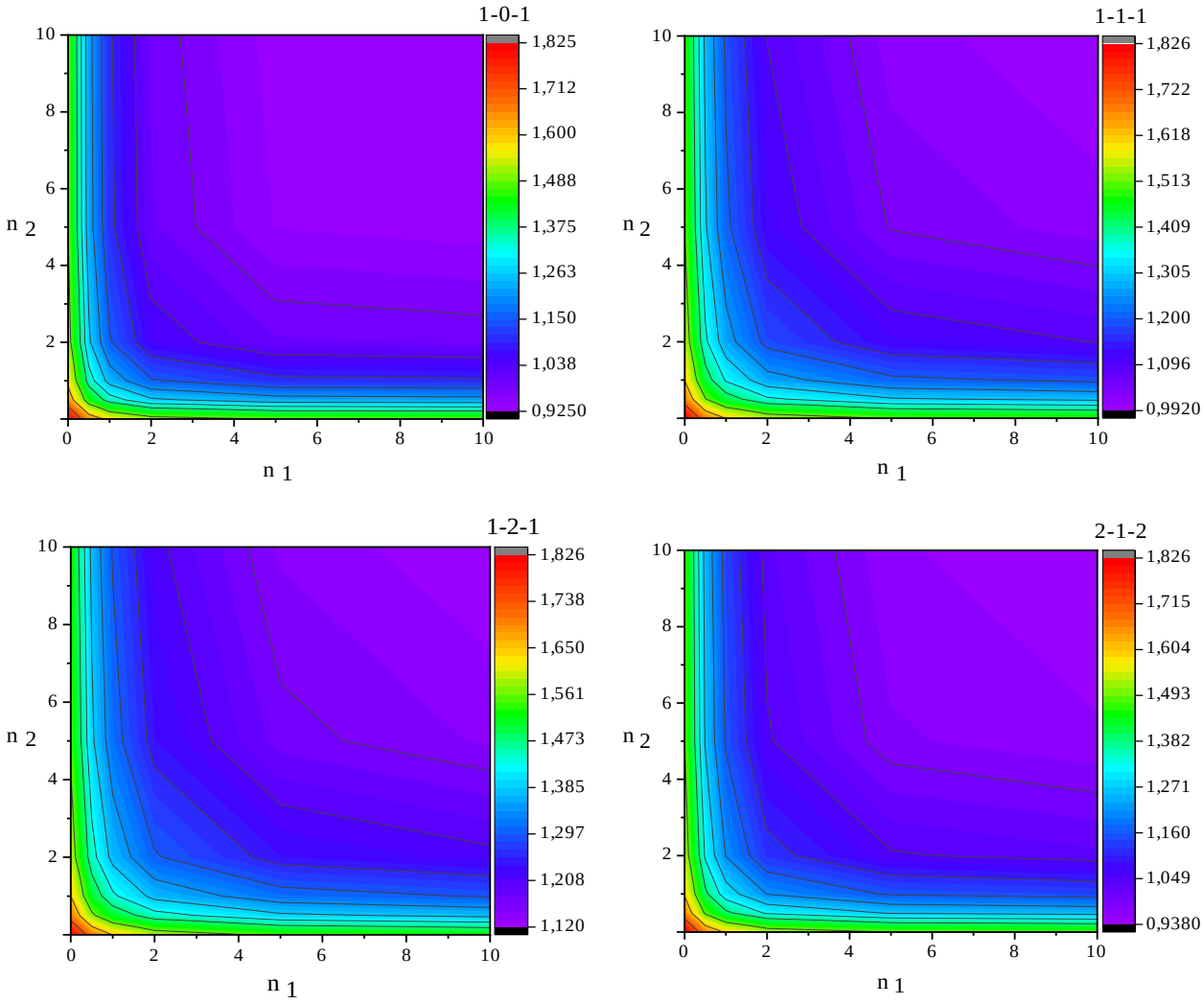

Figure IV-5: Contour plot of frequency parameters for symmetric FGM sandwich plates

Figure IV-6 illustrate the contour plots of the frequency parameters for the non-symmetric FGM sandwich plates. This contour was plotted as a function of the volume fraction exponent for the calculated values of the linear frequency parameters. the increasing of the volume fraction exponents (n_1) and (n_2) produces a reduction of frequency parameters. Non-symmetric FGM plates produced non-symmetric plots. The greatest variation is in the direction of bottom layers (n_1), which reflects the influence of the mixture of the bottom layers on the frequency parameters of the FGM sandwich plates.

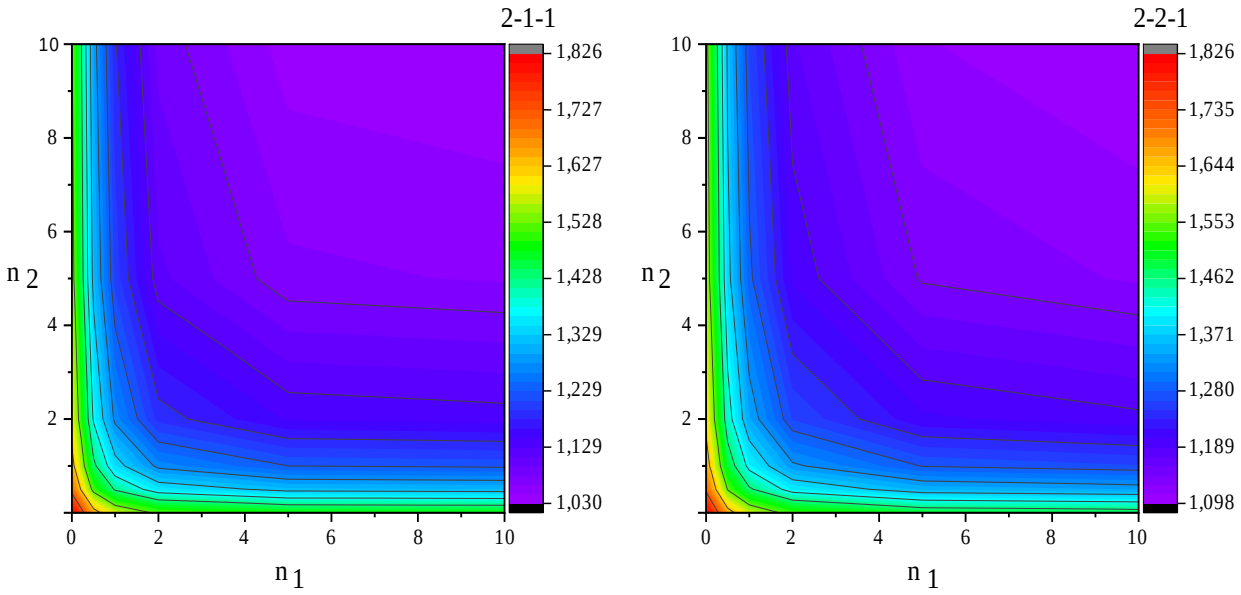

Figure IV-6: Contour plot of frequency parameter for FGM sandwich non-symmetric plates

IV.8 Summary

In this chapter, we define the model, analyze, and integrate the p-version of the finite element method and FSDT. We discuss the practical implementation of the solutions in the computational code. The validity of the results was confirmed through comparisons with existing literature, and the results obtained using the p-version of the FEM were in excellent agreement with those obtained by isotropic and FGM sandwich plates with analytical and semi-analytical solutions. For a degree of polynomials of order six, the convergence investigation conducted in this study provides the stability of the results with a precision of six digits. To test the quality and precision of the proposed p-element, a comparative study was conducted between the present results and those obtained using other methods (TSDT, SSDT, DQM, HypSDT, and HSDT). Excellent agreement was found between the two results, with an order of precision of five digits. Finally, the non-symmetric FGM plates produced the greatest variation in the direction of the bottom layers, reflecting the influence of the mixture of the bottom layers on the frequency parameters of the FGM sandwich plates.

Chapter V

Effect of Porosity Distribution on FGM Sandwich Plates

Chapter V

Effect of Porosity Distribution on FGM Sandwich Plates

The distribution of porosity within FGM sandwich plates presents a notable challenge, as it affects various mechanical properties, such as stiffness, strength, and durability, impacting the structural integrity and overall performance of the plates. Understanding and managing this porosity distribution is crucial for optimizing the design and manufacturing processes of FGM sandwich structures.

In this final chapter, we aim to explore the effect of porosity distribution on FGM sandwich plates using the p-version of the FEM and FSDT. Our study commences with the definition of five porosity distribution models and model validation against the existing literature, ensuring the reliability of our findings. Subsequently, we conducted a comprehensive parametric study to investigate the influence of key factors, including the effect of the thickness ratio, boundary conditions, volume fraction exponents, and porosity coefficients of the top and bottom layers of the FGM sandwich plates on the natural frequency.

V.1 Porosity distribution models

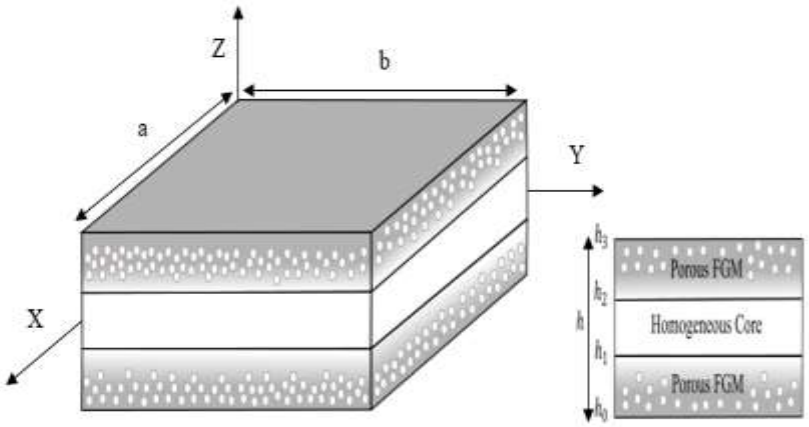

Figure V-1: FGM sandwich plate with porosity model

Researchers have presented several models of porosity distribution to calculate the useful material properties of porous FGM plates [34]. Five even and uneven porosity models were considered in the current work to account for the porosity in each FGM layer of the sandwich plates:

V.1.1 FGM model with even porosities (Imperfect I)

The porosities are evenly distributed across the FGM sandwich layers in this model, whereas the core layer is nonporous (perfect). Having porosities equally distributed (imperfect I), the effective material properties $P^{(l)}$ of FGM layers l (l = 1, 2, 3) are expressed as [34]:

$$\begin{cases} P^1(z) = P_m + (P_c - P_m)V^{(1)}(z) - \frac{\xi_1}{2}(P_c + P_m), \\ P^2(z) = P_m + (P_c - P_m)V^{(2)}(z), \\ P^3(z) = P_m + (P_c - P_m)V^{(3)}(z) - \frac{\xi_2}{2}(P_c + P_m), \end{cases} \quad \text{(V.1)}$$

P_m and P_c are the equivalent characteristics of the metal and ceramic, respectively.

ξ_1, ξ_2 denote the porosity coefficients (ξ_1, ξ_2 "1).

The nonporous FGM sandwich plate is indicated by $\xi_1 = \xi_2 = 0$.

V.1.2 FGM model with uneven porosities (Imperfect II)

The porosities of the FGM sandwich plate expanded along the thickness direction. by the following formulae:

$$\begin{cases} P^1(z) = P_m + (P_c - P_m)V^{(1)}(z) - \frac{\xi_1}{2}(P_c + P_m)\left[1 - \frac{|2z-(h_0+h_1)|}{h_1-h_0}\right], \\ P^2(z) = P_m + (P_c - P_m)V^{(2)}(z), \\ P^3(z) = P_m + (P_c - P_m)V^{(3)}(z) - \frac{\xi_2}{2}(P_c + P_m)\left[1 - \frac{|2z-(h_3+h_2)|}{h_3-h_2}\right], \end{cases} \quad \text{(V.2)}$$

V.1.3 FGM model with logarithmic-uneven porosities (Imperfect III)

A logarithmic function is used in the third model of porosity distribution, and it is expressed as:

$$\begin{cases} P^1(z) = P_m + (P_c - P_m)V^{(1)}(z) - log\left(1 + \frac{\xi_1}{2}\right)(P_c + P_m)\left[1 - \frac{|2z-(h_0+h_1)|}{h_1-h_0}\right], \\ P^2(z) = P_m + (P_c - P_m)V^{(2)}(z), \\ P^3(z) = P_m + (P_c - P_m)V^{(3)}(z) - log\left(1 + \frac{\xi_2}{2}\right)(P_c + P_m)\left[1 - \frac{|2z-(h_3+h_2)|}{h_3-h_2}\right], \end{cases} \quad \text{(V.3)}$$

V.1.4 FGM model with linear-uneven porosities (Imperfect IV)

In this model, the density of porosity changes linearly across the FGM layers and is low at the sandwich's outer surfaces and high at its two interfaces.

$$\begin{cases} P^1(z) = P_m + (P_c - P_m)V^{(1)}(z) - \frac{\xi_1}{2}(P_c + P_m)\left[1 - \frac{z-h_1}{h_0-h_1}\right], \\ P^2(z) = P_m + (P_c - P_m)V^{(2)}(z), \\ P^3(z) = P_m + (P_c - P_m)V^{(3)}(z) - \frac{\xi_2}{2}(P_c + P_m)\left[\frac{z+h_3}{h_2-h_3}\right], \end{cases} \quad \text{(V.4)}$$

V.1.5 FGM model with sinusoidal-uneven porosities (Imperfect V)

The fifth porosity distribution model, which is based on a sinusoidal function, is written as:

$$\begin{cases} P^1(z) = P_m + (P_c - P_m)V^{(1)}(z) - \frac{\xi_1}{2}sin\left(\frac{\pi}{4} + \frac{zh}{2}\right)(P_c + P_m)\left[1 - \frac{|2z-(h_0+h_1)|}{h_1-h_0}\right], \\ P^2(z) = P_m + (P_c - P_m)V^{(2)}(z), \\ P^3(z) = P_m + (P_c - P_m)V^{(3)}(z) - \frac{\xi_2}{2}sin\left(\frac{\pi}{4} + \frac{zh}{2}\right)(P_c + P_m)\left[1 - \frac{|2z-(h_3+h_2)|}{h_3-h_2}\right], \end{cases} \quad \text{(V.5)}$$

V.2 Convergence and Comparison

To verify the accuracy of the proposed model for FGM sandwich plates with porosity, a Convergence and Comparison was performed for the linear free vibration of the results available in the literature.

Table V-1 provides a comprehensive comparison of the nondimensional frequencies of the square FGM sandwich plates as a function of the porosity model (imperfect I) with those predicted by alternative theories, exhibiting convergence among these values, as highlighted in studies by Daikh and Zankour [28] and Van Vinh and Huy [33]. By gradually increasing the polynomial order from 2 to 8, the numerical results achieved the desired accuracy for the simply supported configurations. The tabulated data distinctly reveal a rapid convergence trend with increasing polynomial order, which is particularly evident beyond p = 6, emphasizing the effectiveness and stability of the convergence process in yielding precise solutions.

Table V-1: The convergency and comparison of porosity on the non-dimensional frequencies of FGM square sandwich plate (a/h=10, n=2)

ξ	*p*	Methods	1-0-1	1-1-1	1-2-1	2-1-2	2-2-1	2-1-1
0	2	Present	1.12263	1.25777	1.37901	1.18754	1.34199	1.26450
	4		1.05862	1.18595	1.30045	1.11974	1.26338	1.18971
	6		1.05855	1.18591	1.30040	1.11965	1.26310	1.18951
	8		1.05855	1.18591	1.30040	1.11965	1.26310	1.18951
		HSDT [28]	1.06155	1.18847	1.30244	1.12248	1.24391	1.16529
		HypSDT [33]	1.05205	1.18913	1.30326	1.12305	1.24464	1.16595
0.1	2	Present	1.03963	1.18668	1.32321	1.10846	1.28682	1.20212
	4		0.98015	1.11867	1.24760	1.04486	1.21031	1.12950
	6		0.97007	1.11856	1.24758	1.04478	1.21010	1.12937
	8		0.97007	1.11856	1.24758	1.04478	1.21010	1.12937
		HSDT [28]	0.98258	1.12071	1.24933	1.04712	1.18195	1.09355
		HypSDT [33]	0.98307	1.12134	1.25012	1.04766	1.18265	1.09417
0.2	2	Present	0.93047	1.10396	1.26253	1.01157	1.22558	1.12930
	4		0.87685	1.04040	1.19015	0.95329	1.15118	1.05883
	6		0.87684	1.04036	1.19014	0.95317	1.15094	1.05860
	8		0.87684	1.04036	1.19014	0.95317	1.15094	1.05860
		HSDT [28]	0.87867	1.04201	1.19156	0.95491	1.11054	1.00557
		HypSDT [33]	0.87912	1.04260	1.19231	0.95542	1.11120	1.00616

The non-dimensional frequencies of the square FGM sandwich plates as a function of four porosity models (imperfect I, …., IV) are considered with two values of porosity coefficients

$\xi_1 = \xi_2 = \xi = 0.1$ and 0.2, and the volume fraction exponents $n_1 = n_2 = n = 2$ are presented in Table V-2, and compared with the dose of Daikh and Zankour [29]. We note that in the four porosity models, these findings closely matched those of the analysis.

Table V-2: The comparison of the non-dimensional frequencies of square FGM sandwich plate with porosity distribution (a/h=10)

Porosity	ξ	Methods	1-0-1	1-1-1	1-2-1	2-1-2	2-2-1	2-1-1
Perfect	0	Present	1.05855	1.18591	1.30040	1.11965	1.26310	1.18951
		HSDT [29]	1.06155	1.18847	1.30244	1.12248	1.24391	1.16529
Imperfect I	0.1	Present	0.98007	1.11856	1.24758	1.04478	1.21010	1.12937
		HSDT [29]	0.98258	1.12071	1.24933	1.04712	1.18195	1.09355
	0.2	Present	0.87684	1.04036	1.19014	0.95317	1.15094	1.05860
		HSDT [29]	0.87867	1.04201	1.19156	0.95491	1.11054	1.00557
Imperfect II	0.1	Present	1.02932	1.15520	1.27528	1.08732	1.23895	1.16414
		HSDT [29]	1.03235	1.15768	1.27723	1.09008	1.21572	1.13481
	0.2	Present	0.99729	1.12290	1.24953	1.05262	1.21398	1.13740
		HSDT [29]	1.00033	1.12524	1.25140	1.05528	1.18609	1.10199
Imperfect III	0.1	Present	1.03006	1.15597	1.27589	1.08813	1.23954	1.16477
		HSDT [29]	1.03308	1.15844	1.27785	1.09089	1.21642	1.13558
	0.2	Present	1.00044	1.12599	1.25198	1.05599	1.21637	1.13998
		HSDT [29]	1.00347	1.12837	1.25386	1.05867	1.18894	1.10519
Imperfect IV	0.1	Present	1.02190	1.15354	1.27464	1.08408	1.24395	1.16975
		HSDT [29]	1.05559	1.17079	1.28422	1.10840	1.22699	1.15122
	0.2	Present	1.03187	1.11935	1.24820	1.04566	1.22430	1.14914
		HSDT [29]	1.05213	1.15260	1.26581	1.09394	1.20966	1.13763

V.3 Parametric Study

After verifying the accuracy of the current formulation, a parametric investigation was conducted. The influences of the thickness ratio, boundary conditions, two-volume fraction exponents (n_1, n_2) and two porosity coefficients (ξ_1, ξ_2) of the top and bottom layers of the FGM sandwich plate on the natural frequencies were investigated.

Table V-3 shows the non-dimensional frequencies of a square FGM sandwich plate with two different face's porosities. Five models are considered. The table illustrates that when $\xi_1 = \xi_2 = 0$ for different imperfect porosity models, the non-dimensional frequencies remain consistent, indicating what is termed the "perfect model." The 1-2-1 model shows higher non-dimensional frequency values compared to the 1-0-1 model, which, in contrast, shows the smallest frequencies. The higher the porosity coefficient, the lower non-dimensional frequencies are observed.

Table V-3: non-dimensional frequencies of square FGM sandwich plate with two porosities distribution ($a/h = 10, n_1 = 2, n_2 = 0.5$) for different Imperfect model

Porosity	ξ_1	ξ_2	1-0-1	1-1-1	1-2-1	2-1-2	2-2-1	2-1-1
Imperfect I	0.0	0.0	1.27162	1.36589	1.44579	1.31866	1.39920	1.35396
		0.1	1.25113	1.34233	1.42468	1.29523	1.37679	1.32836
		0.2	1.23056	1.31894	1.40408	1.27177	1.35494	1.30305
	0.1	0.0	1.25204	1.34431	1.42669	1.29692	1.38179	1.33931
		0.1	1.22914	1.31883	1.40428	1.27123	1.35787	1.31181
		0.2	1.20588	1.29338	1.38234	1.24529	1.33445	1.28450
	0.2	0.0	1.23090	1.32236	1.40775	1.27432	1.36382	1.32348
		0.1	1.20525	1.29480	1.38399	1.24613	1.33826	1.29388
		0.2	1.17886	1.26709	1.36061	1.21740	1.31313	1.26434
Imperfect II	0.0	0.0	1.27162	1.36589	1.44579	1.31866	1.39920	1.35396
		0.1	1.26413	1.35461	1.43530	1.30810	1.38795	1.34127
		0.2	1.25698	1.34364	1.42514	1.29782	1.37704	1.32888
	0.1	0.0	1.26478	1.35586	1.43654	1.30918	1.39173	1.34929
		0.1	1.25692	1.34415	1.42574	1.29815	1.38015	1.33620
		0.2	1.24940	1.33275	1.41528	1.28740	1.36889	1.32342
	0.2	0.0	1.25795	1.34594	1.42748	1.29975	1.38436	1.34466
		0.1	1.24970	1.33380	1.41637	1.28824	1.37242	1.33118
		0.2	1.24179	1.32194	1.40560	1.27699	1.36082	1.31800
Imperfect III	0.0	0.0	1.27162	1.36589	1.44579	1.31866	1.39920	1.35396
		0.1	1.26430	1.35488	1.43555	1.30835	1.38822	1.34157
		0.2	1.25764	1.34466	1.42608	1.29877	1.37805	1.33003

	0.1	0.0	1.26495	1.35610	1.43676	1.30941	1.39191	1.34940
		0.1	1.25728	1.34469	1.42623	1.29865	1.38061	1.33664
		0.2	1.25027	1.33407	1.41648	1.28865	1.37013	1.32474
	0.2	0.0	1.25859	1.34687	1.42832	1.30063	1.38505	1.34510
		0.1	1.25057	1.33506	1.41751	1.28944	1.37343	1.33197
		0.2	1.24323	1.32405	1.40749	1.27901	1.36265	1.31973
Imperfect IV	0.0	0.0	1.27162	1.36589	1.44579	1.31866	1.39920	1.35396
		0.1	1.24892	1.34784	1.43174	1.29816	1.38562	1.33731
		0.2	1.22599	1.32994	1.41798	1.27766	1.37233	1.32089
	0.1	0.0	1.27414	1.36114	1.43949	1.31637	1.39838	1.35790
		0.1	1.25102	1.34266	1.42513	1.29540	1.38453	1.34098
		0.2	1.22764	1.32432	1.41106	1.27441	1.37098	1.32429
	0.2	0.0	1.27693	1.35658	1.43342	1.31426	1.39776	1.36213
		0.1	1.25340	1.33767	1.41875	1.29282	1.38365	1.34494
		0.2	1.22957	1.31888	1.40437	1.27133	1.36984	1.32797
Imperfect V	0.0	0.0	1.27162	1.36589	1.44579	1.31866	1.39920	1.35396
		0.1	1.26627	1.35787	1.43832	1.31114	1.39119	1.34493
		0.2	1.26110	1.35001	1.43103	1.30378	1.38337	1.33607
	0.1	0.0	1.26679	1.35879	1.43924	1.31196	1.39392	1.35065
		0.1	1.26126	1.35056	1.43162	1.30421	1.38574	1.34143
		0.2	1.25590	1.34248	1.42417	1.29661	1.37774	1.33237
	0.2	0.0	1.26198	1.35177	1.43279	1.30530	1.38869	1.34739
		0.1	1.25626	1.34332	1.42502	1.29731	1.38035	1.33797
		0.2	1.25071	1.33502	1.41741	1.28948	1.37217	1.32871

Table V-4 shows the non-dimensional frequencies of a square FGM sandwich plate with diverse volume fraction exponents across various models of imperfect porosity. This demonstrates that higher volume fraction exponents result in lower non-dimensional frequencies across all imperfect porosity models.

Table V-4: non-dimensional frequencies of square FGM sandwich plate with two different face's volume fraction exponents and different coefficients of porosity($a/h = 10, \xi_1 = 0.1, \xi_2 = 0.2$)

Porosity	n_1	n_2	1-0-1	1-1-1	1-2-1	2-1-2	2-2-1	2-1-1
Imperfect I	0.0	0.0	1.84368	1.80545	1.79465	1.81887	1.80077	1.81031
		0.1	1.79069	1.76332	1.76037	1.77170	1.77177	1.77568
		0.2	1.74662	1.72802	1.73162	1.73227	1.74744	1.74663
	0.1	0.0	1.79001	1.76273	1.75987	1.77107	1.75400	1.75762
		0.1	1.73407	1.71887	1.72449	1.72167	1.72371	1.72120
		0.2	1.68740	1.68205	1.69477	1.68027	1.69826	1.69058
	0.2	0.0	1.74541	1.72696	1.73070	1.73114	1.71496	1.71388
		0.1	1.68687	1.68157	1.69435	1.67977	1.68354	1.67588
		0.2	1.63788	1.64342	1.66379	1.63663	1.65711	1.64388
Imperfect II	0.0	0.0	1.83901	1.81652	1.81021	1.82428	1.81378	1.81966
		0.1	1.78835	1.77581	1.77682	1.77892	1.78552	1.78615
		0.2	1.74645	1.74182	1.74888	1.74117	1.76187	1.75812
	0.1	0.0	1.78818	1.77562	1.77663	1.77873	1.76863	1.76911
		0.1	1.73486	1.73330	1.74219	1.73133	1.73916	1.73394
		0.2	1.69063	1.69792	1.71335	1.69179	1.71446	1.70446
	0.2	0.0	1.74614	1.74146	1.74853	1.74082	1.73106	1.72731
		0.1	1.69048	1.69775	1.71318	1.69162	1.70053	1.69068
		0.2	1.64418	1.66114	1.68356	1.65051	1.67492	1.65993
Imperfect III	0.0	0.0	1.83834	1.81678	1.81073	1.82422	1.81423	1.81994
		0.1	1.78777	1.77613	1.77738	1.77894	1.78601	1.78648
		0.2	1.74596	1.74220	1.74948	1.74126	1.76239	1.75849
	0.1	0.0	1.78762	1.77595	1.77721	1.77877	1.76915	1.76948
		0.1	1.73439	1.73371	1.74281	1.73144	1.73972	1.73435
		0.2	1.69025	1.69839	1.71401	1.69198	1.71505	1.70492
	0.2	0.0	1.74567	1.74187	1.74915	1.74093	1.73164	1.72775
		0.1	1.69011	1.69822	1.71385	1.69182	1.70115	1.69117
		0.2	1.64391	1.66168	1.68426	1.65079	1.67557	1.66048
Imperfect IV	0.0	0.0	1.82450	1.80987	1.80643	1.81482	1.81474	1.81935
		0.1	1.77423	1.76966	1.77348	1.76995	1.78694	1.78638

		0.2	1.73255	1.73602	1.74586	1.73253	1.76364	1.75874
	0.1	0.0	1.77289	1.76861	1.77264	1.76877	1.76950	1.76866
		0.1	1.71993	1.72680	1.73865	1.72185	1.74051	1.73405
		0.2	1.67590	1.69178	1.71013	1.68264	1.71617	1.70499
	0.2	0.0	1.73016	1.73415	1.74435	1.73041	1.73185	1.72673
		0.1	1.67484	1.69094	1.70946	1.68170	1.70181	1.69068
		0.2	1.62872	1.65469	1.68016	1.64091	1.67657	1.66037
Imperfect V	0.0	0.0	1.83426	1.81860	1.81419	1.82402	1.81670	1.82080
		0.1	1.78430	1.77838	1.78112	1.77925	1.78870	1.78765
		0.2	1.74300	1.74482	1.75346	1.74201	1.76528	1.75993
	0.1	0.0	1.78417	1.77824	1.78099	1.77911	1.77207	1.77090
		0.1	1.73161	1.73645	1.74690	1.73235	1.74288	1.73612
		0.2	1.68805	1.70153	1.71835	1.69337	1.71843	1.70699
	0.2	0.0	1.74277	1.74455	1.75320	1.74175	1.73494	1.72965
		0.1	1.68794	1.70139	1.71823	1.69325	1.70472	1.69346
		0.2	1.64237	1.66528	1.68891	1.65274	1.67937	1.66309

The effect of the thickness ratio (h/a) on the nondimensional natural frequency parameters is presented in Figs. V-2-V-3. Four porosity models (imperfect I …., IV) were considered with two values of the porosity coefficients $\xi_1 = \xi_2 = \xi = 0.1$ and 0.2. A six-layer FGM-sandwich plate was used. It can be seen from the figures that for the model with imperfect porosity IV, the fundamental frequency parameters decrease with an increase in the thickness ratio. For the first model $\xi = 0.1$ and $\xi = 0.2$ for the second model of porosity. However, the frequency parameters of the third model (imperfect III) increased from h/a=0.05. A similar behavior is observed for the first model with $\xi = 0.2$, and the second model with $\xi = 0.1$.

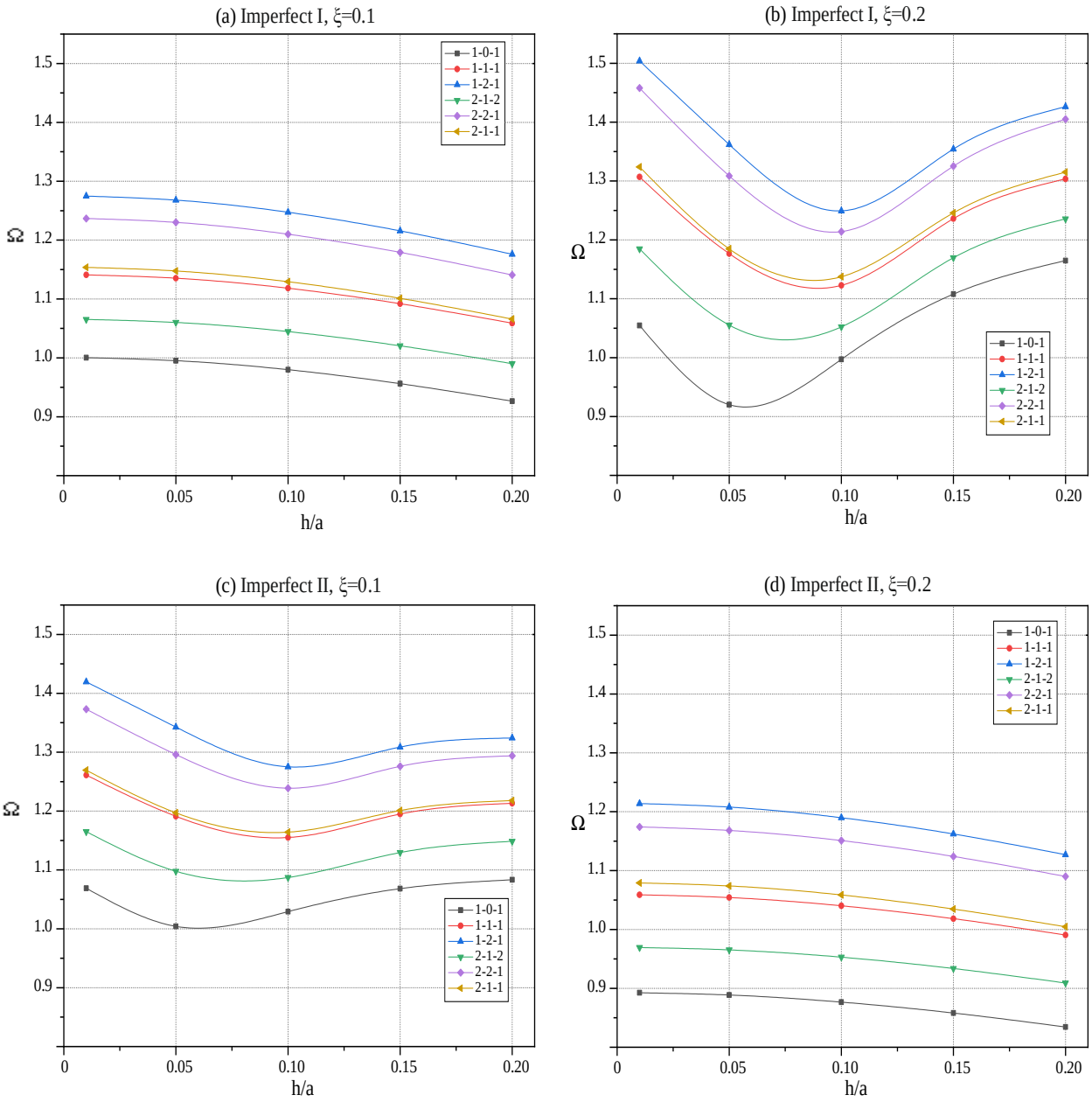

Figure V-2: Effect of thickness ratio index of fundamental frequency parameters for FGM sandwich models with porosity (n=2; imperfect I and II)

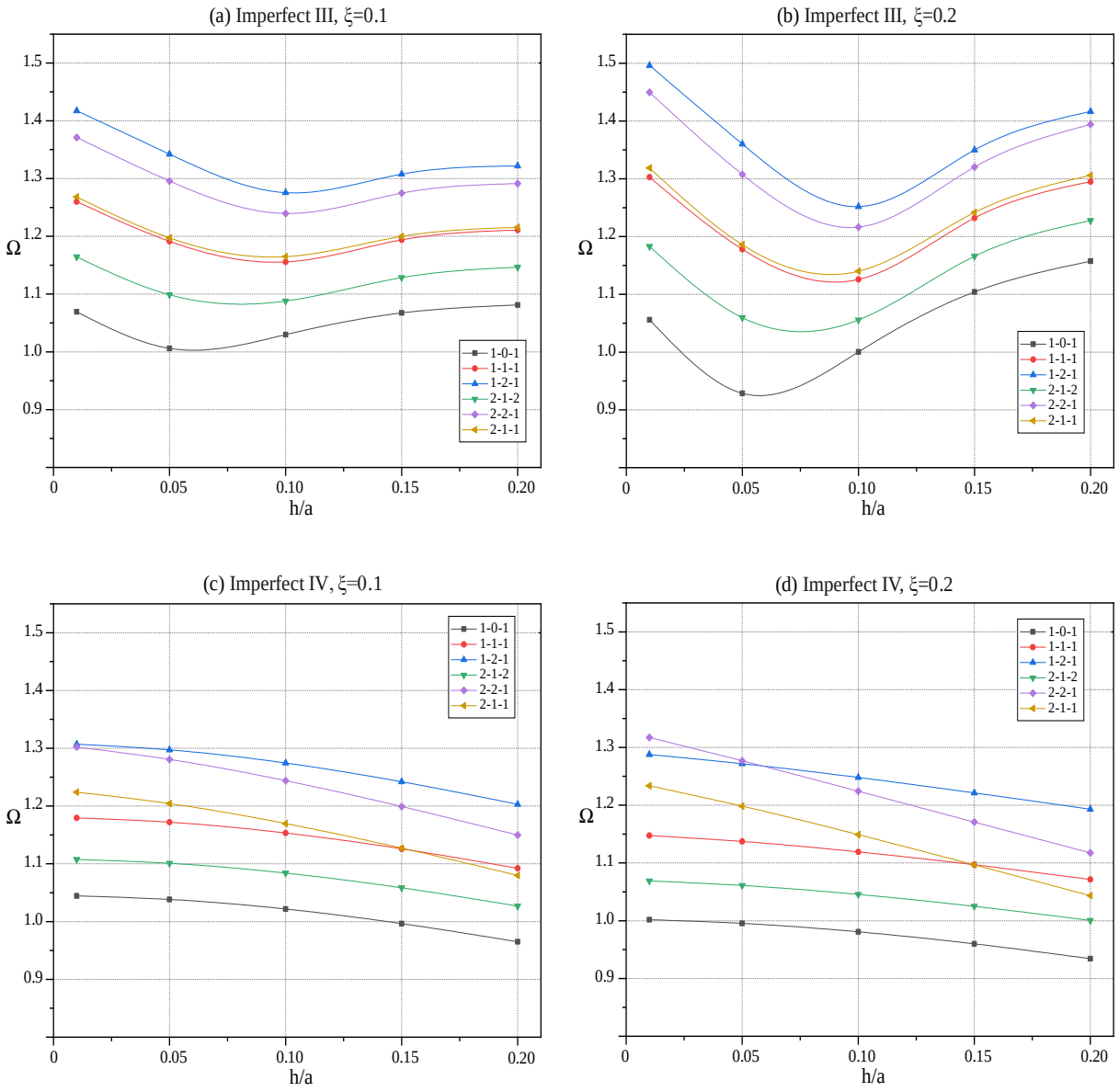

Figure V-3: Effect of thickness ratio index of fundamental frequency parameters for FGM sandwich models with porosity (n=2; imperfect III and IV)

The nondimensional frequencies as a function of the thickness ratio (h/a) for perfect and five porosity distributions are presented in Figure V-4. When the thickness ratio increased from 0 to 0.2, and the porosity coefficient $\xi = \xi_1 = \xi_2 = 0.2$, two behaviors were observed. In the first case, the frequency parameters decrease as the models become perfect, imperfect I, and imperfect IV. However, in the second case, they increased after decreasing in models imperfect II, imperfect III, and imperfect V. A similar behavior was observed for the symmetric and non-symmetric FGM sandwich plates.

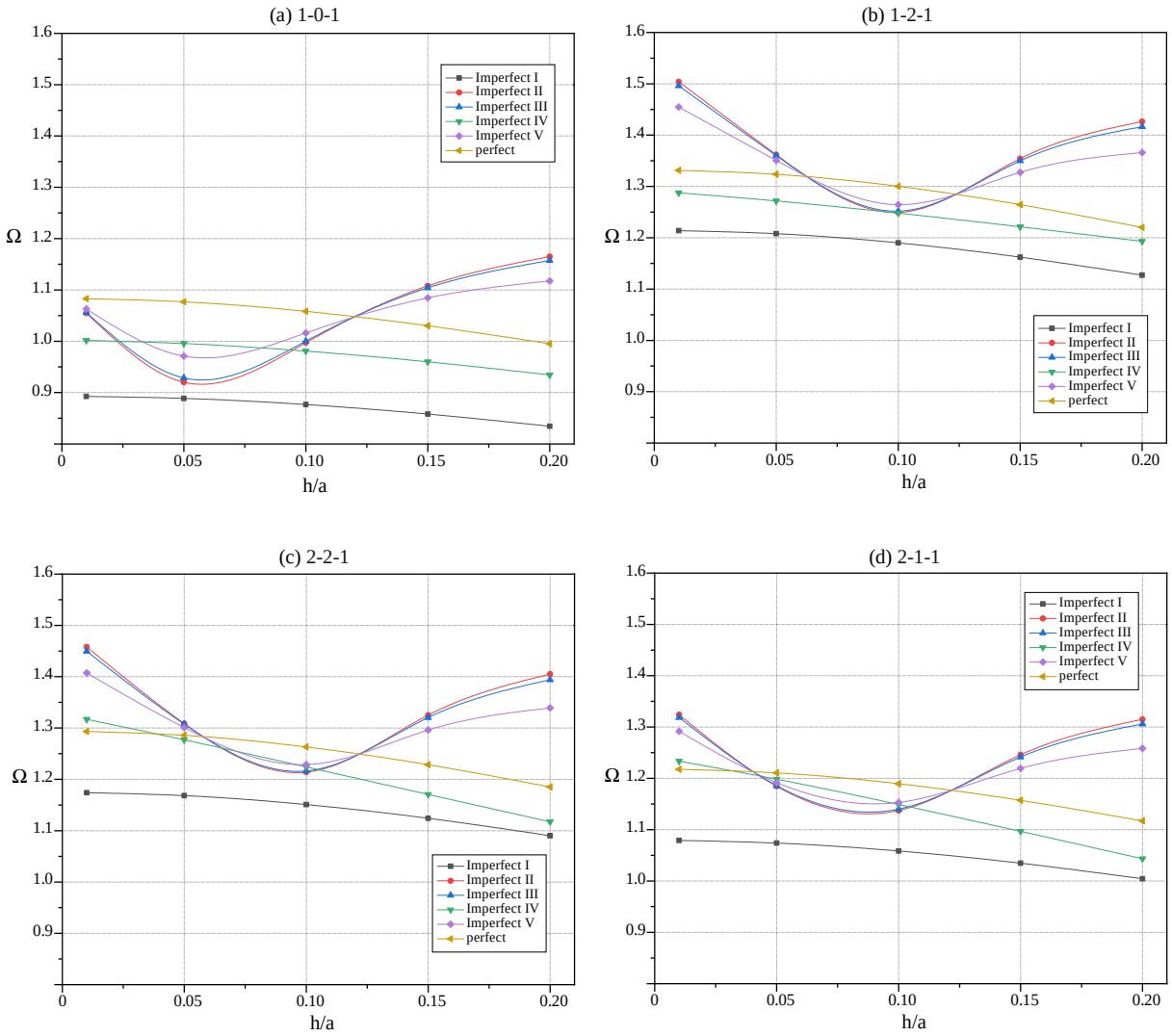

Figure V-4: effect of thickness ratio index of the linear frequency parameters for perfect and porosity distribution of FGM sandwich plates (n=2; ξ=0.2)

The influence of the boundary conditions is presented in Figure V-5, fully clamped (CCCC), clamped at two opposite edges and simply supported at two opposite edges (CSCS), simply supported at two continuous edges and clamped at next two edges (SSCC), and fully simply supported (SSSS) are considered. It can be observed from the figure that the frequencies decrease as the porosity coefficient increases. The highest values of the frequency parameters were obtained under the CCCC boundary conditions. However, SSSS yields the smallest value. Similar behavior was observed for the five porosity distributions. This is due to the increase in edge constraints.

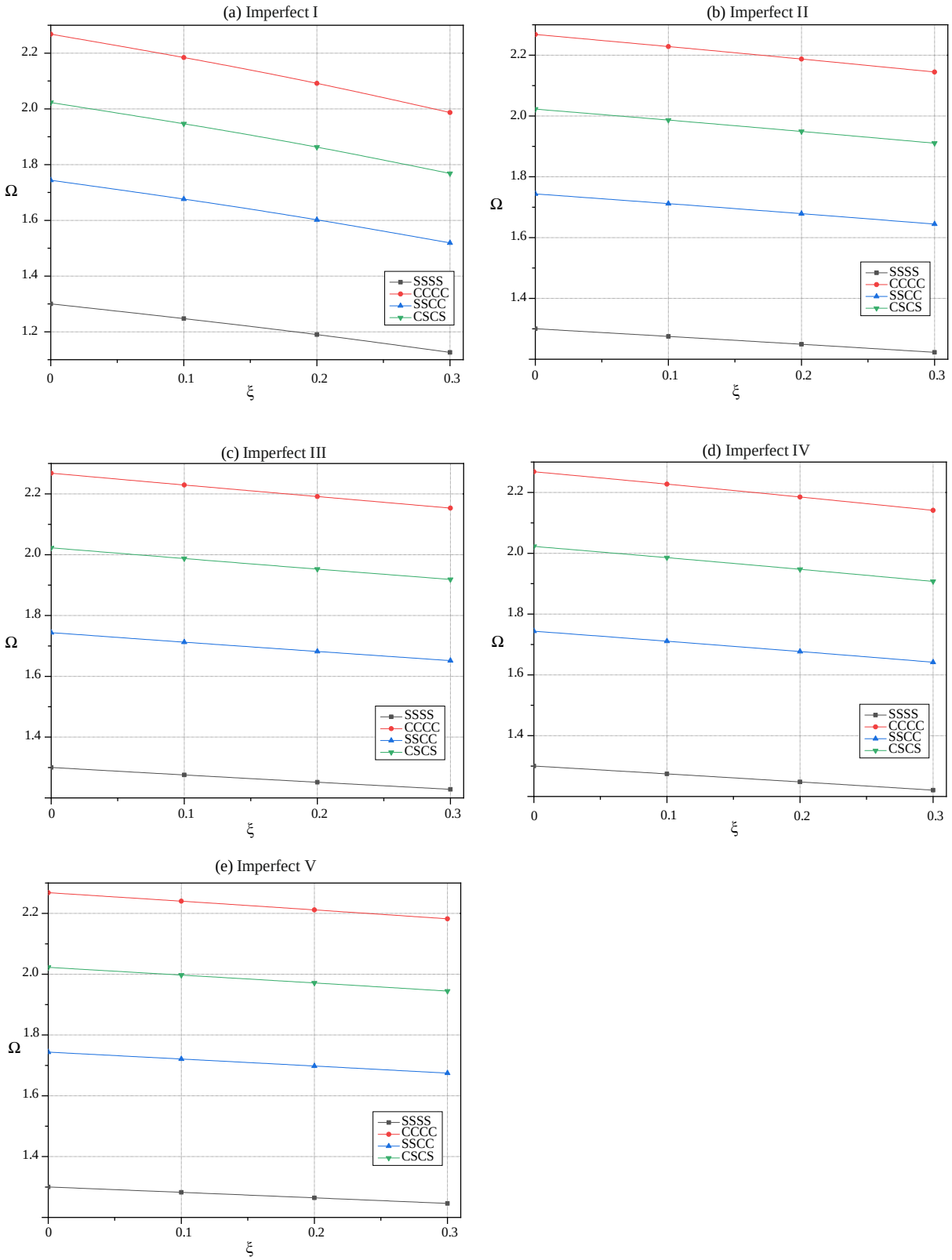

Figure V-5: effect of the porosity coefficient on frequency parameters for different boundary condition of square FGM sandwich plates (n=2; 1-2-1)

Figure V-6 shows the influence of the volume fraction exponent $(n = n_1 = n_2 = 0, \dots, 5)$ on the frequency parameters of the SSSS square FGM sandwich plate with a porosity coefficient of $\xi = 0.2$. It can be observed from this figure that imperfect I (even porosity model) is obtained from the separated curve of the other models. The curves of the uneven models (imperfections II, ..., V) are indistinguishable. Increasing the volume fraction exponent value causes a more significant separation of the first model (even the porosity model).

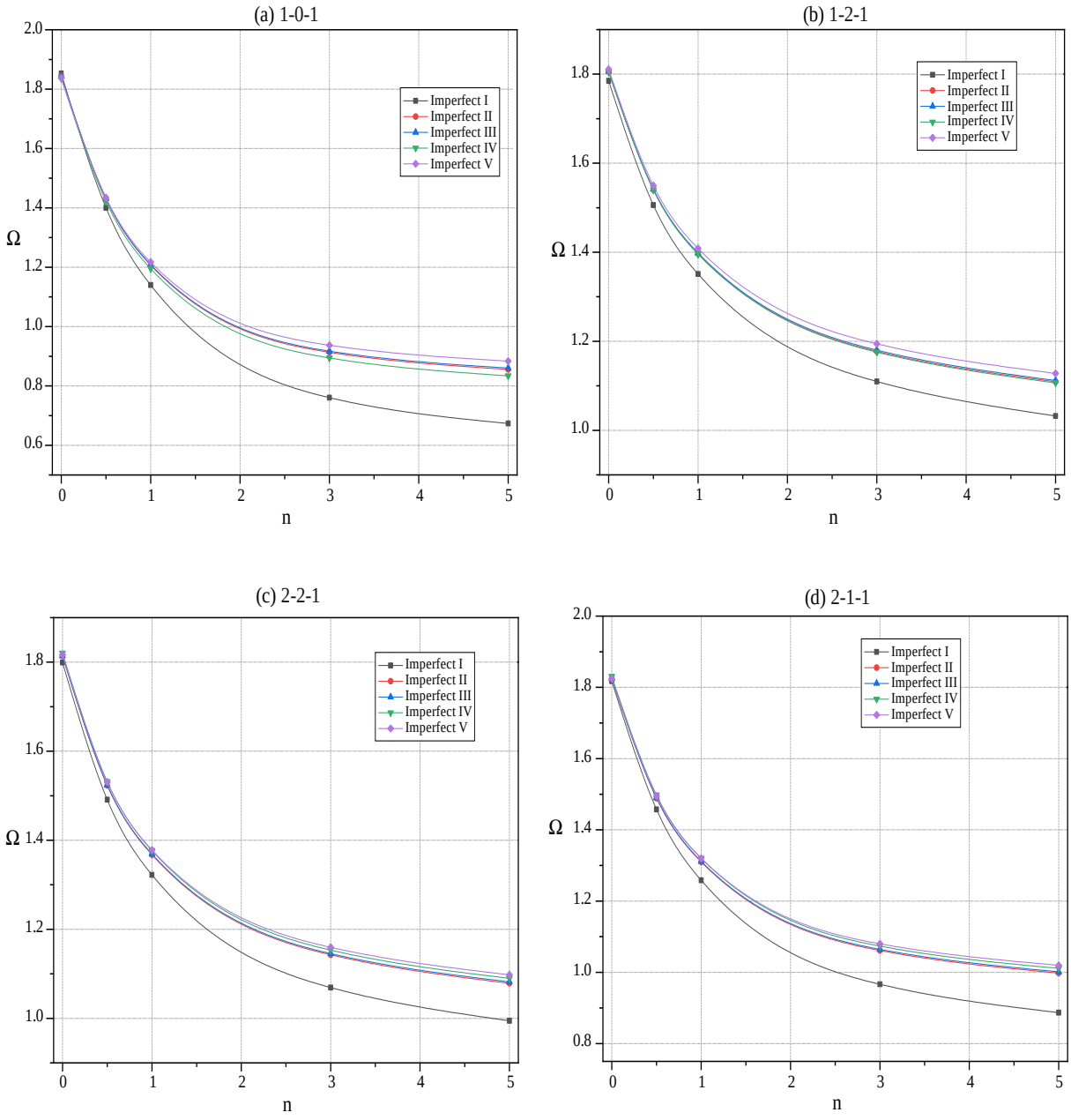

Figure V-6: the effect of the volume fraction exponent and porosity models on the frequency parameters of SSSS square FGM sandwich plates (ξ=0.2)

Figure V-7 plots the influence of the porosity coefficient on the vibration frequency parameters of the square porous FGM sandwich plates for the five imperfect types. The types of FGM sandwich plates considered in this example are (1-0-1, 1-2-1, 1-1-1, and 2-1-1), and the values of the volume fraction exponent taken are (n=n_1=n_2=0.5). For the first two cases where n=0.5 the variation curves are straight lines; that is, the variation is linear between the frequency parameters and the porosity coefficient. For this volume fraction value, the dominant physical properties of the FGM sandwich plate were the properties of the ceramic. However, for the last two cases, the increase in the porosity coefficient values decreases with a non-linear curve, which can result in the fact that in these two cases, the dominant physical properties of the plate are the properties of the metal. Therefore, the influence of the porosity coefficient on the vibration behavior of an FGM sandwich plate depends on the rate of mixing of the layers of this plate.

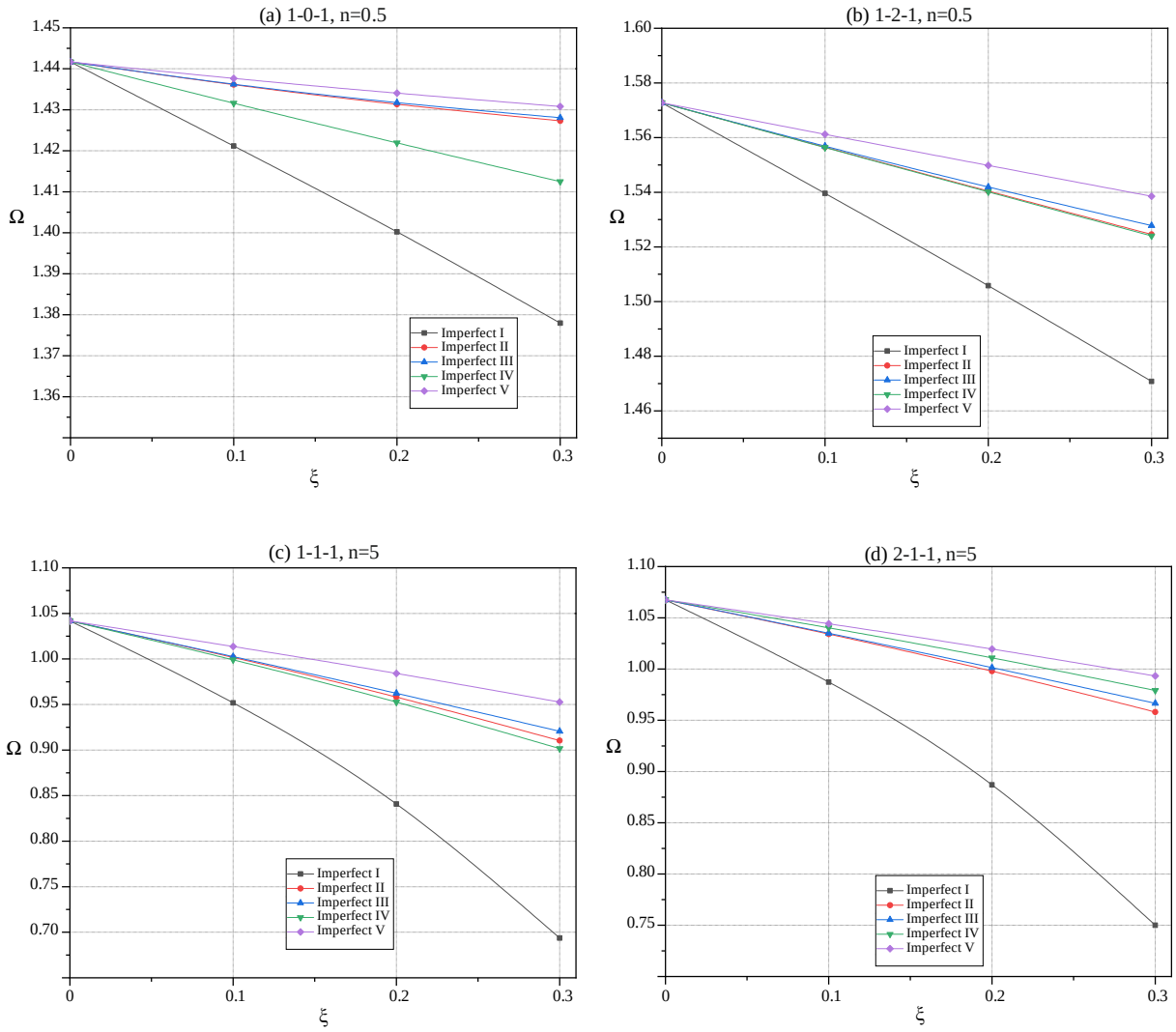

Figure V-7: the influence of the porosity coefficient models on the free vibration frequencies of square FGM sandwich plates

Figures V-8-V-9 illustrate the contour plot of the linear frequency parameters as a function of the volume fraction exponent for the SSSS square FGM sandwich plate with porosity. This contour was plotted for the calculated values of the frequency parameters as a function of the two-volume fraction exponents, (n_1) of the bottom, and (n_2) of the top layers. An increase in the volume fraction exponents n_1 and n_2 from 0 to 10 reduces the frequency parameters. The maximum frequency is denoted by red and is associated with lower values of (n_1) and (n_2), whereas the minimum frequency is indicated in purple. If we take the 1st case of Figure 5.8, the red color represents the maximum values of the frequency parameters ($\Omega \geq 1.711$), whereas the purple color represents the smallest values of the frequency parameters in this contour ($\Omega \leq 0.9344$); for example, the green color represents the values of the frequency parameters ($1.322 \leq \Omega \leq 1.452$). For the other colors (yellow, orange blue, and sky blue), each color represents a range of frequency parameter values.

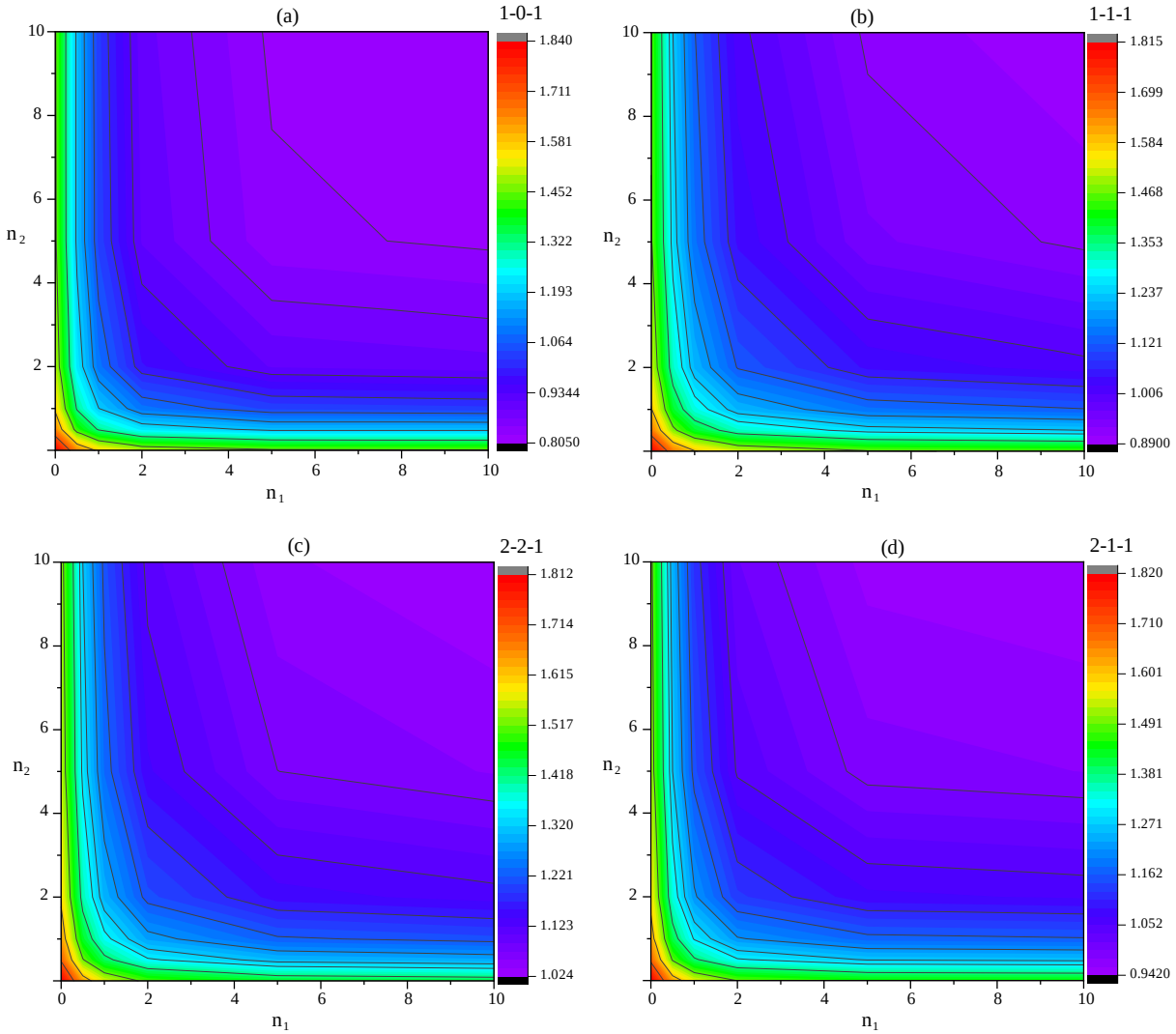

Figure V-8: Contour plot of linear frequency parameter of the volume fraction exponent for SSSS square FGM sandwich plate with porosity (ξ=0.1; Imperfect I)

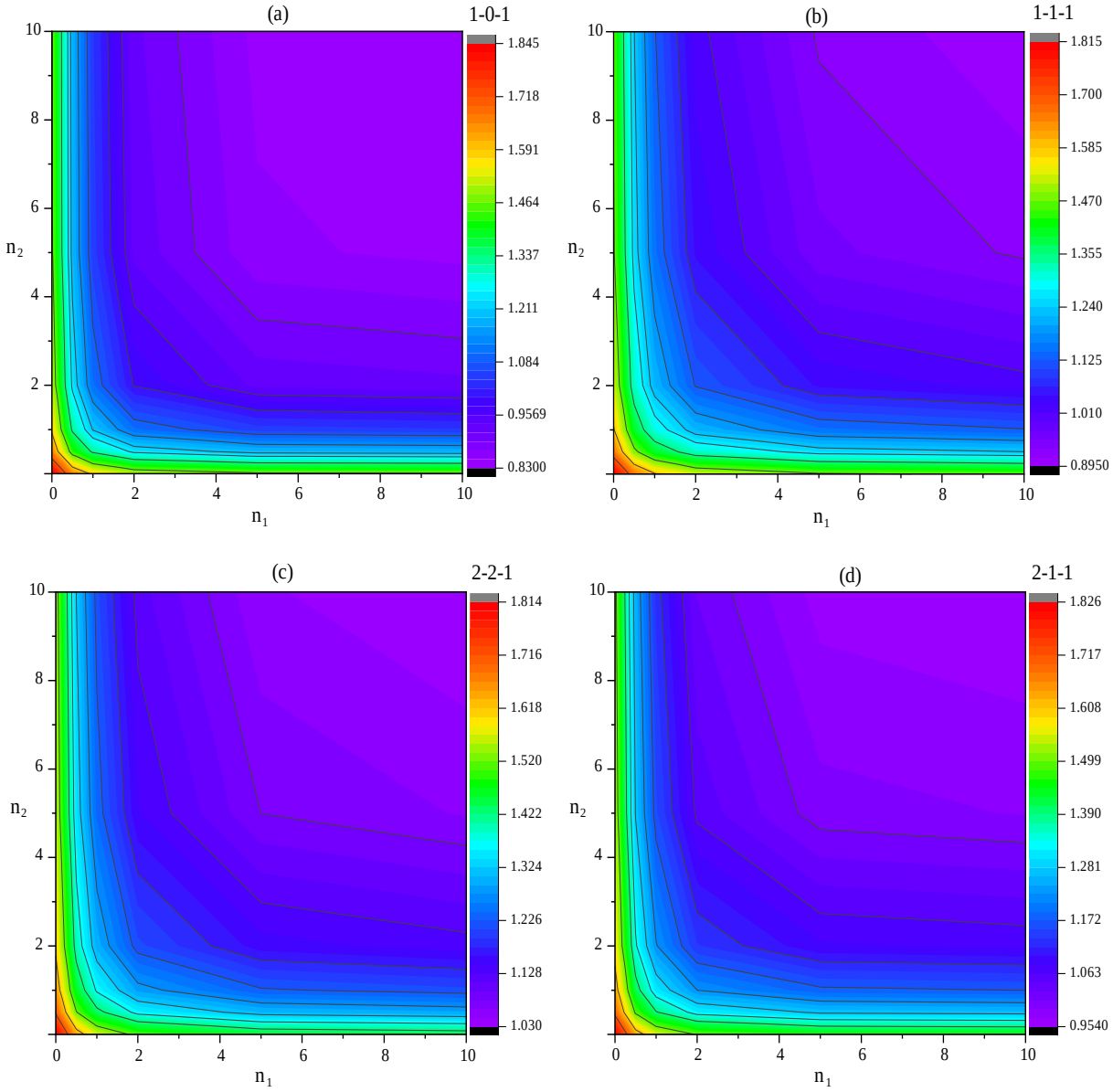

Figure V-9: Contour plot of linear frequency parameter of the volume fraction exponent for SSSS square FGM sandwich plate with porosity (ξ=0.2; Imperfect II)

The effect of the porosity coefficient on the frequency parameters of the SSSS square FGM sandwich plates is plotted in Figures V-10, V-11.

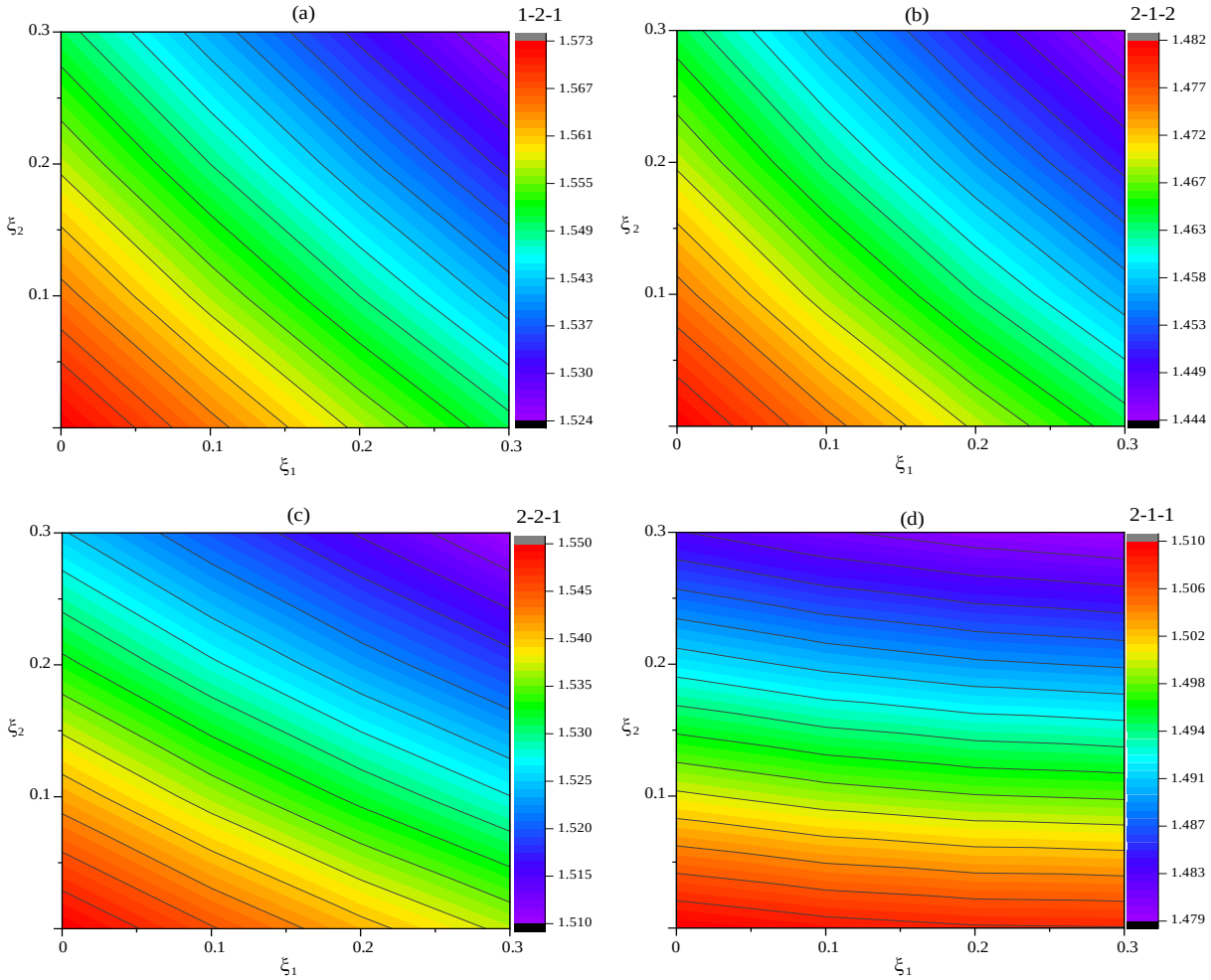

Figure V-10: Contour plot of linear frequency parameter of porosity coefficient for FGM sandwich plates. (n=0.5; Imperfect II)

The frequency parameters decreased when the porosity coefficients ξ_1 and ξ_2 increased. This can be observed from the figures. V-8, V-11 that the geometrical and physical symmetric plates produced symmetric plots. The most significant variations are in the directions of (n_1) and (ξ_1). This illustrates the effect of the bottom layer mixture on the frequency parameters of the porous FGM sandwich plates. The maximum results of the frequency parameter values for the symmetric plates were obtained for small values of (ξ_1, n_1) or (ξ_2, n_2) and for large values of (ξ_1, n_1) or (ξ_2, n_2). For the other types (non-symmetric), the maximum values of the frequency parameters can only be obtained by increasing the values of the bottom layers and decreasing those of the top layers.

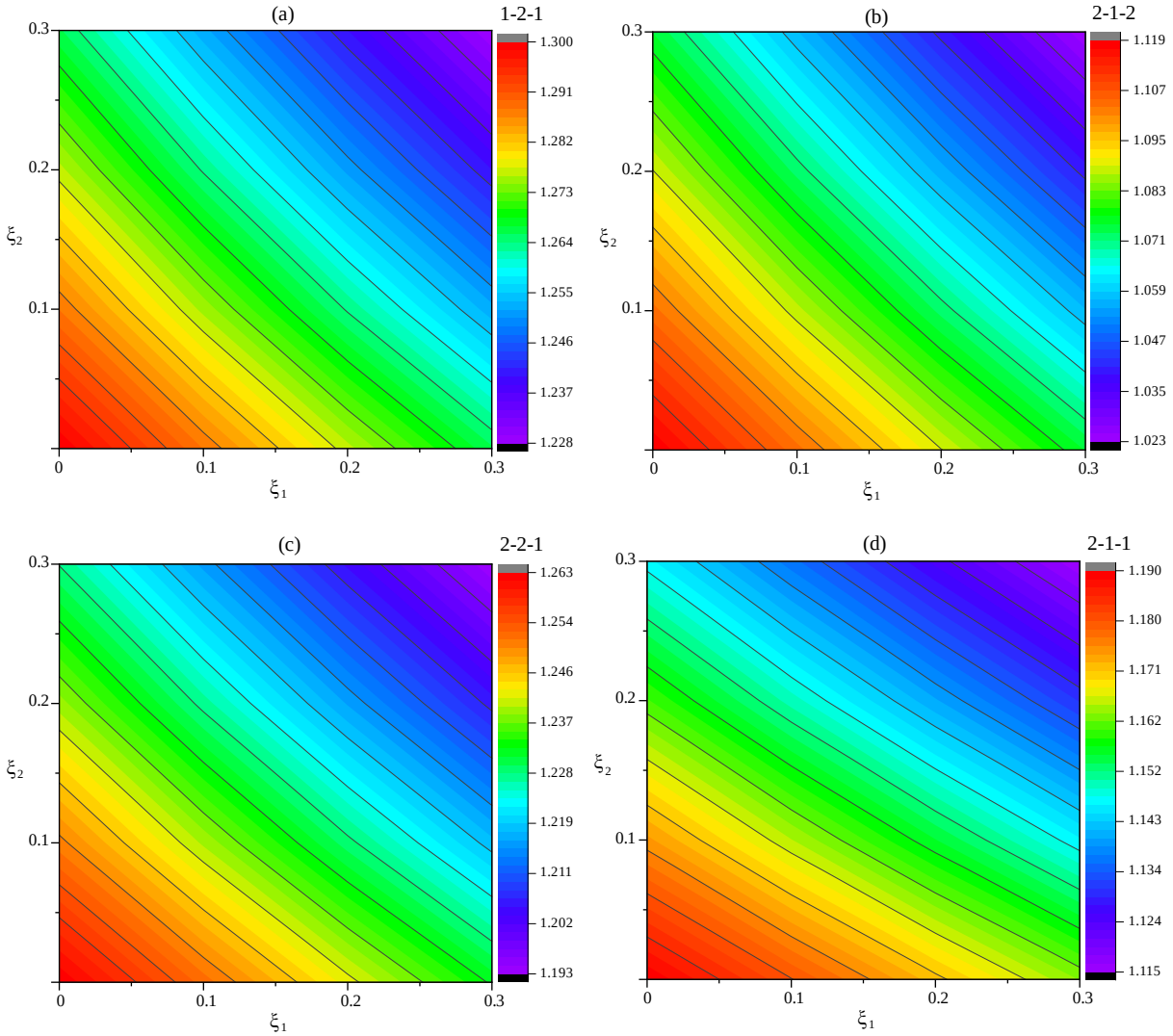

Figure V-11: Contour plot of linear frequency parameter of porosity coefficient for FGM sandwich plates. (n=2; Imperfect III)

Figure. V-12 shows a contour plot of the frequency parameters for simply supported FGM sandwich plates as a function of the porosity coefficient and volume fraction exponent. It can be observed that the frequency decreased as the porosity coefficient increased from 0 to 0.3, and the volume fraction increased from 0 to 10. This type of graph is new in the literature, which varies the porosity coefficient and exponent of the volume fraction at the same time. This variation gives contour plots for the frequency parameters for four types of FGM sandwich plates (1-0-1, 1-1-1, 2-2-1 and 2-1-1). The black curves indicate the same frequency parameter values. Note that for the values of ($0 \leq n \leq 1$), where the mixture contains more ceramic, we obtained straight curves from which the variation is linear of the frequency parameters as a function of the porosity coefficient. On the other hand, in the zone where the mixture contains

the most metal (1≤n≤10), if ξ is changed while n is fixed, the trajectory will cross several contour curves. This provides a nonlinear variation in the frequency parameters as a function of the porosity coefficient. According to these results, the porosity coefficient and mixing rate of the layers influence the rigidity or flexibility of the porous FGM sandwich plate.

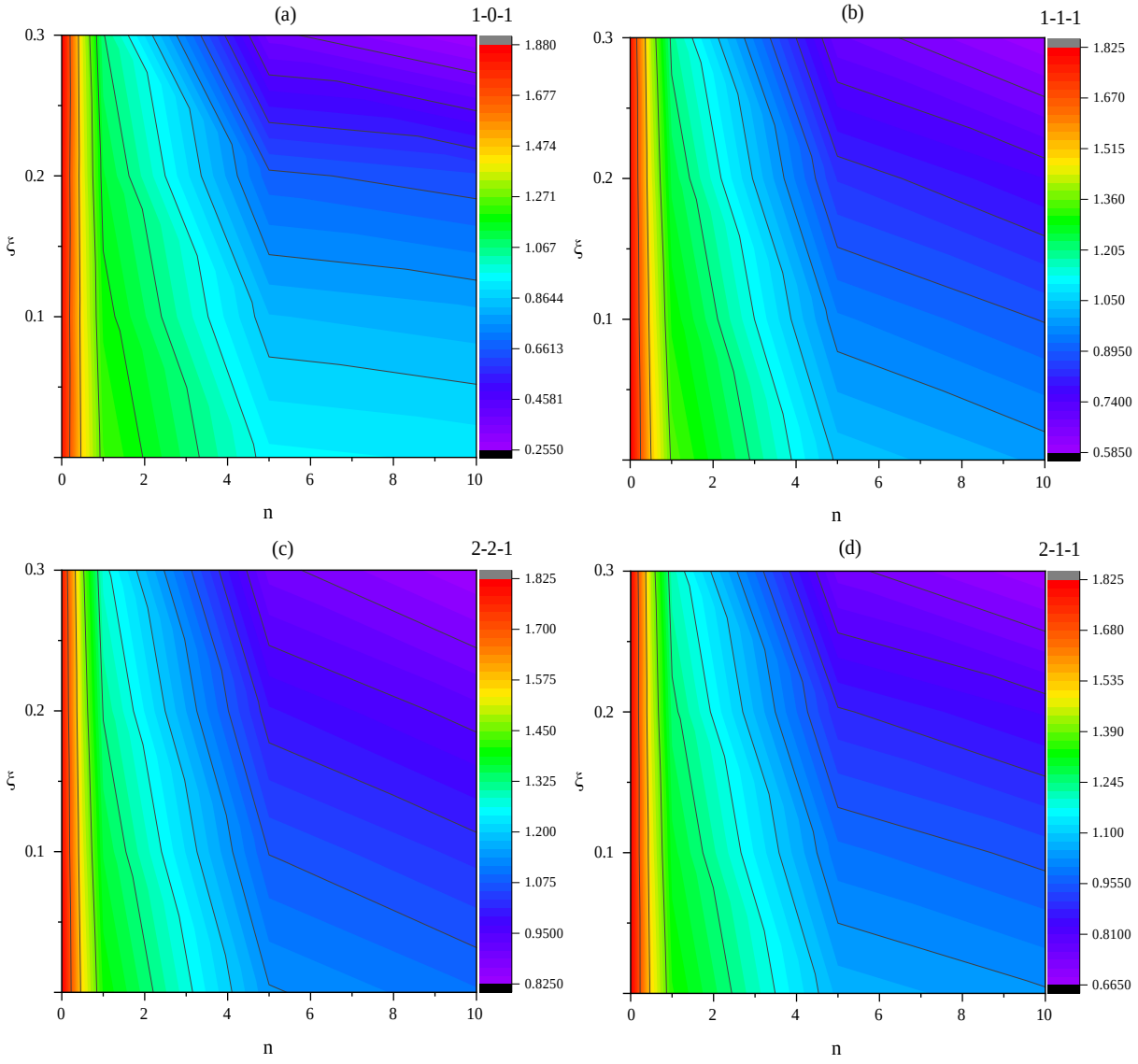

Figure V-12: Contour plot of linear frequency parameter of porosity and the volume fraction exponent for FGM sandwich plates (Imperfect I)

V.4 Summary

In this concluding chapter, the effect of porosity distribution on FGM sandwich plates was investigated using the p-version of FEM and FSDT. The study demonstrated accuracy compared to the literature results and explored the effects of various parameters on the natural frequency. The stability of the results with a precision of six digits for polynomials of order six, excellent agreement with other methods, nonlinear frequency parameter trends influenced by plate thickness and porosity type, and significant impacts of volume fraction exponents and porosity coefficients on frequency parameters lead to insights into vibrational behavior and material properties. This work has opened the way to an in-depth discussion of the parameters influencing the free vibration behavior of FGM sandwich plates with unequal layer porosities for the first time.

Chapter VI

General Conclusion and Future Directions

Chapter VI

General Conclusion and Future Directions

This thesis presents the linear free vibrations of an FGM sandwich plate with a porosity. First-order shear deformation theory has been applied to derive equations of motion describing the free vibrations of plates. A p-version of the FEM model was developed to handle the above-mentioned problems accurately and efficiently. Several parametric studies have been conducted on the subject of linear free vibrations of FGM sandwich plates with porosity, and detailed conclusions have been drawn at the end of each chapter. In the following sections, some important conclusions are summarized with respect to the numerical model, its implementation and results of parametric studies mentioned in previous chapters, and recommendations for future work.

VI.1 Conclusions

Our study successfully validated the combined use of first-order shear deformation theory and the p-version of the FEM. When applied to plates, these theories have demonstrated accuracy and reliability in capturing the mechanical behavior of the system.

For a degree of polynomials of order six, the convergence investigation conducted in this work provides stability of the results with a precision of six digits. To test the quality and precision of the proposed p-element, a comparative study was conducted between the present results and those obtained by other methods (TSDT, SSDT, DQM, HypSDT, and HSDT).

Excellent agreement was found between the two results, with an order of precision of five digits. The effect of the plate thickness on the frequency parameters is not governed by a linear law; sometimes, there is a decrease followed by an increase in the values of the frequency parameters. The FGM sandwich plates that exhibit this behavior are Imperfects II, III, and V.

This type of imperfect is a model of FGM sandwich plates with uneven porosities, logarithmic-uneven porosities, and sinusoidal-uneven porosities. Thus, we conclude that there is an interaction between the effect of the thickness and type of imperfection on the vibrational behavior of the FGM sandwich plate with porosity.

An increase in the porosity coefficient led to a decrease in the frequency parameters for all the five types of imperfections. The largest values were obtained for the clamped plate with a sinusoidal-uneven type of porosity. This results in the fact that this plate is more rigid than other plates. This influence is especially focused on the values of $(0 \leq n_1, n_2 \leq 2)$, and these values represent a change in physical properties from ceramic to metal. This decrease in the frequency parameter makes the sandwich plate more flexible. The influence of the porosity coefficients on the frequency parameters decreases almost linearly when the values of $(\xi_1 and\ \xi_2)$ increase. By increasing the values of $(\xi_1 and\ \xi_2)$, the values of the physical properties of the plate and its mass decrease, making the plate less rigid.

This work has opened the way to an in-depth discussion of the parameters influencing the free vibration behavior of FGM sandwich plates with unequal layer porosities for the first time.

VI.2 Suggestions for potential future work

The work in this thesis is limited and future improvements should be considered:

- Extension to Include Nonlinear Effects: Investigate the effects of nonlinearities on the free vibration behavior of FGM sandwich plates with porosity. This could involve incorporating material nonlinearity, geometric nonlinearity, or both, to provide a more

comprehensive understanding of the structural response under varying loading conditions.

- Consideration of temperature effects: The influence of temperature variations on the free vibration characteristics of the FGM sandwich plates with porosity was explored. Incorporating thermal effects into the analysis can help assess the structural stability and performance of the FGM sandwich plates in real-world operating environments.
- Optimization Studies for Performance Enhancement: Conduct optimization studies to maximize the free vibration characteristics of the FGM sandwich plates with porosity. This could involve optimizing the material distribution, porosity levels, or geometric configurations to achieve the desired vibration modes or enhance the structural performance while considering the manufacturing constraints.
- Experimental validation and verification: Numerical models developed for the free vibration analysis of porous FGM sandwich plates were experimentally validated and verified. Experimental testing can provide crucial insights into the accuracy and reliability of numerical predictions, thereby ensuring confidence in the analytical results.
- Exploration of Advanced Material Models: Explore advanced material models beyond first-order shear deformation theory (FSDT) to capture more complex behaviors exhibited by porous FGM sandwich plates. We consider higher-order theories and models that account for material microstructures or nonlocal effects to improve the accuracy of the analysis.
- Dynamic stability and response: The dynamic stability and response of the FGM sandwich plates with porosity subjected to external excitations or dynamic loading conditions were investigated. Phenomena such as flutter, resonance, and dynamic buckling were analyzed to assess the structural integrity and resilience of FGM sandwich plates in dynamic environments.
- The presented model can be further extended to nanostructures (e.g., shells, 3D solids...)

Bibliography

[1] B. Saleh, J. Jiang, A. Ma, D. Song, D. Yang, and Q. Xu, ‘Review on the Influence of Different Reinforcements on the Microstructure and Wear Behavior of Functionally Graded Aluminum Matrix Composites by Centrifugal Casting’, *Metals and Materials International*, vol. 26, no. 7. 2020. doi: 10.1007/s12540-019-00491-0.

[2] K. Swaminathan, D. T. Naveenkumar, A. M. Zenkour, and E. Carrera, ‘Stress, vibration and buckling analyses of FGM plates-A state-of-the-art review’, *Composite Structures*, vol. 120. Elsevier Ltd, pp. 10–31, Feb. 01, 2015. doi: 10.1016/j.compstruct.2014.09.070.

[3] K. Swaminathan and D. M. Sangeetha, ‘Thermal analysis of FGM plates – A critical review of various modeling techniques and solution methods’, *Composite Structures*, vol. 160. Elsevier Ltd, pp. 43–60, Jan. 15, 2017. doi: 10.1016/j.compstruct.2016.10.047.

[4] M. Alimoradzadeh, S. D. Akbas, M. Alimoradzadeh, and S. D. Akbas, ‘Structural Engineering and Mechanics’, *Structural Engineering and Mechanics*, vol. 81, no. 6, p. 705, Mar. 2022, doi: 10.12989/SEM.2022.81.6.705.

[5] H. T. Thai and S. E. Kim, ‘A review of theories for the modeling and analysis of functionally graded plates and shells’, *Composite Structures*, vol. 128. 2015. doi: 10.1016/j.compstruct.2015.03.010.

[6] A. Gupta and M. Talha, ‘Recent development in modeling and analysis of functionally graded materials and structures’, *Progress in Aerospace Sciences*, vol. 79. 2015. doi: 10.1016/j.paerosci.2015.07.001.

[7] N. J. Kanu, U. K. Vates, G. K. Singh, and S. Chavan, ‘Fracture problems, vibration, buckling, and bending analyses of functionally graded materials: A state-of-the-art review including smart FGMS’, *Particulate Science and Technology*, vol. 37, no. 5. Taylor and Francis Inc., pp. 579–604, Jul. 04, 2019. doi: 10.1080/02726351.2017.1410265.

[8] A. Toudehdehghan, J. W. Lim, K. E. Foo, M. I. N. Ma'Arof, and J. Mathews, 'A brief review of functionally graded materials', in *MATEC Web of Conferences*, 2017. doi: 10.1051/matecconf/201713103010.

[9] A. Garg, M. O. Belarbi, H. D. Chalak, and A. Chakrabarti, 'A review of the analysis of sandwich FGM structures', *Composite Structures*, vol. 258. Elsevier Ltd, Feb. 15, 2021. doi: 10.1016/j.compstruct.2020.113427.

[10] P. T. Dat, D. Van Thom, and D. T. Luat, 'Free vibration of functionally graded sandwich plates with stiffeners based on the third-order shear deformation theory', *Vietnam Journal of Mechanics*, vol. 38, no. 2, pp. 103–122, Jun. 2016, doi: 10.15625/0866-7136/38/2/6730.

[11] Y. Wang, 'Mesh refinement of finite element method for free vibration analysis of variable geometrical rotating cylindrical shells', *Engineering Computations (Swansea, Wales)*, vol. 40, no. 1, pp. 210–228, Feb. 2023, doi: 10.1108/EC-02-2022-0082.

[12] Y. Wang, J. Hu, D. Kennedy, J. Wang, and J. Wu, 'Adaptive mesh refinement for finite element analysis of the free vibration disturbance of cylindrical shells due to circumferential micro-crack damage', *Engineering Computations (Swansea, Wales)*, vol. 39, no. 9, pp. 3271–3295, Nov. 2022, doi: 10.1108/EC-09-2021-0555.

[13] S. A. Belalia, 'Investigation of the mechanical properties on the large amplitude free vibrations of the functionally graded material sandwich plates', *Journal of Sandwich Structures and Materials*, vol. 21, no. 3, pp. 895–916, Mar. 2019, doi: 10.1177/1099636217701299.

[14] S. A. Belalia, 'A new analysis of nonlinear free vibration behavior of bi-functionally graded sandwich plates using the p-version of the finite element method', *Mechanics of Advanced Materials and Structures*, vol. 26, no. 8, pp. 727–740, Apr. 2019, doi: 10.1080/15376494.2017.1410912.

[15] S. A. Belalia, 'A curved hierarchical finite element method for the nonlinear vibration analysis of functionally graded sandwich elliptic plates', *Mechanics of Advanced Materials and Structures*, vol. 26, no. 13, pp. 1115–1129, Jul. 2019, doi: 10.1080/15376494.2018.1430277.

[16] Y. Wang, ‘Adaptive mesh refinement for finite element analysis of elastic buckling disturbance of circularly curved beams due to multiple micro-cracks damage’, *Engineering Computations (Swansea, Wales)*, vol. 40, no. 1, pp. 191–209, Feb. 2023, doi: 10.1108/EC-01-2022-0016.

[17] Y. Wang and J. Wang, ‘An hp-version adaptive finite element algorithm for eigensolutions of moderately thick circular cylindrical shells via error homogenisation and higher-order interpolation’, *Engineering Computations (Swansea, Wales)*, vol. 39, no. 5, pp. 1874–1901, May 2022, doi: 10.1108/EC-07-2021-0430.

[18] V. N. Burlayenko and T. Sadowski, ‘Free vibrations and static analysis of functionally graded sandwich plates with three-dimensional finite elements’, *Meccanica*, vol. 55, no. 4, pp. 815–832, Apr. 2020, doi: 10.1007/s11012-019-01001-7.

[19] S. IRFAN and F. SIDDIQUI, ‘A review of recent advancements in finite element formulation for sandwich plates’, *Chinese Journal of Aeronautics*, vol. 32, no. 4. Chinese Journal of Aeronautics, pp. 785–798, Apr. 01, 2019. doi: 10.1016/j.cja.2018.11.011.

[20] M. Yaylacı *et al.*, ‘Structural Engineering and Mechanics’, *Structural Engineering and Mechanics*, vol. 76, no. 3, p. 325, Nov. 2020, doi: 10.12989/SEM.2020.76.3.325.

[21] J. Zhang, W. Yang, J. Chen, and R. Xu, ‘Direct evaluation of the stress intensity factors for the single and multiple crack problems using the p-version finite element method and contour integral method’, *Applied Sciences (Switzerland)*, vol. 11, no. 17, Sep. 2021, doi: 10.3390/app11178111.

[22] M. H. Ghazwani, ‘A Novel nth-Order Shear Deformation Theory for the Bending and Free Vibration Analysis of Bi-functionally Graded Sandwich Plates’, *Iranian Journal of Science and Technology - Transactions of Civil Engineering*, vol. 48, no. 1, 2024, doi: 10.1007/s40996-023-01162-2.

[23] P. Van Vinh, ‘Deflections, stresses and free vibration analysis of bi-functionally graded sandwich plates resting on Pasternak’s elastic foundations via a hybrid quasi-3D theory’, *Mechanics Based Design of Structures and Machines*, vol. 51, no. 4, 2023, doi: 10.1080/15397734.2021.1894948.

[24] P. Kumar and C. V. Srinivasa, ‘On buckling and free vibration studies of sandwich plates and cylindrical shells: A review’, *Journal of Thermoplastic Composite Materials*, vol. 33, no. 5. 2020. doi: 10.1177/0892705718809810.

[25] R. Meksi, S. Benyoucef, A. Mahmoudi, A. Tounsi, E. A. Adda Bedia, and S. R. Mahmoud, ‘An analytical solution for bending, buckling and vibration responses of FGM sandwich plates’, *Journal of Sandwich Structures and Materials*, vol. 21, no. 2, 2019, doi: 10.1177/1099636217698443.

[26] L. Hadji, A. Fallah, M. M. Aghdam, L. Hadji, A. Fallah, and M. M. Aghdam, ‘Influence of the distribution pattern of porosity on the free vibration of functionally graded plates.’, *Structural Engineering and Mechanics*, vol. 82, no. 2, p. 151, Apr. 2022, doi: 10.12989/SEM.2022.82.2.151.

[27] M. Heshmati and S. K. Jalali, ‘Effect of radially graded porosity on the free vibration behavior of circular and annular sandwich plates’, *European Journal of Mechanics, A/Solids*, vol. 74, pp. 417–430, Mar. 2019, doi: 10.1016/j.euromechsol.2018.12.009.

[28] A. A. Daikh and A. M. Zenkour, ‘Effect of porosity on the bending analysis of various functionally graded sandwich plates’, *Mater Res Express*, vol. 6, no. 6, Mar. 2019, doi: 10.1088/2053-1591/ab0971.

[29] A. A. Daikh and A. M. Zenkour, ‘Free vibration and buckling of porous power-law and sigmoid functionally graded sandwich plates using a simple higher-order shear deformation theory’, *Mater Res Express*, vol. 6, no. 11, Oct. 2019, doi: 10.1088/2053-1591/ab48a9.

[30] Y. Zhang, G. Jin, M. Chen, T. Ye, C. Yang, and Y. Yin, ‘Free vibration and damping analysis of porous functionally graded sandwich plates with a viscoelastic core’, *Compos Struct*, vol. 244, Jul. 2020, doi: 10.1016/j.compstruct.2020.112298.

[31] T. T. Tran, Q. H. Pham, and T. Nguyen-Thoi, ‘Static and free vibration analyses of functionally graded porous variable-thickness plates using an edge-based smoothed finite element method’, *Defence Technology*, vol. 17, no. 3, pp. 971–986, Jun. 2021, doi: 10.1016/j.dt.2020.06.001.

[32] T. Q. Quan, D. T. T. Ha, and N. D. Duc, 'Analytical solutions for nonlinear vibration of porous functionally graded sandwich plate subjected to blast loading', *Thin-Walled Structures*, vol. 170, Jan. 2022, doi: 10.1016/j.tws.2021.108606.

[33] P. Van Vinh and L. Q. Huy, 'Finite element analysis of functionally graded sandwich plates with porosity via a new hyperbolic shear deformation theory', *Defence Technology*, vol. 18, no. 3, pp. 490–508, Mar. 2022, doi: 10.1016/j.dt.2021.03.006.

[34] S. Kumar Sah and A. Ghosh, 'Influence of porosity distribution on free vibration and buckling analysis of multi-directional functionally graded sandwich plates', *Compos Struct*, vol. 279, Jan. 2022, doi: 10.1016/j.compstruct.2021.114795.

[35] S. Hirannaiah, K. Swaminathan, and T. Rajanna, 'Thermo-mechanical vibration and buckling analysis of porous FG sandwich plates with geometric discontinuity based on physical neutral surface', *Mechanics of Advanced Materials and Structures*, 2023, doi: 10.1080/15376494.2023.2220493.

[36] Y. Belkhodja, M. El Amine Belkhodja, H. Fekirini, and D. Ouinas, 'New quasi-three-, and two-dimensional trigonometric-cubic monomial HSDT for thermal buckling and thermo-mechanical bending analyses of FGM symmetrical/non-symmetrical sandwich plates with hard/soft core', *Compos Struct*, vol. 304, 2023, doi: 10.1016/j.compstruct.2022.116402.

[37] A. Karakoti, S. Pandey, and V. R. Kar, 'Nonlinear transient analysis of porous P-FGM and S-FGM sandwich plates and shell panels under blast loading and thermal environment', *Thin-Walled Structures*, vol. 173, 2022, doi: 10.1016/j.tws.2022.108985.

[38] S. Merdaci, H. M. Adda, B. Hakima, R. Dimitri, and F. Tornabene, 'Higher-order free vibration analysis of porous functionally graded plates', *Journal of Composites Science*, vol. 5, no. 11, 2021, doi: 10.3390/jcs5110305.

[39] N. K. Hosur Shivaramaiah, S. Kattimani, M. Shariati, and T. Nguyen-Thoi, 'Geometrically nonlinear behavior of two-directional functionally graded porous plates with four different materials', *Proc Inst Mech Eng C J Mech Eng Sci*, vol. 236, no. 22, 2022, doi: 10.1177/09544062221111038.

[40] L. J. Gibson and M. F. Ashby, 'Cellular solids: Structure and properties, second edition', *Cellular Solids: Structure and Properties, Second Edition*, pp. 1–510, Jan. 2014, doi: 10.1017/CBO9781139878326.

[41] B. Alan, D. Stuart, and K. Donald, 'composite materials for aircraft structures, second edition', ISBN 1-56347-540-5, 2004, DOI: 10.2514/4.861680.

[42] D. ZENKERT, 'SANDWICH STRUCTURES, second edition' Stockholm, March 1995.

[43] I. M. Daniel, E. E. Gdoutos, I. M. Daniel, R. R. Mccormick, and E. E. Gdoutos, 'Failure Modes of Composite Sandwich Beams', January 2010, DOI: 10.1007/978-90-481-3141-9_9.

[44] H.G. Allen, Analysis and Design of Structural Sandwich Panels, Pergamon Press, Oxford, 1969.

[45] R. M. Jones, 'Mechanics of composite materials. McGraw Hill, New York (1975).

[46] J.-M. Berthelot, Book, Matériaux composites : comportement mécanique et analyse des structures , 2012.

[47] V. R. Kar and S. K. Panda, 'Nonlinear thermomechanical behavior of functionally graded material cylindrical/hyperbolic/ elliptical shell panel with temperature-dependent and temperature-independent properties', *Journal of Pressure Vessel Technology, Transactions of the ASME*, vol. 138, no. 6, Dec. 2016, doi: 10.1115/1.4033701.

[48] H. LAZREG, 'contribution à l'étude de la vibration des plaques Sandwiches en FGM, thèse de doctorat en sciences, 2012-2013, Universite Djillali Liabes Sidi Bel Abbes'.

[49] C. R. Kumar and G. Nagarajan, 'Performance and emission characteristics of a low heat rejection spark ignited engine fuelled with E20', *Journal of Mechanical Science and Technology*, vol. 26, no. 4, pp. 1241–1250, Apr. 2012, doi: 10.1007/s12206-012-0206-0.

[50] S. Uemura, 'The activities of FGM on new application', in *Materials Science Forum*, Trans Tech Publications Ltd, 2003, pp. 1–10. doi: 10.4028/www.scientific.net/msf.423-425.1.

[51] T. Hirai and L. Chen, 'Recent and prospective development of functionally graded materials in Japan', *Materials Science Forum*, vol. 308–311, pp. 509–514, 1999, doi: 10.4028/www.scientific.net/msf.308-311.509.

[52] M. Talha and B. N. Singh, 'Static response and free vibration analysis of FGM plates using higher order shear deformation theory', *Appl Math Model*, vol. 34, no. 12, pp. 3991–4011, Dec. 2010, doi: 10.1016/j.apm.2010.03.034.

[53] M. Sasaki, T. Hashida, T. Hirai, and H. Takahashi, 'Thermal Shock Resistance of SiC/C Functionally Gradient Material Prepared by Chemical Vapor Deposition', *Journal of the Japan Society of Powder and Powder Metallurgy*, vol. 37, no. 7, 1990, doi: 10.2497/jjspm.37.966.

[54] B. Saleh *et al.*, '30 Years of functionally graded materials: An overview of manufacturing methods, Applications and Future Challenges', *Composites Part B: Engineering*, vol. 201. Elsevier Ltd, Nov. 15, 2020. doi: 10.1016/j.compositesb.2020.108376.

[55] I. M. El-Galy, B. I. Saleh, and M. H. Ahmed, 'Functionally graded materials classifications and development trends from industrial point of view', *SN Applied Sciences*, vol. 1, no. 11. Springer Nature, Nov. 01, 2019. doi: 10.1007/s42452-019-1413-4.

[56] J. H. Adair, S. A. Touse, and P. J. Melling, 'CHEMICALLY DERIVED MULTILAYER CERAMICS.', *American Ceramic Society Bulletin*, vol. 66, no. 10, 1987.

[57] S. Put, J. Vleugels, G. Anné, and O. Van Der Biest, 'Functionally graded ceramic and ceramic-metal composites shaped by electrophoretic deposition', in *Colloids and Surfaces A: Physicochemical and Engineering Aspects*, 2003. doi: 10.1016/S0927-7757(03)00227-9.

[58] N. Espallargas, 'Introduction to thermal spray coatings', in *Future Development of Thermal Spray Coatings: Types, Designs, Manufacture and Applications*, 2015. doi: 10.1016/B978-0-85709-769-9.00001-4.

[59] Y. Watanabe, H. Sato, and E. Miura-Fujiwara, 'Functionally Graded Metallic Biomaterials', 2015. doi: 10.1007/978-3-662-46842-5_9.

[60] G. H. Loh, E. Pei, D. Harrison, and M. D. Monzón, 'An overview of functionally graded additive manufacturing', *Additive Manufacturing*, vol. 23. 2018. doi: 10.1016/j.addma.2018.06.023.

[61] Z. Pan, D. Ding, B. Wu, D. Cuiuri, H. Li, and J. Norrish, 'Arc Welding Processes for Additive Manufacturing: A Review', in *Transactions on Intelligent Welding Manufacturing*, 2018. doi: 10.1007/978-981-10-5355-9_1.

[62] S. Rathee, S. Maheshwari, A. N. Siddiquee, and M. Srivastava, 'A Review of Recent Progress in Solid State Fabrication of Composites and Functionally Graded Systems Via Friction Stir Processing', *Critical Reviews in Solid State and Materials Sciences*, vol. 43, no. 4. 2018. doi: 10.1080/10408436.2017.1358146.

[63] Z. L. Chao *et al.*, 'Ballistic behavior and microstructure evolution of B4C/AA2024 composites', *Ceram Int*, vol. 45, no. 16, 2019, doi: 10.1016/j.ceramint.2019.07.033.

[64] J.S. Moya, A.J. Sanchez-Herencia, R. Moreno, (1992). Functionally Gradient Ceramics by Sequential Slip Casting, Materials Letters 14, 333–35.

[65] R. E. Mistler, 'HIGH STRENGTH ALUMINA SUBSTRATES PRODUCED BY A MULTIPLE - LAYER CASTING TECHNIQUE.', *American Ceramic Society Bulletin*, vol. 52, no. 11, 1973.

[66] P. Boch, T. Chartier, M. Huttepain, (1986). Casting of AL2O3/ZrO2 laminated Composites, Journal of the American Ceramic Society 69 (8), 191–192.

[67] R. Faddoul, 'Printing processes dedicated for the mass production of ceramic based microelectronic devices. Fluid mechanics [physics.class-ph]. Institut National Polytechnique de Grenoble - INPG, 2012. English. NNT: tel-00825123'.

[68] M. Chmielewski and K. Pietrzak, 'Metal-ceramic functionally graded materials - Manufacturing, characterization, application', *Bulletin of the Polish Academy of Sciences: Technical Sciences*, vol. 64, no. 1, 2016, doi: 10.1515/bpasts-2016-0017.

[69] R. M. Mahamood and E. T. Akinlabi, 'Types of Functionally Graded Materials and Their Areas of Application', in *Topics in Mining, Metallurgy and Materials Engineering*, Springer Science and Business Media Deutschland GmbH, 2017, pp. 9–21. doi: 10.1007/978-3-319-53756-6_2.

[70] S. Matsuo, F. Watari, N. Ohata. Fabrication of functionally graded dental composite resin post and core by laser lithography and finite element analysis of its stress relaxation effect on tooth root. Dental Mater J 2001;20(4):257–74.

[71] F. Watari *et al.*, 'Biocompatibility of materials and development to functionally graded implant for bio-medical application', *Compos Sci Technol*, vol. 64, no. 6, pp. 893–908, May 2004, doi: 10.1016/j.compscitech.2003.09.005.

[72] A. Sadollah, A. Bahreininejad, H. Eskandar, and M. Hamdi, 'Optimum material gradient for functionally graded dental implant using particle swarm optimization', in *Advanced Materials Research*, 2013, pp. 30–36. doi: 10.4028/www.scientific.net/AMR.647.30.

[73] W. W. Chen, A. M. Rajendran, B. Song, and X. Nie, 'Dynamic fracture of ceramics in armor applications', *Journal of the American Ceramic Society*, vol. 90, no. 4, pp. 1005–1018, Apr. 2007, doi: 10.1111/j.1551-2916.2007.01515.x.

[74] M. Niino, K. Kisara, and M. Mori, 'Feasibility Study of FGM Technology in Space Solar Power Systems (SSPS)', *Materials Science Forum*, vol. 492–493, pp. 163–170, Aug. 2005, doi: 10.4028/www.scientific.net/msf.492-493.163.

[75] M. Herrmann and W. Sobek, 'Functionally graded concrete: Numerical design methods and experimental tests of mass-optimized structural components', *Structural Concrete*, vol. 18, no. 1, pp. 54–66, Feb. 2017, doi: 10.1002/suco.201600011.

[76] Y. Miyamoto, W. A. Kaysser, B. H. Rabin, A. Kawasaki, and R. G. Ford, Eds., *Functionally Graded Materials*, vol. 5. in Materials Technology Series, vol. 5. Boston, MA: Springer US, 1999. doi: 10.1007/978-1-4615-5301-4.

[77] D. Delfosse, ‘Fundamentals of Functionally Graded Materials’, *Materials Today*, vol. 1, no. 4, 1998, doi: 10.1016/s1369-7021(98)80023-0.

[78] S. H. Chi and Y. L. Chung, ‘Mechanical behavior of functionally graded material plates under transverse load-Part I: Analysis’, *Int J Solids Struct*, vol. 43, no. 13, 2006, doi: 10.1016/j.ijsolstr.2005.04.011.

[79] S. H. Chi and Y. L. Chung, ‘Cracking in coating-substrate composites with multi-layered and FGM coatings’, *Eng Fract Mech*, vol. 70, no. 10, 2003, doi: 10.1016/S0013-7944(02)00114-5.

[80] J. H. Kim and G. H. Paulino, ‘Finite element evaluation of mixed mode stress intensity factors in functionally graded materials’, *Int J Numer Methods Eng*, vol. 53, no. 8, 2002, doi: 10.1002/nme.364.

[81] C. Zhang, A. Savaidis, G. Savaidis, and H. Zhu, ‘Transient dynamic analysis of a cracked functionally graded material by a BIEM’, in *Computational Materials Science*, 2003. doi: 10.1016/S0927-0256(02)00395-6.

[82] B. Karami, D. Shahsavari, M. Janghorban, and L. Li, ‘Influence of homogenization schemes on vibration of functionally graded curved microbeams’, *Compos Struct*, vol. 216, 2019, doi: 10.1016/j.compstruct.2019.02.089.

[83] F. Delale and F. Erdogan, ‘The crack problem for a nonhomogeneous plane’, *Journal of Applied Mechanics, Transactions ASME*, vol. 50, no. 3, 1983, doi: 10.1115/1.3167098.

[84] I. Elishakoff, D. Pentaras, and C. Gentilini, *Mechanics of functionally graded material structures*. 2015. doi: 10.1142/9505.

[85] J. N. Reddy, *Theory and Analysis of Elastic Plates and Shells, Second Edition*. 2006. doi: 10.1201/9780849384165.

[86] J. N. Reddy, *Mechanics of Laminated Composite Plates and Shells*. 2003. doi: 10.1201/b12409.

[87] H. Deng and W. Cheng, 'Dynamic characteristics analysis of bi-directional functionally graded Timoshenko beams', *Compos Struct*, vol. 141, 2016, doi: 10.1016/j.compstruct.2016.01.051.

[88] G. Kirchhoff, '4. Über das Gleichgewicht und die Bewegung einer elastischen Scheibe', *Journal fur die Reine und Angewandte Mathematik*, vol. 1850, no. 40, 1850, doi: 10.1515/crll.1850.40.51.

[89] M. Şimşek, 'Bi-directional functionally graded materials (BDFGMs) for free and forced vibration of Timoshenko beams with various boundary conditions', *Compos Struct*, vol. 133, 2015, doi: 10.1016/j.compstruct.2015.08.021.

[90] L. F. Qian and R. C. Batra, 'Design of bidirectional functionally graded plate for optimal natural frequencies', *J Sound Vib*, vol. 280, no. 1–2, 2005, doi: 10.1016/j.jsv.2004.01.042.

[91] Reissner, E. (1963). On the Derivation of Boundary Conditions for Plate Theory. Proceedings of the Royal Society A: Mathematical, Physical and Engineering Sciences, 276(1365), 178–186. doi:10.1098/rspa.1963.0201.

[92] K. H. Lo, R. M. Christensen, and E. M. Wu, 'A high-order theory of plate deformation: Part 1: Homogeneous plates', *Journal of Applied Mechanics, Transactions ASME*, vol. 44, no. 4, 1977, doi: 10.1115/1.3424154.

[93] K. H. Lo, R. M. Christensen, and E. M. Wu, 'A high-order theory of plate deformation: Part 2: Laminated plates', *Journal of Applied Mechanics, Transactions ASME*, vol. 44, no. 4, 1977, doi: 10.1115/1.3424155.

[94] M. Levinson, 'An accurate, simple theory of the statics and dynamics of elastic plates', *Mech Res Commun*, vol. 7, no. 6, 1980, doi: 10.1016/0093-6413(80)90049-X.

[95] M. V. V. Murthy, 'IMPROVED TRANSVERSE SHEAR DEFORMATION THEORY FOR LAMINATED ANISOTROPIC PLATES.', *NASA Technical Paper*, 1981.

[96] J. N. Reddy, 'A simple higher-order theory for laminated composite plates', *Journal of Applied Mechanics, Transactions ASME*, vol. 51, no. 4, 1984, doi: 10.1115/1.3167719.

[97] T. Kant and K. Swaminathan, 'Analytical solutions for the static analysis of laminated composite and sandwich plates based on a higher order refined theory', *Compos Struct*, vol. 56, no. 4, 2002, doi: 10.1016/S0263-8223(02)00017-X.

[98] Y. M. Ghugal and R. P. Shimpi, 'A review of refined shear deformation theories of isotropic and anisotropic laminated plates', *Journal of Reinforced Plastics and Composites*, vol. 21, no. 9, 2002, doi: 10.1177/073168402128988481.

[99] J. M. Whitney and C. T. Sun, 'A higher order theory for extensional motion of laminated composites', *J Sound Vib*, vol. 30, no. 1, 1973, doi: 10.1016/S0022-460X(73)80052-5.

[100] M. Touratier, 'An efficient standard plate theory', *Int J Eng Sci*, vol. 29, no. 8, 1991, doi: 10.1016/0020-7225(91)90165-Y.

[101] K. P. Soldatos, 'A transverse shear deformation theory for homogeneous monoclinic plates', *Acta Mech*, vol. 94, no. 3–4, 1992, doi: 10.1007/BF01176650.

[102] M. Karama, K. S. Afaq, and S. Mistou, 'Mechanical behaviour of laminated composite beam by the new multi-layered laminated composite structures model with transverse shear stress continuity', *Int J Solids Struct*, vol. 40, no. 6, 2003, doi: 10.1016/S0020-7683(02)00647-9.

[103] R. P. Shimpi, 'Refined plate theory and its variants', *AIAA Journal*, vol. 40, no. 1, 2002, doi: 10.2514/2.1622.

[104] H. T. Thai and S. E. Kim, 'A simple quasi-3D sinusoidal shear deformation theory for functionally graded plates', *Compos Struct*, vol. 99, 2013, doi: 10.1016/j.compstruct.2012.11.030.

[105] A. CHABOT, 'analyse des efforts à l'interface entre les couches des materiaux composite à l'aide de modeles multiparticulaires des materiaux multicouches(M4), thése de doctorat en sciences, l'ecole nationale des ponts et chaussées (1997).

[106] E. Carrera, 'An assessment of mixed and classical theories on global and local response of multilayered orthotropic plates', *Compos Struct*, vol. 50, no. 2, 2000, doi: 10.1016/S0263-8223(00)00099-4.

[107] D. Baptiste, R. O. Polit, R. A. Chabot, E. M. Boussu, and J. F. Caron, Thèse, MODELISATION GLOBALE ET LOCALE DES STRUCTURES MULTICOUCHES PAR ELEMENTS FINIS DE PLAQUE, 'Viet Tung NGUYEN', 2004.

[108] Di Sciuva, M. (1987). An Improved Shear-Deformation Theory for Moderately Thick Multilayered Anisotropic Shells and Plates. Journal of Applied Mechanics, 54(3), 589–. doi:10.1115/1.3173074.

[109] U. Icardi, 'Higher-order zig-zag model for analysis of thick composite beams with inclusion of transverse normal stress and sublaminates approximations', *Composites Part B:Engineering*, vol. 32, no. 4, 2001, doi: 10.1016/S1359-8368(01)00016-6.

[110] C. Ossadzow; M. Touratier (2001). An improved shear-membrane theory for multilayered shells., 52(1), 85–95. doi:10.1016/s0263-8223(00)00194-x.

[111] M. Karama, B. Abou Harb, S. Mistou, and S. Caperaa, 'Bending, buckling and free vibration of laminated composite with a transverse shear stress continuity model', *Compos B Eng*, vol. 29, no. 3, 1998, doi: 10.1016/S1359-8368(97)00024-3.

[112] I. Babuskat, B. A. Szabo, and I. N. Katz, (1981). The p-version of the finite element method. SlAM J. Numer. Anal, Vol. 18, pp. 515-545.

[113] I. Babuška and M. Suri, 'The p- and h-p versions of the finite element method, an overview', *Comput Methods Appl Mech Eng*, vol. 80, no. 1–3, pp. 5–26, Jun. 1990, doi: 10.1016/0045-7825(90)90011-A.

[114] B. A. Szabb, 'MESH DESIGN FOR THE p-VERSION OF THE FINITE ELEMENT METHOD', 1986, Computer Methods in Applied Mechanics and Engineering, Vol. 55, pp. 181-197.

[115] A. Peanot and E. Y. Rodin, 'HIERARCHIES OF CONFORMING FINITE ELEMENTS FOR PLANE ELASTICITY AND PLATE BENDING*', Pergamon Press, 1916.

[116] A. Houmat, 'Three-dimensional hierarchical finite element free vibration analysis of annular sector plates', *J Sound Vib*, vol. 276, no. 1–2, 2004, doi: 10.1016/j.jsv.2003.07.020.

[117] A. Côté and F. Charron, 'On the selection of p-version shape functions for plate vibration problems', *Comput Struct*, vol. 79, no. 1, 2001, doi: 10.1016/S0045-7949(00)00115-2.

[118] A. Necira, 'Etude des Vibrations Libres des Nano-Plaques Arbitraires, thèse de doctorat en sciences, (2022), Universite Aboubakr Belkaïd Tlemcen.

[119] R. Szilard, (2004), Theories and Applications of Plate Analysis, JohnWiley & Sons Inc., Hoboken, New Jersey, [120] M. Amabili, 'Nonlinear vibrations and stability of shells and plates', p. 374, 2008.

[121] A. W. Leissa, (1973), "The free vibration of rectangular plates", J. Sound Vib., 31(3), 257-293. https://doi.org/10.1016/S0022- 460X(73)80371-2.

[122] M. Malik, and C.W. Bert, (1998), "Three-dimensional elasticity solutions for free vibrations of rectangular plates by the differential quadrature method", Int. J. Solid. Struct., 35(3-4), 299-318. https://doi.org/10.1016/S0020-7683(97)00073-5.

[123] A. M. Zenkour, 'A comprehensive analysis of functionally graded sandwich plates: Part 2-Buckling and free vibration', *Int J Solids Struct*, vol. 42, no. 18–19, pp. 5243–5258, Sep. 2005, doi: 10.1016/j.ijsolstr.2005.02.016.